

## Transition State Models for Probing Stereoinduction in Evans Chiral Auxiliary-Based Asymmetric Aldol Reactions

C. B. Shinisha and Raghavan B. Sunoj\*

*Department of Chemistry, Indian Institute of Technology Bombay, Powai, Mumbai 400076, India*

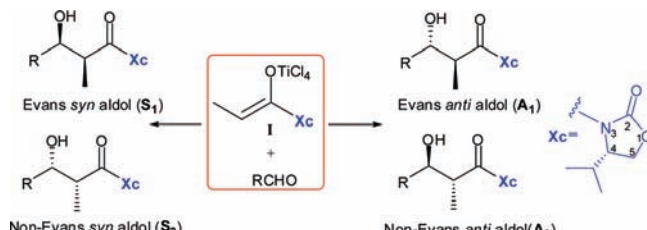
Received March 7, 2010; E-mail: sunoj@chem.iitb.ac.in

**Abstract:** The use of chiral auxiliaries is one of the most fundamental protocols employed in asymmetric synthesis. In the present study, stereoselectivity-determining factors in a chiral auxiliary-based asymmetric aldol reaction promoted by  $TiCl_4$  are investigated by using density functional theory methods. The aldol reaction between chiral titanium enolate [derived from Evans propionyl oxazolidinone (**1a**) and its variants oxazolidinethione (**1b**) and thiazolidinethione (**1c**)] and benzaldehyde is examined by using transition-state modeling. Different stereochemical possibilities for the addition of titanium enolates to aldehyde are compared. On the basis of the coordination of the carbonyl/thiocarbonyl group of the chiral auxiliary with titanium, both pathways involving nonchelated and chelated transition states (TSs) are considered. The computed relative energies of the stereoselectivity-determining C–C bond formation TSs in the nonchelated pathway, for both **1a** and **1c**, indicate a preference toward Evans *syn* aldol product. The presence of a ring carbonyl or thiocarbonyl group in the chiral auxiliary renders the formation of neutral  $TiCl_3$ -enolate, which otherwise is energetically less favored as compared to the anionic  $TiCl_4$ -enolate. Hence, under suitable conditions, the reaction between titanium enolate and aldehyde is expected to be viable through chelated TSs leading to the selective formation of non-Evans *syn* aldol product. Experimentally known high stereoselectivity toward Evans *syn* aldol product is effectively rationalized by using the larger energy differences between the corresponding diastereomeric TSs. In both chelated and nonchelated pathways, the attack by the less hindered face of the enolate on aldehyde through a chair-like TS with an equatorial disposition of the aldehydic substituent is identified as the preferred mode. The steric hindrance offered by the isopropyl group and the possible chelation are identified as the key reasons behind the interesting stereodivergence between Evans and non-Evans products normally reported for the title reaction. The application of an *activation strain model* on the critical TSs has been effective toward rationalizing the origin of stereoselectivity. Improved interaction energy between the reactants is found to be the key stabilizing factor for the lowest energy TS in both chelated and nonchelated pathways. The present study provides newer insights on the role of titanium(IV) toward modulating stereoselectivity in aldol reactions.

### Introduction

Asymmetric induction by using covalent incorporation of chiral auxiliaries is a widely employed strategy in organic synthesis. Oxazolidinones, popularly known as Evans chiral auxiliaries, originally developed for efficient C–C bond construction in an asymmetric fashion, are a classic example of chiral auxiliary-based stereoinduction.<sup>1</sup> The ability of acylated oxazolidinones to engage in chelation with metal ions, along with the steric shielding of one of the enolate faces (due to the presence of suitable substituents at the fourth position oxazolidinone ring, Scheme 1), gives versatility to this group of chiral auxiliaries.<sup>2</sup> Over the years, application of oxazolidinone and

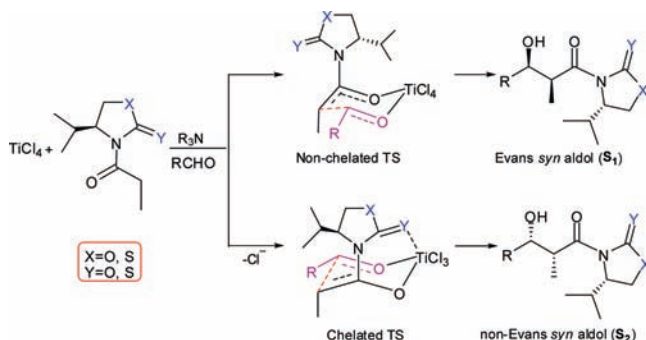
**Scheme 1.** Possible Stereoisomeric Products Resulting from an Oxazolidinone-Mediated Aldol Reaction between a Titanium Enolate (**I**) and an Aldehyde



its variants as chiral auxiliaries has continued to gain increased prominence in organic synthesis.<sup>3</sup>

- (1) (a) Evans, D. A.; Bartroli, J.; Shih, T. L. *J. Am. Chem. Soc.* **1981**, *103*, 2127. (b) Evans, D. A. *Aldrichim. Acta* **1982**, *15*, 23. (c) Abdel-Magid, A.; Pridgen, L. N.; Eggleston, D. S.; Lantos, I. *J. Am. Chem. Soc.* **1986**, *108*, 4595. (d) Ager, D. J.; Prakash, I.; Schaad, D. R. *Aldrichim. Acta* **1997**, *30*, 3. (e) Phoon, C. W.; Abell, C. *Tetrahedron Lett.* **1998**, *39*, 2655. (f) Evans, D. A.; Helmchen, G.; Rüping, M. In *Asymmetric Synthesis—The Essentials*; Christmann, M., Bräse, S., Eds.; Wiley-VCH & Co.: Weinheim, 2007; Vol. 3.
- (2) (a) Evans, D. A.; Rieger, D. L.; Bilodeau, M. T.; Urpi, F. *J. Am. Chem. Soc.* **1991**, *113*, 1047. (b) Chiral *N*-propionyloxazolidinone is shown in Figure S1 of the Supporting Information.
- (3) (a) Cosp, A.; Romea, P.; Talavera, P.; Urpi, F.; Vilarrasa, J.; Font-Bardia, M.; Solans, X. *Org. Lett.* **2001**, *3*, 615. (b) Evans, D. A.; Starr, J. T. *Angew. Chem., Int. Ed.* **2002**, *41*, 1787. (c) Zhang, Y.; Sammakia, T. *Org. Lett.* **2004**, *6*, 3139. (d) Crimmins, M. T.; Christie, H. S.; Chaudhary, K.; Long, A. *J. Am. Chem. Soc.* **2005**, *127*, 13810. (e) Patel, J.; Clavé, G.; Renard, P.-Y.; Franck, X. *Angew. Chem., Int. Ed.* **2008**, *47*, 4224. (f) Tessier, A.; Lahmar, N.; Pytkowicz, J.; Briguid, T. *J. Org. Chem.* **2008**, *73*, 2621. (g) Crimmins, M. T.; King, B. W. *J. Am. Chem. Soc.* **1998**, *120*, 9084.

**Scheme 2.** Illustration of Stereodivergence in *syn*-Aldol Reactions through Chelated and Nonchelated Transition States



Asymmetric aldol reactions using chiral auxiliaries are indeed one of the quintessential examples,<sup>4</sup> wherein chiral titanium or boron enolates are typically produced. The addition of chiral metal enolates thus generated to suitable electrophiles can result in different stereoisomeric products, as shown in Scheme 1. The original studies on oxazolidinone as chiral auxiliary in titanium- or boron-promoted reactions reported the formation of Evans *syn* aldol product with high diastereoselectivity.<sup>5</sup> Titanium enolates are also known to yield non-Evans *syn* aldol product, presumably through a chelation-controlled pathway.<sup>6</sup> Other factors such as the nature of the bound ligands are known to influence the stereochemical outcome of oxazolidinone-mediated aldol reactions using titanium enolates.<sup>7</sup> The generation of *anti* aldol products is now increasingly available in more recent literature.<sup>8</sup>

A closer perusal of related literature conveys that the stereochemical outcome of asymmetric aldol reactions using Evans chiral auxiliary protocol is delicately dependent on the nature of the auxiliary group. For instance, changing the carbonyl of oxazolidinone to a thiocarbonyl group can alter the product stereochemistry. In the early 1990s, Yan et al. noticed opposite facial selectivity preferences in the aldol reaction of a variety of electrophiles with chlorotitanium enolates of camphor-based *N*-propionyloxazolidinethione and *N*-propionyloxazolidinone. The former afforded non-Evans *syn* aldol products, while the latter resulted in Evans *syn* aldol products.<sup>9</sup> Crimmins and co-workers also reported the change in stereoselectivity from Evans *syn* aldol to non-Evans *syn* aldol when the chiral auxiliary was changed from oxazolidinone (**1a**) to thiazolidinethione (**1c**). A description of Evans and non-Evans aldol products is provided in Scheme 2. The formation of Evans or non-Evans *syn* aldol adducts when oxazolidinethione and thiazolidinethione are used as the chiral auxiliary is reported to

depend on the nature and quantity of the base employed in the reaction.<sup>10,11</sup> The selectivity toward Evans *syn* aldol or non-Evans *syn* aldol products is also known to depend on the bulkiness of the aldehyde.<sup>14a</sup> It has been proposed that increasing the chelation potential of the enolate ligand could lead to modulation of facial selectivity promoted by the chelation effect. The improved nucleophilicity of thiazolidinethione has also been suggested to result in a highly ordered chelated transition state (TS), albeit without any verification. The ligands bound to the titanium center are also found to be efficient in promoting  $\pi$ -facial differentiation.<sup>2a,12</sup> The stereochemical differences that result upon varying the reaction conditions with these chiral auxiliaries are also exploited in organic synthesis.<sup>3d,13</sup>

Qualitative models have thus far been adopted to explain the molecular origin of stereoselectivity in these reactions.<sup>12,14</sup> Since hexacoordinate arrangement is one of the preferred modes of coordination in titanium Lewis acids, it is reasonable to expect that the reaction may proceed through an open TS or through a chelated complex resulting from the displacement of chloride ions. The nonchelated TS models are generally employed to explain the formation of Evans *syn* aldol product. In this model, titanium coordinates with the enolate oxygen and the carbonyl group of the approaching aldehyde. The formation of non-Evans *syn* aldol product, on the other hand, is usually accounted for by invoking a chelated TS model. The Lewis acidity of  $\text{Ti(IV)}$  permits chelation with the oxazolidinone carbonyl, thereby leading to a conformational change of the oxazolidinone ring as compared to the nonchelated model (Scheme 2). As a result, the change in the orientation of the isopropyl group in the chelated TS will have a direct bearing on the stereochemical outcome of the reaction.<sup>13</sup>

Though the above-mentioned models of chiral auxiliary-based stereoselective aldol reactions are widely employed toward rationalizing the observed selectivities, a clear picture of the stereoselectivity-controlling TSs is seldom reported.<sup>15</sup> In this article, we present the results of a comprehensive investigation on Evans chiral auxiliary-based asymmetric aldol reaction, where titanium salts are used as the Lewis acid. We have examined different possible modes, involving both chelated and nonchelated pathways, to establish the factors that control the stereochemical course of this fundamentally important reaction. The key TSs are identified that are responsible for the formation of four stereochemically important products. Another key objective is to examine the role of a heteroatom on the chiral auxiliary. To address these issues, competing chelated and nonchelated TSs for an aldol reaction using three different chiral

- (4) (a) Palomo, C.; Oiarbide, M.; García, J. M. *Chem. Soc. Rev.* **2004**, *33*, 65. (b) Davies, S. G.; Garner, A. C.; Roberts, P. M.; Smith, A. D.; Sweet, M. J.; Thomson, J. E. *Org. Biomol. Chem.* **2006**, *4*, 2753.
- (5) Details of the stereochemical descriptions and nomenclature employed here are in accordance with the standard practices found in the current literature. Further details are provided on page S2 of Supporting Information.
- (6) Bonner, M. P.; Thornton, E. R. *J. Am. Chem. Soc.* **1991**, *113*, 1299.
- (7) Shirodkar, S.; Nerz-Stormes, M.; Thornton, E. R. *Tetrahedron Lett.* **1990**, *31*, 4699.
- (8) (a) Evans, D. A.; Tedow, J. S.; Shaw, J. T.; Downey, C. W. *J. Am. Chem. Soc.* **2002**, *124*, 392. (b) Evans, D. A.; Downey, C. W.; Shaw, J. T.; Tedow, J. S. *Org. Lett.* **2002**, *4*, 1127. (c) Crimmins, M. T.; McDougall, P. J. *Org. Lett.* **2003**, *5*, 591. (d) Hajra, S.; Giri, A. K.; Karmakar, A.; Khatua, S. *Chem. Commun.* **2007**, *23*, 2408.
- (9) (a) Yan, T.-H.; Tan, C.-W.; Lee, H.-C.; Lo, H.-C.; Huang, T.-Y. *J. Am. Chem. Soc.* **1993**, *115*, 2613. (b) Yan, T.-H.; Lee, H.-C.; Tan, C.-W. *Tetrahedron Lett.* **1993**, *34*, 3559.
- (10) (a) Crimmins, M. T.; King, B. W.; Tabet, E. A. *J. Am. Chem. Soc.* **1997**, *119*, 7883. (b) Crimmins, M. T.; Chaudhary, K. *Org. Lett.* **2000**, *2*, 775. (c) Crimmins, M. T.; King, B. W.; Tabet, E. A.; Chaudhary, K. *J. Org. Chem.* **2001**, *66*, 894.
- (11) Evans, D. A.; Shaw, J. T. *Act. Chim.* **2003**, *35*.
- (12) Nerz-Stormes, M.; Thornton, E. R. *Tetrahedron Lett.* **1986**, *27*, 897.
- (13) Zhang, W.; Carter, R. G.; Yokochi, A. F. T. *J. Org. Chem.* **2004**, *69*, 2569.
- (14) (a) Nerz-Stormes, M.; Thornton, E. R. *J. Org. Chem.* **1991**, *56*, 2489. (b) Siegel, C.; Thornton, E. R. *J. Am. Chem. Soc.* **1989**, *111*, 5722. (c) Crimmins, M. T.; Shamszad, M. *Org. Lett.* **2007**, *9*, 149.
- (15) A few examples for Zimmerman–Traxler-type transition-state models for aldol reactions have been reported: (a) Li, Y.; Paddon-Row, M. N.; Houk, K. N. *J. Am. Chem. Soc.* **1988**, *110*, 3684. (b) Li, Y.; Paddon-Row, M. N.; Houk, K. N. *J. Org. Chem.* **1990**, *55*, 481.

auxiliaries such as oxazolidinone, oxazolidinethione, and thiazolidinethione are considered.

## Computational Methods

Geometry optimizations of all key stationary points were carried out in the gas phase at the B3LYP (L1),<sup>16</sup> mPW1K (L2),<sup>17</sup> mPW1PW91 (L3),<sup>18</sup> M05-2X (L5),<sup>19</sup> and B98 (L6)<sup>20</sup> levels of theory by using the Gaussian 03 and Gaussian 09 suites of quantum chemical programs.<sup>21</sup> These functionals are frequently used in contemporary literature for addressing various situations where reaction barrier heights are calculated.<sup>22</sup> For all atoms, the 6-31G\* basis set is employed for geometry optimization. We have also examined the effect of using a different basis set on titanium at the B3LYP level, by choosing the Los Alamos pseudopotential basis set (LANL2DZ), while the rest of the elements were treated by using the 6-31G\* basis set (L4).<sup>23,24</sup> The geometries of the critical TSs were again optimized at the levels of theory L1–L6 by using a more flexible basis set (6-311G\*\*), and single-point energies were then evaluated by including diffuse functions. The single-point energies on the optimized geometries were also evaluated by using the dispersion-corrected DFT-D (L7)<sup>25</sup> method as implemented in the ORCA quantum chemical package (B3LYP-D).<sup>26</sup>

All stationary points on the respective potential energy surfaces were characterized at the same levels of theory by evaluating the corresponding Hessian indices. Careful verification of the unique imaginary frequencies for the TSs has been carried out to examine whether the frequency indeed pertains to the desired reaction coordinate. Further, intrinsic reaction coordinate calculations were carried out to authenticate the TSs.<sup>27</sup> Single-point energies were calculated at the respective levels of theory using a more flexible triple- $\zeta$ -quality basis set, including polarization functions on the hydrogen atoms along with diffuse functions on non-hydrogen atoms (6-311+G\*\* (with 6d functions)). The solvent effects were then incorporated with the continuum solvation model using the SCRF-PCM framework. Dichloromethane (DCM) was taken as the continuum solvent dielectric ( $\epsilon = 8.93$ ) since it has been used as solvent previously in these kinds of reactions.<sup>8,28</sup> The energy in solution ( $G_{\text{solvation}}$ , denoted as  $E$  in the text) is comprised of the electronic energy of the polarized solute and the electrostatic solute–solvent interaction energy. The solvent effects in the case

of the DFT-D method (L7) are included at the same level of theory by using the COSMO solvation model.<sup>29</sup> We have focused on the stereoselectivity-controlling C–C bond formation step as well as on the relative energies of the crucial diastereomeric TSs. The relative energies are reported with respect to the lowest energy TS in respective cases.

**Terminology.** The terms “chelated” and “nonchelated” transition states respectively refer to coordination by the ring carbonyl (or thiocarbonyl) group of oxazolidinone (or oxazolidinethione/thiazolidinethione) with the metal center. In the chelated pathway, one of the metal coordination site is occupied by the carbonyl oxygen, while in the nonchelated form, the coordination site is saturated by a chloride ion (Scheme 2). The letters S and A are used to represent the TS leading respectively to *syn* and *anti* aldol products. The subscripts 1 and 2 respectively correspond to Evans and non-Evans products. The TSs **S**<sub>1</sub>, **S**<sub>2</sub>, **A**<sub>1</sub>, and **A**<sub>2</sub> therefore correspond to Evans *syn*, non-Evans *syn*, Evans *anti*, and non-Evans *anti* products.<sup>5</sup> In the nonchelated TSs, additional descriptors *a* and *s* indicate the orientation of the carbonyl group of the chiral auxiliary with respect to the enolate carbonyl as *anti* and *syn*, respectively. The chelated TSs are represented by a prime after the product descriptors, e.g., **TS-S**<sub>1</sub>'.

## Results and Discussion

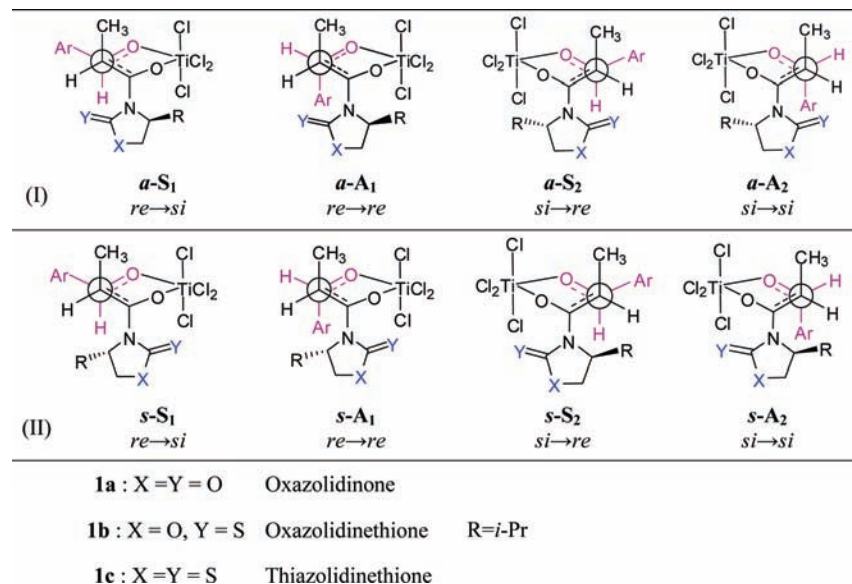
The aldol reaction between benzaldehyde and acyl derivatives of different chiral auxiliaries such as oxazolidinone (**1a**), oxazolidinethione (**1b**), and thiazolidinethione (**1c**) with TiCl<sub>4</sub> as Lewis acid is chosen for the present investigation, with an objective to unravel the molecular origin of stereoselectivity. The asymmetric carbon (C<sub>4</sub> position) of the auxiliary with an isopropyl group is retained in the *S* configuration in this study.<sup>1a</sup> All critical transition states and intermediates that directly influence the stereochemical course of the reaction are identified by using DFT, and their stereoelectronic features are analyzed in detail.

The TiCl<sub>4</sub>-promoted enolization process has been studied previously by using both <sup>1</sup>H and <sup>13</sup>C NMR spectroscopic methods.<sup>30</sup> The computed energies in the present study indicate that the Z-enolates are 2–3 kcal/mol more stable than the corresponding E-enolates.<sup>31</sup> The experimental reports on aldol reactions of *N*-acyloxazolidinones indicate that the stereoselectivities are consistent with the involvement of Z-enolates.<sup>32</sup> The evidence for the existence of enolate in the Z-configuration received further support from NMR spectroscopic as well as isotopic labeling studies.<sup>33</sup> Examples are also available wherein the isomeric purity of enolate intermediates could be confirmed by X-ray crystallography conducted on suitably trapped enolates.<sup>6</sup> Hence, in the present study, we have primarily focused on the aldol reaction of Z-enolates.<sup>34</sup>

The aldehyde and the titanium Z-enolate offer prochiral faces and give rise to two key modes of approach between them.

- (16) (a) Becke, A. D. *J. Chem. Phys.* **1993**, *98*, 5648. (b) Becke, A. D. *Phys. Rev. A* **1998**, *38*, 3098. (c) Lee, C.; Yang, W.; Parr, R. G. *Phys. Rev. A* **1998**, *37*, 785.
- (17) (a) Lynch, B. J.; Fast, P. L.; Harris, M.; Truhlar, D. G. *J. Phys. Chem. A* **2000**, *104*, 4811. (b) Lynch, B. J.; Zhao, Y.; Truhlar, D. G. *J. Phys. Chem. A* **2003**, *107*, 1384.
- (18) Adamo, C.; Barone, V. *J. Chem. Phys.* **1998**, *108*, 664.
- (19) Zhao, Y.; Schultz, N. E.; Truhlar, D. G. *J. Chem. Theory. Comput.* **2006**, *2*, 364.
- (20) Becke, A. D.; Schmid, H. L. *J. Chem. Phys.* **1998**, *108*, 9624.
- (21) (a) Frisch, M. J.; et al. *Gaussian 03*, Revisions C.02 and E.01; Gaussian, Inc.: Wallingford, CT, 2004. (b) Frisch, M. J.; et al. *Gaussian 09*, Revision A.02; Gaussian, Inc.: Wallingford, CT, 2009.
- (22) (a) Lynch, B. J.; Fast, P. L.; Harris, M.; Truhlar, D. G. *J. Phys. Chem. A* **2000**, *104*, 4811. (b) Lynch, B. J.; Truhlar, D. G. *J. Phys. Chem. A* **2001**, *105*, 2936. (c) Curtiss, L. A.; Redfern, P. C.; Raghavachari, K. *J. Chem. Phys.* **2005**, *123*, 124107. (d) Wheeler, S. E.; Moran, A.; Pieniazek, S. N.; Houk, K. N. *J. Phys. Chem. A* **2009**, *113*, 10376. (e) Patel, C.; Sunoj, R. B. *J. Org. Chem.* **2010**, *75*, 359.
- (23) (a) Ditchfield, R.; Hehre, W. J.; Pople, J. A. *J. Chem. Phys.* **1971**, *54*, 724. (b) Hehre, W. J.; Ditchfield, R.; Pople, J. A. *J. Chem. Phys.* **1972**, *56*, 2257. (c) Hariharan, P. C.; Pople, J. A. *Theor. Chim. Acta* **1973**, *28*, 213.
- (24) (a) Hay, P. J.; Wadt, W. R. *J. Chem. Phys.* **1985**, *82*, 270. (b) Hay, P. J.; Wadt, W. R. *J. Chem. Phys.* **1985**, *82*, 299.
- (25) (a) Grimme, S. *J. Comput. Chem.* **2004**, *25*, 1463. (b) Grimme, S. *J. Comput. Chem.* **2006**, *27*, 1787.
- (26) Neese, F. *ORCA—An Ab Initio, Density Functional and Semiempirical Program Package*; University of Bonn: Bonn, Germany, 2007.
- (27) Gonzalez, C.; Schlegel, H. B. *J. Chem. Phys.* **1989**, *90*, 2154.
- (28) Evans, D. A.; Urpi, F.; Somers, T. C.; Clark, J. S.; Bilodeau, M. T. *J. Am. Chem. Soc.* **1990**, *112*, 8215.
- (29) Sinnecker, S.; Rajendran, A.; Klamt, A.; Diedenhofen, M.; Neese, F. *J. Phys. Chem. A* **2006**, *110*, 2235.
- (30) Mechanistic studies on titanium-promoted enolization of  $\alpha$ -hydroxy ketones have been reported: Moreira, I. de P. R.; Bofill, J. M.; Anglada, J. M.; Solsona, J. G.; Nebot, J.; Romea, P.; Urpi, F. *J. Am. Chem. Soc.* **2008**, *130*, 3242.
- (31) The energy difference as well as the optimized geometries of enolates is provided in Figure S2 in the Supporting Information.
- (32) Itoh, Y.; Yamamoto, M.; Mikami, K. *J. Am. Chem. Soc.* **2004**, *126*, 13174.
- (33) Kimball, D. B.; Michalczyk, R.; Moody, E.; Ollivault-Shiflett, M.; Jesus, K. D.; Silks, L. A., III *J. Am. Chem. Soc.* **2003**, *125*, 14666.
- (34) However, the reaction of titanium *E*-enolate with benzaldehyde for representative cases through chelated as well as nonchelated pathways has also been examined. The selectivity is found to be toward Evans *anti* aldol, and the results are tabulated in Table S1 in the Supporting Information.

**Scheme 3.** Important Modes of Addition of Titanium Enolate to Benzaldehyde in the Nonchelated Pathway with the Ring Carbonyl Thiocarbonyl Group Oriented Either *anti* (I) or *syn* (II) with Respect to the Enolate Oxygen: View along the Incipient C–C Bond (Reaction Coordinate)



Depending on the orientation of the chiral auxiliary, additions by both the hindered and unhindered faces of the *Z*-enolate of *N*-propionyl derivatives of **1a** and **1b** as well as **1c** on the *si/re* face of benzaldehyde are considered. In these cases, both chelated and nonchelated pathways are examined as well. Coordination of the carbonyl (or thiocarbonyl) group with the titanium is present in the former, while it is absent in the latter, wherein the oxazolidinone ring is away from the metal center. These stereochemical possibilities can lead to unique diastereomeric products. Three important questions demand immediate attention: (a) What is the most favored mode of addition between the enolate and the electrophile? (b) What are the relative preferences between different pathways responsible for stereochemically different products? (c) What are the contributing stereoelectronic factors operating in the corresponding TSs? These questions are addressed in the following manner. A pre-reacting complex (PRC) is envisaged first, wherein the C=O group of the incoming electrophile (benzaldehyde) coordinates to the titanium atom. Coordination from the carbonyl oxygens of the enolate and the electrophile results in a hexacoordinate titanium complex. The number of possible conformers for such complexes is therefore restricted. A schematic diagram representing important nonchelated TSs for C–C bond formation between titanium *Z*-enolate and benzaldehyde is provided in Scheme 3. An additional model, as shown in Scheme 3-II, wherein the oxazolidinone ring is oriented differently with respect to the enolate oxygen, is additionally examined. Such reorientation within the nonchelated model can give rise to different conformers. In the first set of approaches, depicted as **S**<sub>1</sub> or **A**<sub>1</sub> and **S**<sub>2</sub> or **A**<sub>2</sub>, the orientation of the ring carbonyl (or thiocarbonyl) is *anti* with respect to the enolate oxygen, while in the additional set, the corresponding orientation is *syn*. The modes of approach leading to products **S**<sub>1</sub> and **A**<sub>1</sub> involve the attack of the enolate through its unhindered face on benzaldehyde, **a**-**S**<sub>1</sub> and **a**-**A**<sub>1</sub> as shown in Scheme 3-I. The corresponding representations are *s*-**S**<sub>1</sub> and *s*-**A**<sub>1</sub> for the additional possibility (Scheme 3-II).

All key nonchelated TSs for the C–C bond formation are first located. The carbonyl groups of the enolate as well as benzaldehyde are found to maintain coordination with the

titanium center in the optimized geometries. The relative energies of these TSs with respect to the lowest energy TS are given in Table 1. In the nonchelated TS model, attack by the less hindered *re* face of enolate on the *si* face of benzaldehyde is found to be energetically the most favored approach. In this mode of addition, the ring carbonyl orientation is *anti* to the enolate oxygen. The geometry of **TS-a-S**<sub>1</sub>, as provided in Figure 1, reveals that the methyl group and the developing alkoxide oxygen (which would eventually be the new –OH group) are on the same side, evidently suggesting the formation of Evans *syn* aldol product. Interestingly, the computed relative energies of the TSs for chiral auxiliaries **1a–c** indicate a preference toward Evans *syn* aldol product. It is of additional significance at this juncture to note that the computed relative energies of TSs obtained at different levels of theory are in very good mutual agreement (Table 1). With larger differences in the energies of the competing diastereomeric TSs, higher levels of stereoselectivity can be expected with these chiral auxiliaries.

The optimized geometries of the diastereomeric TSs for the C–C bond formation reaction are provided in Figure 1.<sup>35</sup> The stereoelectronic features of these TSs are carefully examined to establish the factors that could influence the stereochemical outcome of the reaction. Some of the pertinent details are summarized here. The incipient C–C bond lengths (reaction coordinate) in **TS-a-S**<sub>1</sub> (2.33 Å) indicate a tighter TS as compared to **TS-a-A**<sub>2</sub> (2.42 Å). The geometric features of *syn* TSs, namely, **TS-a-S**<sub>1</sub> and **TS-a-S**<sub>2</sub>, indicate a chair-like geometry, whereas *anti* TSs, **TS-a-A**<sub>1</sub> and **TS-a-A**<sub>2</sub>, present a boat-like conformer. The substituents around the developing C–C bond in the higher energy boat-like TSs, such as in **TS-a-A**<sub>1</sub> and **TS-a-A**<sub>2</sub>, tend to remain eclipsed ( $d_2 = -13^\circ$  and  $12^\circ$ ) as compared to the lower energy chair-like **TS-a-S**<sub>1</sub> and **TS-a-S**<sub>2</sub>, wherein the substituents maintain a staggered orientation ( $d_2 = -66^\circ$  and  $69^\circ$ , Figure 1-I). Similar torsional preferences of the substituents around the developing bond are

(35) The optimized TS geometries for chiral auxiliaries oxazolidinethione and thiazolidinethione are provided in Figure S4 in the Supporting Information.

**Table 1.** Computed Relative Energies<sup>a</sup> (in kcal/mol) of Important Transition States in the Nonchelated Pathway Obtained at Various Levels of Theory<sup>b</sup> for the Addition of Titanium Enolate to Benzaldehyde

transition state	mode of approach	relative energies						
		L1	L2	L3	L4	L5	L6	L7
Oxazolidinone ( <b>1a</b> )								
<b>TS-a-S<sub>1</sub></b>	<i>re</i> → <i>si</i>	<b>0.0</b> (0.0)	<b>0.0</b> (0.0)	<b>0.0</b> (0.0)	<b>0.0</b> (0.0)	<b>0.0</b> (0.0)	<b>0.0</b> (0.0)	<b>0.0</b> (0.0)
<b>TS-a-A<sub>1</sub></b>	<i>re</i> → <i>re</i>	3.2 (3.2)	5.1 (10.3)	5.6 (6.6)	3.4 (3.6)	5.8 (6.6)	3.9 (3.9)	5.8 (7.0)
<b>TS-a-S<sub>2</sub></b>	<i>si</i> → <i>re</i>	4.6 (5.2)	5.6 (11.9)	6.5 (7.6)	4.7 (5.1)	6.8 (7.6)	4.9 (6.1)	6.0 (7.2)
<b>TS-a-A<sub>2</sub></b>	<i>si</i> → <i>si</i>	6.0 (7.9)	7.9 (9.7)	8.0 (9.8)	6.2 (5.9)	8.6 (10.4)	5.9 (8.4)	7.0 (8.9)
<b>TS-s-S<sub>1</sub></b>	<i>re</i> → <i>si</i>	9.5 (16.9)	8.9 (15.4)	13.2 (20.9)	10.3 (17.5)	10.8 (18.6)	11.6 (17.0)	9.3 (17.3)
<b>TS-s-A<sub>1</sub></b>	<i>re</i> → <i>re</i>	12.4 (19.8)	12.1 (18.5)	10.0 (18.0)	12.8 (20.3)	10.8 (22.3)	14.2 (19.6)	12.7 (20.3)
<b>TS-s-S<sub>2</sub></b>	<i>si</i> → <i>re</i>	8.5 (14.6)	13.9 (21.6)	8.5 (15.4)	11.6 (17.9)	8.6 (15.8)	9.7 (15.0)	7.8 (15.0)
<b>TS-s-A<sub>2</sub></b>	<i>si</i> → <i>si</i>	11.1 (17.2)	10.5 (18.3)	11.6 (18.2)	9.2 (15.2)	12.2 (18.6)	12.7 (17.6)	11.3 (17.7)
Oxazolidinethione ( <b>1b</b> )								
<b>TS-a-S<sub>1</sub></b>	<i>re</i> → <i>si</i>	<b>0.0</b> (0.0)	<b>0.0</b> (0.0)	<b>0.0</b> (0.0)	<b>0.0</b> (0.0)	<b>0.0</b> (0.0)	<b>0.0</b> (0.0)	<b>0.0</b> (0.0)
<b>TS-a-A<sub>1</sub></b>	<i>re</i> → <i>re</i>	4.0 (3.8)	5.8 (6.8)	5.0 (9.3)	4.2 (4.1)	5.9 (7.0)	4.1 (3.5)	6.9 (7.8)
<b>TS-a-S<sub>2</sub></b>	<i>si</i> → <i>re</i>	4.2 (4.8)	5.3 (6.5)	4.6 (5.7)	4.3 (4.8)	6.6 (7.5)	4.7 (5.2)	5.4 (6.7)
<b>TS-a-A<sub>2</sub></b>	<i>si</i> → <i>si</i>	5.7 (7.3)	7.6 (9.4)	5.7 (7.4)	6.0 (7.4)	8.3 (9.7)	6.0 (7.2)	6.6 (8.4)
<b>TS-s-S<sub>1</sub></b>	<i>re</i> → <i>si</i>	11.1 (17.6)	12.6 (15.9)	10.9 (17.5)	11.8 (18.3)	12.7 (20.6)	12.6 (17.8)	11.2 (18.7)
<b>TS-s-S<sub>2</sub></b>	<i>si</i> → <i>re</i>	8.8 (14.2)	9.6 (19.9)	8.2 (14.0)	9.6 (14.7)	8.5 (16.1)	9.9 (14.0)	8.3 (14.9)
Thiazolidinethione ( <b>1c</b> )								
<b>TS-a-S<sub>1</sub></b>	<i>re</i> → <i>si</i>	<b>0.0</b> (0.0)	<b>0.0</b> (0.0)	<b>0.0</b> (0.0)	<b>0.0</b> (0.0)	<b>0.0</b> (0.0)	<b>0.0</b> (0.0)	<b>0.0</b> (0.0)
<b>TS-a-A<sub>1</sub></b>	<i>re</i> → <i>re</i>	4.1 (4.0)	6.1 (7.2)	5.4 (4.9)	4.2 (5.5)	5.8 (7.4)	5.2 (6.8)	7.1 (7.8)
<b>TS-a-S<sub>2</sub></b>	<i>si</i> → <i>re</i>	2.0 (3.9)	4.8 (6.5)	4.0 (4.7)	3.3 (5.0)	6.1 (7.8)	3.9 (4.6)	4.6 (6.0)
<b>TS-a-A<sub>2</sub></b>	<i>si</i> → <i>si</i>	5.1 (6.4)	7.3 (9.4)	6.3 (7.3)	5.2 (6.6)	7.9 (10.1)	4.2 (4.0)	6.3 (7.8)
<b>TS-s-S<sub>2</sub></b>	<i>si</i> → <i>re</i>	— <sup>c</sup> (15.5)	8.6 (16.2)	8.1 (14.8)	— <sup>c</sup> (14.8)	7.6 (12.7)	8.5 (12.7)	7.2 (13.5)

<sup>a</sup> L1 = PCM<sub>(DCM)</sub>/B3LYP/6-311+G\*\*//B3LYP/6-31G\*; L2 = PCM<sub>(DCM)</sub>/mPW1K/6-311+G\*\*//mPW1K/6-31G\*; L3 = PCM<sub>(DCM)</sub>/mPW1PW91/6-311+G\*\*//mPW1PW91/6-31G\*; L4 = PCM<sub>(DCM)</sub>/B3LYP/LANL2DZ (Ti), 6-311+G\*\*//B3LYP/LANL2DZ(Ti),6-31G\* for all other atoms; L5 = PCM<sub>(DCM)</sub>/M05-2X/6-311+G\*\*//M05-2X/6-31G\*; L6 = PCM<sub>(DCM)</sub>/B98/6-311+G\*\*//B98/6-31G\*; L7 = COSMO<sub>(DCM)</sub>/B3LYP-D/6-311+G\*\*//B3LYP/6-31G\*. <sup>b</sup> Gas-phase relative energies at the respective levels of theory are given in parentheses. <sup>c</sup> The TS at the levels of theory of L1 and L4 could not be located after repeated attempts.

found to influence the stereoselectivity in a variety of reactions.<sup>36</sup> The dihedral angles describing the orientation of (i) the oxazolidinone ring with respect to the enolate double bond (d1) and (ii) the substituents around the developing C–C bond (d2) are provided in Figure 1. In the lower energy TSs (**TS-a-S<sub>1</sub>** and **TS-a-A<sub>1</sub>**), the oxazolidinone ring tends to remain in-plane with the enolate moiety (d1 = −162° and −179°), whereas out-of-plane arrangement is noticed for the higher energy TSs (**TS-a-S<sub>2</sub>** and **TS-a-A<sub>2</sub>**, d1 = −136° and −139°). In both *anti* TSs (**A<sub>1</sub>** and **A<sub>2</sub>**), the phenyl group of benzaldehyde and the oxazolidinone ring of the enolate are found to remain in a 1,3-*cis* disposition. The 1,3-destabilizing interaction in this situation is minimized in the boat conformer.<sup>37</sup> However, these groups are farther apart in the TSs responsible for *syn* aldol products.

(36) (a) Behnam, S. M.; Behnam, S. E.; Ando, K.; Green, N. S.; Houk, K. N. *J. Org. Chem.* **2000**, *65*, 8970. (b) Janardanan, D.; Sunoj, R. B. *Chem.–Eur. J.* **2007**, *13*, 4805. (c) Janardanan, D.; Sunoj, R. B. *J. Org. Chem.* **2008**, *73*, 8163.

The unfavorable interaction between the isopropyl group on the oxazolidinone and the approaching phenyl ring of benzaldehyde appears to be quite high in **TS-a-A<sub>2</sub>**. In **TS-a-S<sub>1</sub>** and **TS-a-S<sub>2</sub>**, the methyl group of the titanium enolate is found to be at a favorable distance from the phenyl ring to enable weak CH···π interactions.<sup>38</sup> Interestingly, all TSs leading to *anti* aldol products lack CH···π interactions owing to the relative orientations of the phenyl and the methyl groups (Figure 1). Another weak interaction between the axial chloride ligands of titanium and the methylene hydrogens of the oxazolidinone ring is also

(37) In fact, the initial guess geometry with a chair-like conformation has been identified to converge into a boat-like arrangement during the geometry optimization of the transition states.

(38) (a) The shortest contact distances of CH···π interactions are identified as 2.79 and 2.74 Å respectively in **TS-S<sub>1</sub>** and **TS-S<sub>2</sub>**. (b) These distances fit well within the range of CH···π contacts usually reported in literature. (c) Takahashi, O.; Kohno, Y.; Saito, K.; Nishio, M. *Chem.–Eur. J.* **2003**, *9*, 756. (d) Suezawa, H.; Ishihara, S.; Umezawa, Y.; Tsuboyama, S.; Nishio, M. *Eur. J. Org. Chem.* **2004**, 4816.

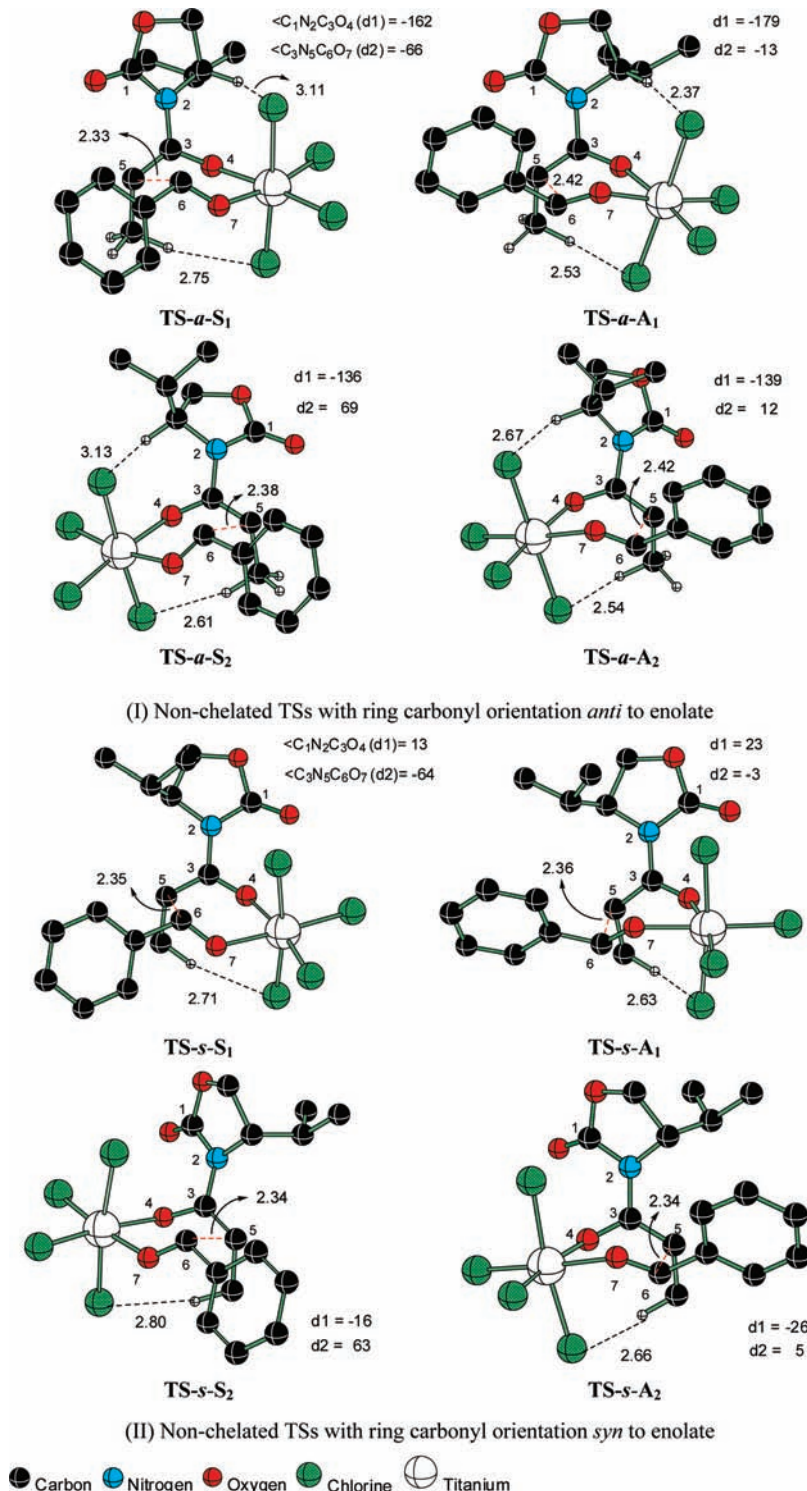


**Figure 1.** B3LYP/6-31G\* optimized geometries of lower energy diastereomeric transition states in the nonchelated pathway for the addition of titanium enolate to benzaldehyde with oxazolidinone (**1a**) as the chiral auxiliary. Only selected hydrogens are shown for clarity. The distances are in Å.

noticed. The CH···Cl distances are found to be in the range of 2.53–2.75 Å. A number of weak interactions between aldehydic or enolate hydrogens and the chloride ligands or the ring carbonyl are also identified. A pictorial representation of all these weak interactions and the calculated electron densities at the corresponding bond critical points are provided in the Supporting Information.<sup>39</sup> The calculated dipole moments of the TSs are also found to exhibit good correlation with the observed selectivity, wherein the lowest energy TS is identified to have

the lowest dipole moment.<sup>40</sup> The cumulative effect of the above-mentioned weak interactions will contribute to the vital energy difference between the diastereomeric TSs required for imparting high levels of stereoselectivity. Moreover, we have carried out distortion–interaction analysis of the key TSs to gain improved insight into the origin of stereoselectivity (*vide infra*).

The energies of TSs wherein the ring carbonyl orientation is *syn* to the enolate carbonyl (as in Scheme 3-I) are found to be much higher than when the ring carbonyl is *anti* to the enolate

carbonyl. The repulsion between the thiocarbonyl and the enolate carbonyl is expected to become stronger in the case of thiocarbonyl (**1b** and **1c**).<sup>41</sup> Other interactions that help stabilize the TSs are found to be either absent or weak in this model.<sup>42</sup> The oxazolidinone ring in **TS-s-S<sub>1</sub>** and **TS-s-S<sub>2</sub>** is found to remain relatively more coplanar with the enolate. The substituents around the developing C–C bond are in a staggered arrangement (Figure 1-II). The stronger dipolar interaction between the ring and enolate carbonyls in the *syn* arrangement could as well destabilize these TSs. The calculated dipole moments for these TSs are found to be larger.<sup>43</sup> For instance, the dipole moment of **TS-a-S<sub>1</sub>** is only 9.8 D, while the corresponding value is 17.6 D for **TS-s-S<sub>1</sub>**. From these trends it is evident that the TSs prefer a dipole-minimized orientation of the chiral auxiliary. Hence, in oxazolidinone-mediated aldol reactions, the dipole effects likely exert a dominant control on the  $\pi$ -facial selectivity in carbonyl addition reactions.<sup>44</sup>

The analyses of the stereoselectivity-determining TSs, as presented in the above sections, convey that the nonchelated TS model can readily explain the formation of Evans *syn* aldol product through **TS-a-S<sub>1</sub>**.<sup>1a,10</sup> It is of further significance that the predicted trends at the different levels of theory employed in the present study (L1–L7) are in good agreement with the experimental selectivities, besides being mutually consistent. Moreover, the trends remained the same as in Table 1 when the critical TSs were reoptimized by using a 6-311G\*\* basis set.<sup>45</sup>

Until now, the discussions have focused on the importance of nonchelated TSs toward rationalizing the stereochemical outcome, such as the formation of Evans *syn* aldol product. It is of high significance to consider that the product stereochemistry can be quite different if the reaction conditions are altered. Among the key modifications to the reaction conditions, changes in the nature and amount of Lewis bases appear more common.<sup>10</sup> More importantly, interesting changes in stereoselectivity have been reported for Evans oxazolidinone-mediated aldol reactions.<sup>6,9a,10a,c,12</sup> In one such fine example, Crimmins and co-workers illustrated a stereodivergent *syn* aldol reaction by changing the number of equivalents of base. The use of 1 and 2 equiv of base respectively led to the formation of non-Evans *syn* and Evans *syn* aldol products while the rest of the reaction conditions were kept the same. In several of these situations, the involvement

of a chelated TS is invoked, although verifications of such models remain largely unavailable in the literature.

The chelation of a chiral auxiliary through carbonyl/thiocarbonyl groups with titanium is possible when a vacant coordination site is created by the removal of one of the chloride ligands. Different scenarios can be envisaged in this context. The base-promoted enolization of TiCl<sub>4</sub>-bound propionyl oxazolidinone can first lead to an anionic intermediate (**I**), as shown in Scheme 1. The protonated base thus produced can subsequently assist in the removal of the chloride ion. The open coordination site can then be occupied by the carbonyl group, leading to a neutral chelated TiCl<sub>3</sub>-bound enolate. In the absence of such coordinating groups, the formation of anionic titanium enolate is reported to be favored over that of neutral titanium enolate.<sup>46</sup> When 2 equiv of base is used, it is quite likely that the base can compete for the vacant coordination site, thereby reducing the chances of chelation with the ring carbonyl (or thiocarbonyl) group. In an effort to establish the significance of chelated TS models and the accompanying changes in the stereochemical outcome, we have investigated the reaction between *N*-propionyloxazolidinone and benzaldehyde. Unlike in the nonchelated TS model, the number of rotameric possibilities in the chelated TSs is far too limited due to the presence of additional chelation. The key possibilities for the addition of enolate to benzaldehyde, along with the corresponding stereochemical descriptions, are presented in Scheme 4.

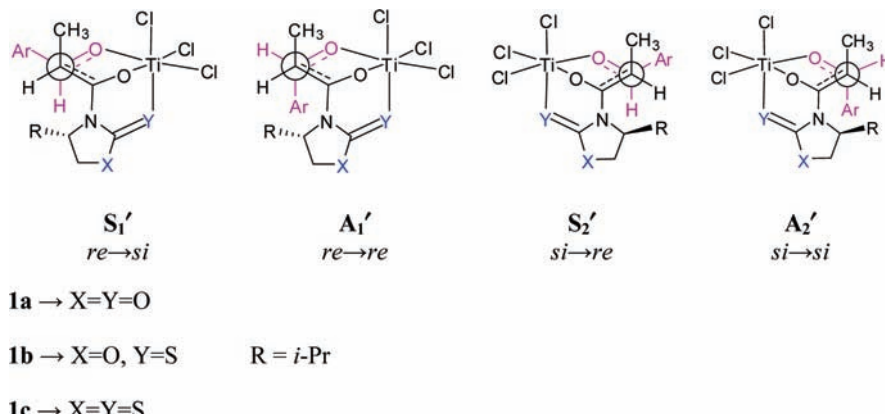
The major difference between the chelated and nonchelated models relates to the orientation of the *N*-propionyloxazolidinone ring in the TS. The chiral auxiliary is rotated by about 180° as a result of the chelation. More significantly, the chelation leads to an interchange of the hindered and unhindered prochiral faces of the enolate with respect to the approaching electrophile.<sup>47</sup> The key TSs for the stereoselectivity-controlling C–C bond formation step for **1a–c** have been identified. The barrier for rotation about the N–C bond for the conversion of nonchelated to chelated enolate is found to be only about 2–3 kcal/mol for the chiral auxiliaries examined in this study.<sup>48</sup> Hence, under the standard reaction conditions, rotation about the N–C bond can result in reversal of the prochiral face offered by the oxazolidinone-tethered enolate. However, in the case of thiocarbonyl coordination, as in **1b** and **1c**, more effective chelation and additional stabilization of the enolate complex is likely.<sup>49</sup>

The computed relative energies of important diastereomeric TSs in the chelated pathway are provided in Table 2. It can be readily noticed that the lowest energy TS is **TS-S<sub>2</sub>'**, which is responsible for the formation of non-Evans *syn* aldol product **S<sub>2</sub>**. This is found to be true for all three chiral auxiliaries. More interestingly, the predicted stereochemical outcome is in full accord with the experimental observations.<sup>10</sup> The energy difference between the lower energy diastereomeric TSs (**TS-S<sub>2</sub>'** and **TS-A<sub>2</sub>'**) is found to vary, depending on the nature of the heteroatom present in the chiral auxiliary, alluding to a possible

- (39) (a) See Figure S3 and Table S2 in the Supporting Information. (b) The topological analysis of electron densities are carried out by using Bader's Atom-in-Molecule formalism and was carried out by using AIM2000 software. (c) Bader, R. F. W. *Atoms in Molecules: A Quantum Theory*; Clarendon Press: Oxford, 1990. (d) AIM2000, Version 2.0; The Buro fur Innovative Software, SBK-Software: Bielefeld, Germany, 2000.
- (40) Calculated dipole moments for all the TSs are tabulated in Table S3 of the Supporting Information. A representative set of TSs is also provided to depict the direction of the dipole in Figure S5.
- (41) In fact, this is reflected in our attempts to optimize some of the TSs in this category. Even after repeated attempts we were able to optimize only the TSs leading to *syn* products (**S<sub>1</sub>** and **S<sub>2</sub>** for oxazolidinethione, and **S<sub>2</sub>** for thiazolidinethione). All other initial guess geometries reverted back, during the course of geometry optimization, to an *anti* orientation, where the ring thiocarbonyl remains *anti* to the enolate oxygen.
- (42) The TSs lack stabilizing weak interactions between the ring carbonyl of enolate and the substrate hydrogens; see Figure S3 in the Supporting Information.
- (43) The dipole moment values are tabulated in Table S7 in the Supporting Information.
- (44) Wipf, P.; Jung, J.-K. *Chem. Rev.* **1999**, *99*, 1469.
- (45) The relative energies with respect to the lowest energy TS obtained by using the triple- $\zeta$  basis set are provided in Table S4 in the Supporting Information.

- (46) Marrone, A.; Renzetti, A.; Maria, P. D.; Gérard, S.; Sapi, J.; Fontana, A.; Re, N. *Chem.—Eur. J.* **2009**, *15*, 11537.
- (47) Although nonchelated TS models generated by the rotation of oxazolidinone ring can result in interchange between the hindered and unhindered faces of the enolate, as shown in Figure 1-II, these are found to be much higher in energy.
- (48) The geometry of TSs and barriers for ring carbonyl/thiocarbonyl coordination are given in Figure S6 of the Supporting Information.
- (49) (a) See Figure S7 in the Supporting Information for plausible reaction pathways for the formation of anionic neutral titanium enolate. (b) Gibbs free energies of formation of chelated enolates are provided in Table S5 in the Supporting Information.

**Scheme 4.** Important Modes of Addition of Titanium Enolate to Benzaldehyde in the Chelated Pathway: View along the Incipient C–C Bond (Reaction Coordinate)<sup>a</sup>



<sup>a</sup> The stereochemical description conveys the mode of addition of the enolate on aldehyde.

**Table 2.** Computed Relative Energies<sup>a</sup> (kcal/mol) of Important Transition States in the Chelated Pathway Obtained at Various Levels of Theory<sup>b</sup> for the Addition of Titanium Enolate to Benzaldehyde

transition state	mode of approach	relative energy						
		L1	L2	L3	L4	L5	L6	
Oxazolidinone ( <b>1a</b> )								
<b>TS-S<sub>1'</sub></b>	<i>re</i> → <i>si</i>	2.7 (3.4)	3.3 (3.8)	2.8 (2.9)	2.7 (3.5)	2.5 (4.2)	2.6 (2.9)	1.0 (1.6)
<b>TS-A<sub>1'</sub></b>	<i>re</i> → <i>re</i>	3.9 (4.9)	4.0 (3.4)	3.7 (3.6)	3.8 (4.1)	2.6 (3.5)	3.5 (3.6)	1.7 (1.6)
<b>TS-S<sub>2'</sub></b>	<i>si</i> → <i>re</i>	0.0 (0.0)	0.0 (0.6)	2.0 (0.9)	0.0 (0.8)	0.0 (1.4)	0.0 (0.4)	0.5 (0.0)
<b>TS-A<sub>2'</sub></b>	<i>si</i> → <i>si</i>	2.2 (1.8)	2.1 (0.0)	0.0 (0.0)	2.0 (0.0)	0.8 (0.0)	2.0 (0.0)	0.0 (0.8)
Oxazolidinethione ( <b>1b</b> )								
<b>TS-S<sub>1'</sub></b>	<i>re</i> → <i>si</i>	2.2 (2.8)	3.1 (7.8)	3.1 (2.7)	2.9 (2.6)	1.3 (3.1)	3.0 (2.9)	0.9 (2.3)
<b>TS-A<sub>1'</sub></b>	<i>re</i> → <i>re</i>	2.9 (3.1)	3.8 (8.3)	3.8 (3.5)	3.5 (3.0)	1.8 (2.5)	3.4 (3.2)	1.2 (1.3)
<b>TS-S<sub>2'</sub></b>	<i>si</i> → <i>re</i>	0.0 (0.3)	0.0 (0.0)	0.0 (0.1)	0.0 (0.03)	0.3 (0.8)	0.0 (0.3)	0.2 (1.2)
<b>TS-A<sub>2'</sub></b>	<i>si</i> → <i>si</i>	1.2 (0.0)	2.2 (4.8)	2.2 (0.0)	1.8 (0.0)	0.0 (0.0)	1.9 (0.0)	0.0 (0.0)
Thiazolidinethione ( <b>1c</b> )								
<b>TS-S<sub>1'</sub></b>	<i>re</i> → <i>si</i>	3.4 (2.8)	3.7 (2.6)	6.5 (6.1)	3.4 (2.6)	4.3 (1.8)	1.0 (1.9)	2.3 (2.7)
<b>TS-A<sub>1'</sub></b>	<i>re</i> → <i>re</i>	3.7 (3.3)	3.9 (2.8)	3.9 (3.5)	3.6 (3.2)	2.3 (2.7)	3.4 (3.1)	1.2 (0.4)
<b>TS-S<sub>2'</sub></b>	<i>si</i> → <i>re</i>	0.0 (0.0)	0.0 (0.0)	0.0 (0.0)	0.0 (0.0)	0.0 (0.0)	0.0 (0.0)	0.0 (0.0)
<b>TS-A<sub>2'</sub></b>	<i>si</i> → <i>si</i>	2.4 (1.0)	2.8 (0.2)	2.7 (0.9)	2.3 (1.1)	1.7 (0.4)	2.3 (1.1)	0.9 (0.1)

<sup>a</sup> L1 = PCM<sub>(DCM)</sub>/B3LYP/6-311+G\*\*//B3LYP/6-31G\*; L2 = PCM<sub>(DCM)</sub>/mPW1K/6-311+G\*\*//mPW1K/6-31G\*; L3 = PCM<sub>(DCM)</sub>/mPW1PW91/6-311+G\*\*//mPW1PW91/6-31G\*; L4 = PCM<sub>(DCM)</sub>/B3LYP/LANL2DZ (Ti), 6-311+G\*\*//B3LYP/LANL2DZ (Ti), 6-31G\* for all other atoms; L5 = PCM<sub>(DCM)</sub>/M05-2X/6-311+G\*\*//M05-2X/6-31G\*; L6 = PCM<sub>(DCM)</sub>B98/6-311+G\*\*//B98/6-31G\*; L7 = COSMO<sub>(DCM)</sub>/B3LYP-D/6-311+G\*\*//B3LYP/6-31G\*. <sup>b</sup> Gas-phase relative energies at respective levels of theory are given in parentheses.

change in the stereochemical outcome by varying the chelation around the titanium center. Subtle changes in the chelation ability of the heteroatom or the use of other substrates bearing functional groups capable of chelation with the titanium might bring about interesting changes in the stereoselectivity.<sup>50</sup> Insights of this kind could perhaps be made use of in rational modification of chiral auxiliaries.

The optimized geometries of a representative set of diastereomeric TSs in the case of thiazolidinethione are provided in

Figure 2.<sup>51</sup> The octahedral coordination topology around the titanium in the chelated TSs is found to be more distorted as compared to that in the nonchelated TSs.<sup>52</sup> It can be noticed that axial ligands such as thiocarbonyl and chloride remain nonlinear and result in a distorted octahedral geometry. The TSs

(51) The optimized geometries of the diastereomeric chelated transition states for **1a** and **1b** are given in Figure S8 in the Supporting Information.

(52) Similar observations are reported earlier with titanium complexes possessing bidentate ligands. See: (a) Reetz, M. T. *Acc. Chem. Res.* **1993**, *26*, 462. (b) Jonas, V.; Frenking, G. *Organometallics* **1993**, *12*, 2111. (c) Jonas, V.; Frenking, G.; Reetz, M. T. *Organometallics* **1995**, *14*, 5316.

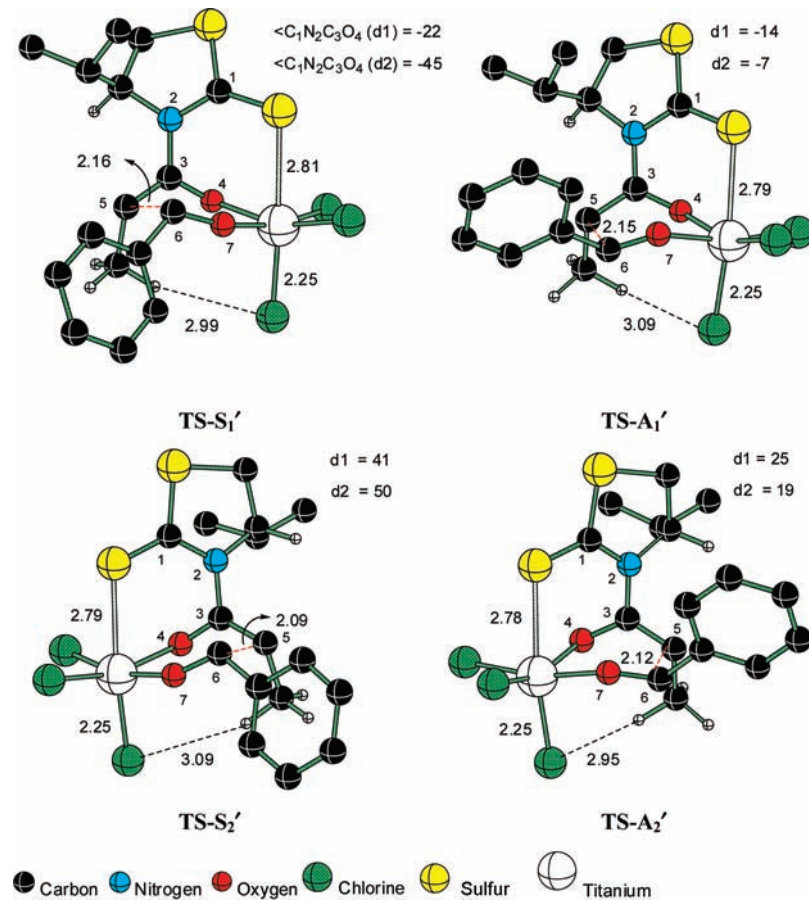


**Figure 2.** B3LYP/6-31G\* optimized geometries of lower energy diastereomeric transition states in the chelated pathway for the addition of titanium enolate to benzaldehyde with thiazolidinethione (**1c**) as the chiral auxiliary. Only selected hydrogens are shown for clarity. The distances are in Å.

leading to Evans (**TS-S<sub>1</sub>'**) and non-Evans *syn* aldol (**TS-S<sub>2</sub>'**) products exhibit a chair-like geometry, similar to that noticed earlier in the nonchelated pathway. The phenyl group of benzaldehyde in both **TS-S<sub>1</sub>'** and **TS-S<sub>2</sub>'** is farther from the chiral auxiliary. In addition to such geometric features that help minimize steric interactions, the phenyl group tends to remain at a favorable distance ( $\sim 2.75$  Å) to develop C–H $\cdots\pi$  interaction with the methyl group of the enolate. In the boat-like TSs, such as in **TS-A<sub>1</sub>'** and **TS-A<sub>2</sub>'**, which are responsible for *anti* aldol products, C–H $\cdots\pi$  stabilizing interactions are absent owing to the orientation of the phenyl group.<sup>31,53</sup> The analysis of various factors that influence the relative energies indicates subtle and interesting variations between these TSs. Among the four lower energy TSs, **TS-A<sub>1</sub>'** leading to Evans *anti* aldol is found to be the highest energy TS. The steric interaction between the phenyl group and the isopropyl group of the chiral auxiliary appears to be the major contributor in this case. The facial selectivity is largely influenced by the substituent on the chiral auxiliary ring. In fact, there have been reports on the use of different substituents at the fourth position of the chiral auxiliary ring.<sup>11</sup> The relative energies computed by using the optimized geometries with a more flexible triple- $\zeta$ -quality basis set are also found to be in good agreement with the results presented here.<sup>54</sup>

(53) Zhao, Y.; Truhlar, D. G. *J. Phys. Chem. A* **2005**, *109*, 5656.

(54) The relative energies computed using geometries optimized with the 6-311G\*\* basis set at the levels of theory L1–L6 are provided in Table S6 in the Supporting Information.

A detailed comparison of the geometric features between chelated and nonchelated TSs is presented in Table 3. The Ti $\cdots$ O=C<sub>enolate</sub> bond length in TSs is generally elongated as compared to that in the corresponding PRCs in both nonchelated and chelated pathways.<sup>55</sup> The efficiency of donation of an enolate oxygen lone pair to the empty d-orbitals of titanium is found to get weaker upon coordination with benzaldehyde. As the C–C bond formation completes, the bond between the oxygen of benzaldehyde and titanium becomes progressively shorter. In accordance with the expectations, further elongation of the Ti $\cdots$ O=C<sub>enolate</sub> distance toward the product side can be noticed as well. In the chelated TSs, stronger Ti $\cdots$ Y=C donor–acceptor interaction is found to weaken the Ti $\cdots$ O=C<sub>enolate</sub> interaction. For instance, in the case of **1a** leading to product **S<sub>2</sub>**, the Ti $\cdots$ O=C<sub>enolate</sub> distance increases from 1.86 Å in the PRC to 2.29 Å in the resulting intermediate toward the product side. In the chelated TSs, an interesting difference between the coordination of carbonyl and thiocarbonyl is noticed. Upon going from TS to product, the enolate coordination breaks in the case of **1a**, whereas it remains intact in **1b** and **1c**. In the latter cases, however, the coordination of the ring thiocarbonyl is found to be absent.

(55) The pre-reacting complexes (PRCs) and succeeding intermediates (Int) are identified using the intrinsic reaction coordinate (IRC) calculations starting from the respective TSs. The last point, as obtained through the IRC runs, has been subjected to further geometry optimization using the ‘opt = calcfc’ option available in the program. The stationary points thus obtained are characterized as true minima by using additional frequency calculations.

**Table 3.** Comparison of Key Structural Parameters for Chelated and Nonchelated Transition States, Pre-reacting Complexes, and Succeeding Intermediates Obtained at the B3LYP/6-31G\* Level of Theory (Distances in Å)

transition state	chiral auxiliary		bond lengths with titanium				
			nonchelated TSs		chelated TSs		
			...O=C <sub>enolate</sub>	...O=C <sub>PhCHO</sub>	...O=C <sub>enolate</sub>	...O=C <sub>PhCHO</sub>	...Y=C <sup>a</sup>
TS-S <sub>1</sub>	1a	PRC	1.86	2.26	1.85	2.31	2.15
		TS	2.03	2.04	2.06	1.94	2.31
		Int	2.40	1.81	4.68	1.76	2.28
	1b	PRC	1.86	2.26	1.85	2.26	2.64
		TS	2.05	2.01	2.03	1.94	2.84
		Int	2.41	1.81	2.25	1.78	4.89
TS-A <sub>1</sub>	1a	PRC	1.85	2.27	1.85	2.26	2.65
		TS	2.07	2.00	2.02	1.94	2.81
		Int	2.43	1.81	2.24	1.78	4.81
	1b	PRC	1.84	2.27	1.86	2.28	2.30
		TS	2.03	2.03	2.07	1.97	2.31
		Int	4.38	1.77	3.67	1.77	2.27
TS-S <sub>2</sub>	1a	PRC	1.84	2.26	1.85	2.26	2.64
		TS	2.05	2.01	2.03	1.97	2.82
		Int	4.28	1.77	2.25	1.77	4.88
	1b	PRC	1.86	2.26	1.85	2.26	2.65
		TS	2.07	1.99	2.03	1.97	2.80
		Int	4.34	1.77	2.25	1.77	4.88
TS-A <sub>2</sub>	1a	PRC	1.86	2.26	1.85	2.24	2.17
		TS	1.99	2.06	2.08	1.93	2.29
		Int	2.29	1.82	5.38	1.75	2.26
	1b	PRC	1.81	2.31	1.83	2.28	2.61
		TS	2.02	2.04	2.06	1.93	2.81
		Int	2.31	1.82	2.34	1.81	3.06
TS-S <sub>2</sub>	1c	PRC	1.82	2.31	1.84	2.27	2.65
		TS	2.04	2.04	2.06	1.94	2.79
		Int	2.31	1.82	2.45	1.80	2.97
	1b	PRC	1.82	2.39	1.84	2.27	2.65
		TS	2.05	2.03	2.04	1.95	2.81
		Int	4.31	1.78	2.26	1.78	4.99
TS-A <sub>2</sub>	1c	PRC	1.82	2.39	1.84	2.26	2.65
		TS	2.07	2.03	2.04	1.95	2.78
		Int	2.27	1.80	2.26	1.77	4.98

<sup>a</sup> Y = O for 1a; Y = S for 1b and 1c.

The comparison between the TSs for **1a** and **1c** provides certain interesting details. It is noticed that the chelation in **1c** is more favored because of the longer C=S bond (1.67 Å) as compared to the ring carbonyl (with a C=O bond distance of 1.20 Å) as in **1a**. Such chelation helps to reduce the crowding around the titanium in **1c**. Further, the inherently higher affinity of sulfur for titanium as compared to oxygen favors the chelated pathway in **1c** more than in **1a**.<sup>56</sup> Enhanced preference of titanium toward sulfur over that of a second oxygen ligand (when one of the coordination sites is preoccupied by oxygen) is borne out by NMR experiments on titanium complexes.<sup>57</sup> The ring sulfur, such as in **1c**, may also influence the donor–acceptor interaction between titanium and the exocyclic thiocarbonyl/carbonyl group through electronic interaction. This is evident from the longer distance between titanium and thiocarbonyl sulfur in **1b** than in **1c**. All the above-mentioned stabilizing/destabilizing interactions and the accompanying subtle changes in the TS geometries can safely be regarded as

(56) In an earlier report Fowles *et al.* reported the preferential coordination of thioxane with titanium through sulfur rather than oxygen: Fowles, G. W. A.; Rice, D. A.; Wilkins, J. D. *J. Chem. Soc. A* **1971**, 1920.

(57) McAlees, A. J.; McCrindle, R.; Woon-Fat, A. R. *Inorg. Chem.* **1976**, 15, 1065.

the factors responsible for the variations in the stereochemical outcome with respect to the changes in the nature of chiral auxiliaries.

**Distortion and Interaction Analysis.** More detailed insights into the trends in the relative energy order between the key TSs are sought by employing the *activation strain* model. The analysis of activation barriers by using this approach could help us understand the origins of stereoselectivity<sup>58</sup> in a more meaningful manner. In this model, the activation energy ( $\Delta E^\ddagger$ ) is decomposed into two key terms, distortion and interaction energies. The distortion energy of the reactants ( $\Delta E_d^\ddagger$ ) is computed as the energy difference between the native unstrained reactant and the corresponding distorted reactant geometries as in the respective TS. The interaction energy ( $\Delta E_i^\ddagger$ ) is calculated as the binding interaction between these distorted reactants at

(58) Through systematic use of the distortion–interaction model, a deeper understanding of chemical reactions can be achieved in terms of the stereoelectronic changes with the reactants. See: (a) Poirier, R. A.; Pye, C. C.; Xidos, J. D.; Burnell, D. J. *J. Org. Chem.* **1995**, 60, 2328. (b) Legault, C. Y.; Garcia, Y.; Merlic, C. A.; Houk, K. N. *J. Am. Chem. Soc.* **2007**, 129, 12664. (c) Ess, D. H.; Houk, K. N. *J. Am. Chem. Soc.* **2008**, 130, 10187. (d) Lam, Y.-h.; Cheong, P. H.-Y.; Blasco Mata, J. M.; Stanway, S. J.; Gouverneur, V.; Houk, K. N. *J. Am. Chem. Soc.* **2009**, 131, 1947.

**Table 4.** Computed Distortion ( $\Delta E^{\ddagger}_d$ )<sup>a</sup> and Interaction ( $\Delta E^{\ddagger}_i$ ) Energies<sup>b</sup> (kcal/mol) for the Nonchelated Transition States Obtained at the PCM<sub>(DCM)</sub>/B3LYP/6-311+G\*\*//B3LYP/6-31G\* Level of Theory

transition state	$\Delta E^{\ddagger}_d$	$\Delta E^{\ddagger}_d(N)$	$\Delta E^{\ddagger}_d(E)$	$\Delta E^{\ddagger}_i$	$\Delta E^{\ddagger c}$
Oxazolidinone ( <b>1a</b> )					
<b>TS-a-S<sub>1</sub></b>	30.7 (30.7) <sup>b</sup>	23.6 (23.1)	7.1 (7.7)	-27.4 (-29.2)	3.3 (1.6)
<b>TS-a-A<sub>1</sub></b>	31.8 (32.6)	26.2 (26.7)	5.6 (6.2)	-25.3 (-27.0)	6.5 (5.9)
<b>TS-a-S<sub>2</sub></b>	31.8 (31.4)	26.0 (25.1)	5.8 (6.3)	-23.9 (-24.2)	7.9 (7.2)
<b>TS-a-A<sub>2</sub></b>	33.6 (35.9)	27.7 (29.5)	5.9 (6.4)	-24.3 (-26.6)	9.3 (9.3)
Oxazolidinethione ( <b>1b</b> )					
<b>TS-a-S<sub>1</sub></b>	36.0 (34.6)	27.8 (25.8)	8.2 (8.8)	-29.9 (-31.5)	6.1 (3.1)
<b>TS-a-A<sub>1</sub></b>	37.0 (36.6)	30.4 (39.4)	6.6 (7.1)	-26.9 (-28.5)	10.1 (8.1)
<b>TS-a-S<sub>2</sub></b>	33.3 (32.0)	27.1 (25.2)	6.3 (6.8)	-23.0 (-23.6)	10.3 (8.4)
<b>TS-a-A<sub>2</sub></b>	39.0 (39.9)	31.3 (31.6)	7.8 (8.3)	-27.3 (-29.5)	11.8 (10.5)
Thiazolidinethione ( <b>1c</b> )					
<b>TS-a-S<sub>1</sub></b>	39.2 (37.5)	30.4 (28.1)	8.8 (9.4)	-31.1 (-32.8)	8.2 (4.8)
<b>TS-a-A<sub>1</sub></b>	40.6 (40.1)	33.0 (31.9)	7.6 (8.2)	-28.3 (-30.2)	12.3 (9.9)
<b>TS-a-S<sub>2</sub></b>	35.5 (37.3)	29.9 (27.5)	7.4 (7.9)	-25.8 (-26.1)	11.4 (9.4)
<b>TS-a-A<sub>2</sub></b>	41.5 (41.9)	33.1 (32.9)	8.4 (9.0)	-28.3 (-30.3)	13.2 (11.6)

<sup>a</sup> Refers to the total distortion energy, consisting of (i) the energy required to distort the geometry of the enolate bound to TiCl<sub>4</sub> to the geometry in the TS, denoted as  $\Delta E^{\ddagger}_d(N)$ , and (ii) the distortion energy of benzaldehyde, denoted as  $\Delta E^{\ddagger}_d(E)$ . <sup>b</sup> Gas-phase energies calculated at the B3LYP/6-311+G\*\*//B3LYP/6-31G\* level are given in parentheses.

<sup>c</sup> Calculated with respect to titanium enolate and benzaldehyde.

the TS geometry. The distortion energy depends on the ability of the reactants to reorganize into their deformed structures in the TS, which is devoid of any interaction between the reactants. The interaction energy, on the other hand, depends on the electronic structure features as well as the relative orientations of the reactants during the bond formation.<sup>59</sup> The results of the activation strain model in terms of *distortion* and *interaction* on the nonchelated TSs are presented in Table 4.

Interesting trends emerge from the analyses of the distortion and interaction energies of stereochemically crucial TSs. A perusal of distortion energies in the case of nonchelated TSs reveals that the contribution to the deformation energy is primarily due to the distortion of the enolate fragment rather than that of benzaldehyde. For instance, with the lowest energy TS (**TS-a-S<sub>1</sub>**), the deformation energies for enolate and benzaldehyde are respectively 23.6 and 7.1 kcal/mol. Similarly, the stabilizing interactions are also found to exhibit interesting variations. In the case of all three chiral auxiliaries, higher stabilizing interaction energy is noticed for the TSs responsible for the formation of Evans *syn* aldol. The  $\Delta E^{\ddagger}_i$  value is -27.4 kcal/mol for the lowest energy TS (**TS-a-S<sub>1</sub>**), whereas it is -25.3 kcal/mol for the next higher energy TS (**TS-a-A<sub>1</sub>**) for oxazolidinone-mediated C–C bond formation. Most strikingly, the net balance between the destabilizing distortion and stabilizing interaction energies is found to follow the predicted energy order between the diastereomeric TSs. In other words, the agreement between the predicted trends in stereoselectivity is consistent with the preferred order as given by the activation strain model. With each of the chiral auxiliaries, the lowest energy TS exhibits the highest  $\Delta E^{\ddagger}_i$  value. It is therefore highly suggestive that the key to the higher stability of **TS-a-S<sub>1</sub>** stems from the improved interaction energy between the reacting partners. In this TS, the unhindered face of the enolate adds to benzaldehyde through

(59) (a) Diefenbach, A.; Bickelhaupt, F. M. *J. Phys. Chem. A* **2004**, *108*, 8460. (b) de Jong, G. T.; Visser, R.; Bickelhaupt, F. M. *J. Organomet. Chem.* **2006**, *691*, 4341. (c) de Jong, G. T.; Bickelhaupt, F. M. *Chem. Phys. Chem.* **2007**, *8*, 1170. (d) de Jong, G. T.; Bickelhaupt, F. M. *J. Chem. Theory Comput.* **2007**, *3*, 514. (e) Fernández, I.; Bickelhaupt, F. M.; Cossío, F. P. *Chem.–Eur. J.* **2009**, *15*, 13022.

**Table 5.** Computed Distortion ( $\Delta E^{\ddagger}_d$ )<sup>a</sup> and Interaction ( $\Delta E^{\ddagger}_i$ ) Energies<sup>b</sup> (kcal/mol) for the Chelated Transition States Obtained at the PCM<sub>(DCM)</sub>/B3LYP/6-311+G\*\*//B3LYP/6-31G\* Level of Theory

transition state	$\Delta E^{\ddagger}_d$	$\Delta E^{\ddagger}_d(N)$	$\Delta E^{\ddagger}_d(E)$	$\Delta E^{\ddagger}_i$	$\Delta E^{\ddagger c}$
Oxazolidinone ( <b>1a</b> )					
<b>TS-S<sub>1</sub>'</b>	49.2 (50.5) <sup>b</sup>	34.7 (35.4)	14.4 (15.2)	-39.3 (-40.1)	9.9 (10.4)
<b>TS-A<sub>1</sub>'</b>	52.2 (47.4)	35.9 (36.3)	16.3 (17.0)	-41.2 (-42.6)	11.0 (10.7)
<b>TS-S<sub>2</sub>'</b>	51.5 (53.1)	33.4 (34.2)	18.1 (18.8)	-44.4 (-44.6)	7.1 (8.4)
<b>TS-A<sub>2</sub>'</b>	49.2 (51.0)	33.4 (34.4)	15.8 (16.6)	-39.9 (-42.7)	9.3 (8.2)
Oxazolidinethione ( <b>1b</b> )					
<b>TS-S<sub>1</sub>'</b>	47.0 (46.8)	33.9 (32.9)	13.1 (13.8)	-35.8 (-37.2)	11.2 (9.5)
<b>TS-A<sub>1</sub>'</b>	49.8 (49.3)	35.2 (33.9)	14.6 (15.3)	-38.0 (-39.7)	11.8 (9.5)
<b>TS-S<sub>2</sub>'</b>	47.7 (47.0)	32.8 (31.3)	14.9 (15.6)	-39.4 (-39.6)	8.3 (7.4)
<b>TS-A<sub>2</sub>'</b>	46.8 (46.8)	32.4 (31.6)	14.4 (15.2)	-36.7 (-39.5)	10.1 (7.3)
Thiazolidinethione ( <b>1c</b> )					
<b>TS-S<sub>1</sub>'</b>	45.2 (46.6)	32.4 (33.1)	12.8 (13.5)	-34.8 (-36.6)	10.4 (10.0)
<b>TS-A<sub>1</sub>'</b>	47.4 (48.4)	33.4 (33.8)	13.9 (14.6)	-36.7 (-38.5)	10.7 (9.9)
<b>TS-S<sub>2</sub>'</b>	45.4 (46.2)	30.7 (30.8)	14.7 (15.4)	-38.4 (-38.8)	7.0 (7.4)
<b>TS-A<sub>2</sub>'</b>	44.1 (45.8)	30.5 (31.5)	13.6 (14.3)	-34.7 (-37.5)	9.4 (8.3)

<sup>a</sup> Refers to the total distortion energy consisting of (i) the energy required to distort the geometry of the enolate bound to TiCl<sub>3</sub> to the geometry in the TS, denoted as  $\Delta E^{\ddagger}_d(N)$ , and (ii) the distortion energy of benzaldehyde, denoted as  $\Delta E^{\ddagger}_d(E)$ . <sup>b</sup> Gas-phase energies calculated at the B3LYP/6-311+G\*\*//B3LYP/6-31G\* level are given in parentheses.

<sup>c</sup> Calculated with respect to titanium enolate and benzaldehyde.

a chair-like geometry; with a staggered arrangement of the substituents around the incipient C–C bond, the maximum stabilizing interaction energy is noticed. A closely related analysis is also carried out on the PRC preceding each stereochemically unique TS for the addition of nucleophile to electrophile. The distortion and interaction energies in these PRCs capture effects due to the ligand reorganization accompanying the formation of a hexacoordinate titanium. In general, the stabilizing interaction energy between the reactants is found to be more than the destabilizing deformation energies in PRCs.<sup>60</sup> This could be regarded as responsible for the improved stability of the PRCs as compared to the separated reactants.

The distortion and interaction energy analysis for the C–C bond formation involving chelated TSs is also performed. The results are summarized in Table 5. The crucial difference here, as compared to the nonchelated pathway, is that the ring carbonyl/thiocarbonyl chelation renders higher rigidity to the titanium complex. As with the nonchelated TSs, higher distortion energy is noticed for the titanium enolate moiety as compared to that in benzaldehyde. More importantly, the distortion of benzaldehyde is found to be more in the chelated TSs. For instance, the distortion energy of benzaldehyde leading to the formation of product **S<sub>1</sub>** is 7.1 kcal/mol in the nonchelated TS, while it is as high as 14.4 kcal/mol in the chelated TS. The interaction energy indeed plays a key role in determining the relative stabilization of the TSs. In all three chiral auxiliaries, the value of  $\Delta E^{\ddagger}_i$  for **TS-S<sub>2</sub>'** is found to be the highest. This implies that the TS responsible for the formation of non-Evans *syn* aldol product (**S<sub>2</sub>**) enjoys the highest stabilizing interaction energy as compared to the other three stereochemically competing TSs. The chair-like C–C bond formation TS geometry, involving the attack of the unhindered face of the enolate on benzaldehyde with a staggered arrangement of the substituents around the developing C–C bond, facilitates improved interaction energy between the fragments. The net effect of these

(59) Complete details of distortion–interaction analysis are provided in Table S8 in the Supporting Information.

factors and the predicted trends are certainly in agreement with the energy ordering between the TSs, as noticed in the present case.

The computed activation barriers for the C–C bond formation ( $\Delta E_{\text{act}}^{\ddagger}$ ), respectively for nonchelated and chelated pathways, are provided in Tables 4 and 5. It is evident that the destabilizing distortion energies dominate over the gain in stability due to the interaction energies. This results in positive activation barriers for the C–C bond formation. However, in the case of PRCs, the stabilizing interaction energy is higher than the distortion energy, leading to a net stabilization of the PRCs with respect to the corresponding reactants.<sup>61</sup> Comparison of the activation barriers between chelated and nonchelated pathways readily reveals that the barriers for the latter are lower. Interestingly, this prediction is along the similar lines as that of an earlier experimental observation by Das and Thornton, wherein the improved speed in a series of diastereoselective aldol reactions between chiral lithium enolate and ketones was attributed to the involvement of a nonchelated TS.<sup>62</sup> It can be further noticed that the barriers associated with **1a**, in both chelated and nonchelated pathways, are lower than those for the other chiral auxiliaries, **1b** and **1c**. Hence, under normal conditions, the reaction is likely to proceed through a nonchelated pathway leading to Evans *syn* aldol as the major product. However, under suitably modified reaction conditions (*vide supra*), the displacement of one of the chloride ions can facilitate the coordination of the ring carbonyl (**1a**) or thiocarbonyl (**1b** and **1c**) to titanium. Such changes can lead to non-Evans *syn* aldol as the major product. It is therefore evident from the present study that the stereodivergence in the chiral auxiliary-mediated asymmetric aldol reaction between titanium enolate and benzaldehyde can be rationalized by using suitable chelated and nonchelated TS models.

The TS models described in this study can shed light on the origin of stereoselectivity and other potential factors capable of influencing the stereochemical outcome of titanium enolate-promoted aldol reactions. The details of the stereoelectronic effects illustrated herein could be applied toward gaining valuable insights on the mechanistic implications of Evans oxazolidinone as well as other chiral auxiliary-mediated reactions.<sup>50</sup>

## Conclusion

The titanium(IV)-promoted aldol reaction between propionyl oxazolidinone and benzaldehyde has been investigated with the help of density functional theory calculations. Other commonly employed oxazolidinone variants such as oxazolidinethione as well as thiazolidinethione have also been examined. Both chelated and nonchelated transition states have been identified

for all the stereochemically important modes of addition between titanium enolate and electrophile. The relative energies of the stereoselectivity-determining TSs are found to be effective toward rationalizing the formation of Evans *syn* and non-Evans *syn* aldol products. In the nonchelated TS pathway, the attack by the less hindered *re* face of titanium enolate on the *si* face of benzaldehyde is found to be energetically the most favored mode of addition, leading to Evans *syn* aldol product. The calculated energy differences of more than 2 kcal/mol between the vital diastereomeric TSs in each of the systems reported herein concur with the experimentally known diastereomeric excess of >90% toward Evans *syn* aldol product. The cumulative effects of steric, electronic, conformational, and electrostatic factors are found to be effective in rationalizing the relative energy order between the critical diastereomeric TSs controlling the stereochemical outcome of the title reaction. Furthermore, in-depth analysis of the TSs by using the *activation strain model* revealed that the balance between the interaction and distortion energies in stereochemically different modes of approach is a crucial controlling factor responsible for the vital differential stabilization of TSs, and hence to the stereochemical outcome. The facial selectivity is found to be largely influenced by the C<sub>4</sub>-substituent, such as an isopropyl group, on the chiral auxiliary. The ring carbonyl or thiocarbonyl chelation with titanium is identified as favoring the formation of neutral titanium enolate. In the chelated TS models, attack by the less hindered *si* face of enolate on the *re* face of benzaldehyde is found to be the favored pathway and results in the formation of non-Evans *syn* aldol product. Further, the steric crowding of ligands around titanium is found to be relatively higher in the case of oxazolidinone as compared to that in oxazolidinethione and thiazolidinethione. The longer C=S...Ti coordinating distance together with the inherently longer C=S bond favors the involvement of a chelated pathway for thiazolidinethione more than that for oxazolidinone. The results are tested across different levels of theory. Gratifyingly, the trends are found to be not only mutually consistent but also in good concurrence with the experimental observations. The results offer a meaningful rationalization of the factors affecting the relative stabilizations of chelated and nonchelated TSs for the critical stereoselectivity-controlling step.

**Acknowledgment.** Generous computing time from the IIT Bombay computer center as well as Center for Modeling Simulation and Design (CMSD) Hyderabad is gratefully acknowledged. S.C.B. acknowledges a senior research fellowship from CSIR New Delhi and Chandan Patel (IIT Bombay) for valuable suggestions.

**Supporting Information Available:** Total electronic energies, optimized coordinates of all the transition state geometries, Figures S1–S8, Tables S1–S9, and complete ref 21. This material is available free of charge via the Internet at <http://pubs.acs.org>.

JA101913K

(61) The deformation interaction analyses done on the PRCs leading to chelated TSs are tabulated in Table S9 in the Supporting Information. The stabilizing interactions between the reactants are again found to dominate over the distortion energies, resulting in net stabilization of the PRCs.

(62) Das, G.; Thornton, E. R. *J. Am. Chem. Soc.* **1993**, *115*, 1302.

# Bicyclic proline analogues as organocatalysts for stereoselective aldol reactions: an *in silico* DFT study

C. B. Shinisha and Raghavan B. Sunoj\*

Received 5th February 2007, Accepted 28th February 2007  
First published as an Advance Article on the web 20th March 2007  
DOI: 10.1039/b701688c

Density functional theory has been employed in investigating the efficiency of a series of bicyclic analogues of proline as stereoselective organocatalysts for the aldol reaction. Three classes of conformationally restricted proline analogues, as part of either a [2.2.1] or [2.1.1] bicyclic framework, have been studied. Transition states for the stereoselective C–C bond formation between enamines derived from [2.2.1] and [2.1.1] bicyclic amino acids and *p*-nitrobenzaldehyde, leading to enantiomeric products, have been identified. Analysis of the transition state geometries revealed that the structural rigidity of catalysts, improved transition state organization as well as other weak interactions influence the relative stabilities of diastereomeric transition states and help contribute to the overall stereoselectivity in the aldol reaction. These bicyclic catalysts are predicted to be substantially more effective in improving the enantiomeric excess than the widely used organocatalyst proline. Enantiomeric excesses in the range 82–95% are predicted for these bicyclic catalysts when a sterically unbiased substrate such as *p*-nitrobenzaldehyde is employed for the asymmetric aldol reaction. More interestingly, introduction of substituents, as simple as a methyl group, at the *ortho* position of the aryl aldehyde bring about an increase in the enantiomeric excess to values greater than 98%. The reasons behind the vital energy separation between diastereomeric transition states has been rationalized with the help of a number of weak interactions such as intramolecular hydrogen bonding and Coulombic interactions operating on the transition states. These predictions could have wider implications for the rational design of improved organocatalysts for stereoselective carbon–carbon bond-forming reactions.

## Introduction

The search for metal-free organocatalysts has been in the forefront of research in organic chemistry in recent years.<sup>1</sup> Proline has evolved as a prototypical example of an organocatalyst with capabilities for a diverse range of asymmetric transformations.<sup>2</sup> The last couple of years have witnessed increasing activities toward identifying improved proline analogues as well as other organocatalysts for asymmetric catalysis.<sup>3</sup> Both theoretical and experimental studies have been reported that propose proline analogues capable of catalyzing stereoselective aldol reactions.<sup>4</sup> The synergy between experimental and theoretical studies has contributed to the evaluation of the mechanism of proline-catalyzed asymmetric reactions.<sup>5</sup>

In one of the earliest examples, reported more than three decades ago, namely the Hajos–Parrish–Eder–Sauer–Wiechert reaction, proline was found to be effective in catalyzing the intramolecular asymmetric cyclodehydration of an achiral ketone to the unsaturated Wieland–Miescher ketone.<sup>6</sup> Whereas a number of mechanisms were initially considered for this reaction, the

one involving two molecules of proline in the catalytic process, proposed by Agami *et al.*, received early acceptance.<sup>7</sup> Recently, Houk and co-workers have examined the involvement of different mechanisms for this reaction using density functional theory (DFT) methods.<sup>8,9</sup> A number of possible transition states for the key C–C bond formation step, which determines the stereochemistry of the reaction, has been proposed. A carboxylic acid assisted enamine mechanism involving only one proline molecule was found to be favourable. In fact, this mechanism, originally proposed by Jung,<sup>10</sup> was overlooked due to the widespread acceptance of Agami's mechanism. The single-proline-catalyzed mechanism for aldol reactions was subsequently re-examined by Houk, List and co-workers with the help of more accurate experimental methods.<sup>11</sup> Proline-catalyzed aldol reactions showed a first-order kinetic dependence on the catalyst concentration, and also exhibited a linear relationship between the enantiomeric excess of proline and that of the product.<sup>3a,11</sup> Thus, the latest experimental results, in concert with DFT studies, support the single-proline-catalyzed mechanism for aldol reactions.

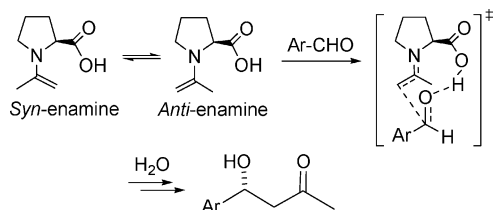
Computational investigations have been used both in conjunction with experimental studies and independently to gaining insights into stereoselective organic reactions. The concurrence between the predicted and experimentally determined enantiomeric excess has generally been quite impressive. Some such examples include the studies on proline-catalyzed aminoxylation,<sup>12</sup> Mannich reactions,<sup>5b</sup> and  $\alpha$ -alkylations.<sup>5d,e</sup> DFT calculations, in particular those using the B3LYP functional,<sup>13</sup> have been effectively employed in probing the differential interactions in diastereomeric

Department of Chemistry, Indian Institute of Technology Bombay, Powai, Mumbai, 400076, India. E-mail: sunoj@chem.iitb.ac.in; Fax: +91 22-2572-3480 or +91 22-2576-7152

† Electronic supplementary information (ESI) available: Total electronic energies, optimized coordinates and single-point energies of all structures reported in the text, Fig. S1–S5, Tables S1–S10 and full list of citations for Gaussian 98 and Gaussian 03 (ref. 47 in the text). See DOI: 10.1039/b701688c

TSs that contribute to the vital energy differences responsible for enantioselectivity in these reactions.<sup>14</sup> Through their studies on the proline-catalyzed asymmetric aldol reaction, Houk and co-workers have demonstrated that enantiomeric excesses predicted using the B3LYP transition state calculations are in remarkable agreement with those obtained experimentally.<sup>15</sup> Weak hydrogen bonding as well as other electrostatic interactions are reported to be crucial in stabilizing the transition states.<sup>14,16</sup>

Mechanistic investigations into the proline-catalyzed direct aldol reaction between ketones and aldehydes using DFT have been reported previously.<sup>17</sup> The stereoselectivity has been identified as being controlled by the crucial C–C bond formation step, which involves the nucleophilic addition of the enamine to the electrophilic aldehyde and concomitant proton transfer from the carboxylic acid group to the developing alkoxide ion (Scheme 1).<sup>15a,18</sup> Finally, hydrolysis of the resulting adduct, with defined stereochemistry, furnishes the desired β-hydroxy ketone as the product.



**Scheme 1** Addition of enamines to the electrophilic aldehyde in the selectivity-determining step.

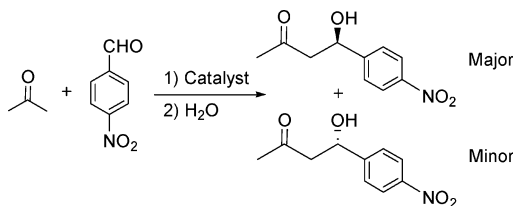
The prochiral faces of the electrophile and the *syn* and *anti* conformations of the enamine could give rise to four different stereochemical modes of approach between the reactants. Additionally, a number of possible TSs with varying dihedral angles between the substituents around the incipient C–C bond can also be envisaged. The lower energy TSs have been suggested to possess intramolecular hydrogen bonding between the developing alkoxide ion and the carboxylic acid group.<sup>15a</sup> The product ratio and the enantiomeric excess calculated using such lower energy TSs was found to be in good agreement with experimental observation. In particular, the computed enantiomeric excess using the gas-phase enthalpy of activation ( $\Delta H^\ddagger_{298\text{K}}$ ) was found to be in close agreement with the experimental results. Furthermore, the activation enthalpies have shown minimum error with respect to the experimentally determined kinetic parameters.<sup>19</sup>

DFT methods have been successfully applied to gain better insights on reaction mechanisms as well as towards rationalizing experimental stereoselectivity in a number of cases other than those described above.<sup>20</sup> We believe that the predictive potential of theoretical models can be further exploited in accelerating this burgeoning area of chemical research. From a slightly different perspective, one can identify an underlying parallelism between the virtual screening protocols adopted in rational drug design and our DFT-based approach to designing new organocatalysts described in the present context. Computer-aided methods using scoring functions and related parameters have significantly contributed to drug discovery, as well as to organic chemistry.<sup>21</sup> In the present thesis, we intend to convey the use of quantum chemical calculations as a virtual screening tool for designing improved organocatalysts.

Among the increasing number of proline analogues reported as potential organocatalysts, the major changes include conversion/replacement of the carboxylic acid group as well as elaborations at the  $\beta$  and  $\gamma$  positions.<sup>22</sup> All such attempts thus far have revolved around monocyclic proline analogues, except for couple of reports on 4,5-methanoprolines.<sup>4b,23</sup> The pyrrolidine ring conformation in proline is believed to be important in chirality transfer,<sup>8</sup> which could play a vital role in organizing the transition state that is formed between the substrate and catalyst along the most enantioselective path.<sup>1c</sup> The pyrrolidine ring is also known to be better suited to aldol reactions than other cyclic secondary amines such as piperolic acid and 2-azetidinecarboxylic acid.<sup>3a</sup> Primary amino acids have also been studied as catalysts for aldol reactions, but good enantiomeric excesses were observed only when the substrates employed were cyclic ketones with reduced conformational flexibility.<sup>24</sup>

Proline can exist in different interconvertible conformations by virtue of the puckered pyrrolidine ring.<sup>25</sup> Therefore, it is logical to anticipate that restricting the conformational freedom of the pyrrolidine ring could have a direct impact on the stereoselectivity of reactions. Greater rigidity of the catalyst could impart improved stability and organization of the transition states, and help keep the entropy loss to a relatively minimal level. Moreover, detailed knowledge on the controlling elements such as structure, conformation and energetics of catalyst, substrate and transitions states will be very valuable towards designing improved catalysts.<sup>14,26</sup>

We reasoned that introducing geometrical constraints on the catalyst can lead to relatively ordered transition states capable of influencing the stereochemical outcome of the reaction. One of the broader objectives at this juncture is to propose how a standard stereoselective aldol reaction can benefit from complete modeling of the reaction and by close inspection of the selectivity-determining transition state. In the present investigation, we have designed a series of novel bicyclic-bifunctional analogues of proline. These catalysts are evaluated for their ability to promote the stereoselective aldol reaction between acetone and *p*-nitrobenzaldehyde (Scheme 2), using DFT methods.

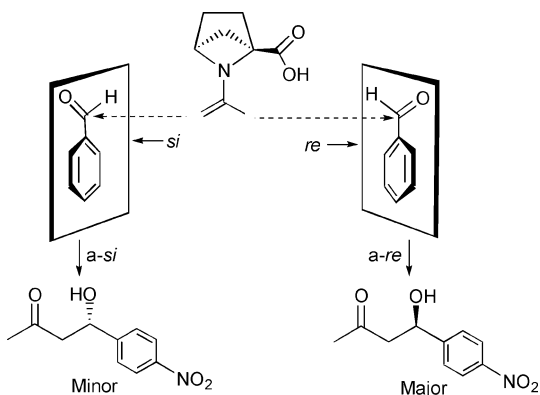


**Scheme 2** General scheme of the model aldol reaction investigated in the present work.

## Results and discussion

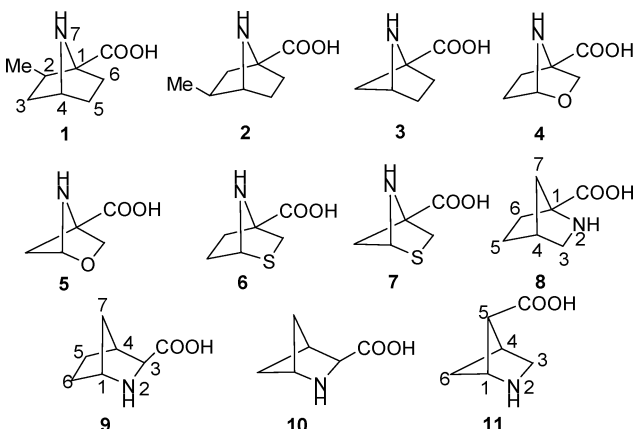
As described above, the mechanism of the organocatalyzed aldol reaction has been proposed to proceed through an enamine intermediate. In this study, we have entirely focused on the selectivity-controlling C–C bond formation step in the aldol reaction between acetone and *p*-nitrobenzaldehyde. This step involves the attack of the enamine formed between acetone and the catalyst (a secondary amine) on the electrophilic aldehyde. Since the aldehyde offers two prochiral faces, the stereoselectivity of the overall reaction will be

critically dependent on this step. In the present study, *re* and *si* facial attack on *p*-nitrobenzaldehyde by *anti*- and *syn*-enamines are investigated. The TSs corresponding to attack of the *anti*-enamine on the *re* and *si* faces of the aldehyde are respectively denoted as *a-re* and *a-si*, and that of the *syn*-enamine are referred to as *s-re* and *s-si*. These stereochemical modes of addition are depicted in Scheme 3. The relative energies between the diastereomeric TSs are then calculated, in order to obtain the kinetic preference for the formation of one enantiomer over the other. This energy difference is then translated into enantiomeric excess (ee) using the absolute rate theory.<sup>15a</sup>



**Scheme 3** Different possible stereochemical modes of addition for the *anti*-enamine (derived from catalyst 3 and acetone) with benzaldehyde.

The catalytic ability of bifunctional amino acids, when tailored onto a rigid bicyclic framework, in the aldol reaction is studied in detail below. We have considered three important conformations of proline contained within a bicyclic framework (Scheme 4). The first set has an envelope conformation in which the -NH is out-of-plane in a [2.2.1] or [2.1.1] bicyclic system and its various analogues (**1–7**). In the second set (**8**), C-7 heads the envelope conformation of the proline skeleton. In the third set, the conformation of proline has been constrained as part of a [2.2.1] or [2.1.1] bicyclic system (**9, 10**). Additionally, a [2.1.1] bicyclic system having a 1,3-relationship between the amino and the carboxylic acid groups (**11**) is also investigated. Interestingly, the synthesis and other applications of a few of these proposed azabicyclic compounds



**Scheme 4** Bicyclic bifunctional asymmetric catalysts for the stereoselective aldol reaction.

are known.<sup>27</sup> Some of these azabicyclics have been reported to be useful as peptidomimetics, since they are capable of inducing conformational changes in peptides, which could be useful in studying receptor recognition.<sup>28</sup>

The pyrrolidine envelope conformer with an out-of-plane -NH group, when contained within a bicyclic framework as in **1** and **2**, will apparently lose its inherent chirality due a plane of symmetry. While restricted conformers, such as that in a [2.2.1] bicyclic system, could have significant nitrogen inversion barriers ( $\Delta G_{\text{expt}} = 13.77 \text{ kcal mol}^{-1}$ ), the molecule will be achiral under most practical conditions.<sup>29</sup> Such a high barrier probably arises due to the repulsion between nitrogen lone pairs and bonding electrons on the two carbon–carbon bridges and the lack of flexibility at the C–N–C bond angle. To impart inherent chirality to these catalysts and also as an early step towards investigating the effect of substituents, we introduced methyl groups at suitable positions on the bicyclic system, as shown in Scheme 4 (**1** and **2**). The azanorbornyl systems bearing a nitrogen at the 7-position (see the numbering for compound **1**, Scheme 4) are known to be highly pyramidal around the nitrogen atom.<sup>30</sup> The orientation of the carboxylic acid group at the bridge-head position is therefore expected to be restricted due to the intramolecular hydrogen bonding with the amino nitrogen.<sup>31</sup> Another logical extension at this juncture is to restrict the amino group to an out-of-plane position with the help of a methylene bridge, as in a [2.1.1] bicyclic system. This will result in catalyst **3**. The predicted enantiomeric excesses for the asymmetric aldol reactions obtained using these bicyclic catalysts, along with the underlying factors responsible for the stereoselectivity, are summarized below.

As described earlier, the stereoselectivity is controlled by the addition of enamines to the electrophile. We have therefore considered two important enamine conformations as a starting point. On the basis of the computed energies, the lowest energy conformer of the enamine derived from different catalysts could either be *syn* or *anti* with respect to the carboxylic acid group. The *syn*-enamines formed from catalysts **1–7** are found to be more stable than the *anti*-enamines.<sup>32</sup> More importantly, the TSs for the addition of enamines to aldehydes are found to be energetically more favourable for the *syn*-enamines than for the corresponding *anti*-enamines. As a representative example, optimized TS geometries for four possible addition modes of enamine **1** to *p*-nitrobenzaldehyde are provided in Fig. 1.

When the enamine adds to the aldehydic group, the developing alkoxide ion tends to abstract the proton from the carboxylic acid group (Scheme 1). The analysis of the TSs revealed that the geometry for such proton transfer is optimal for TSs involving the *syn*-enamine.<sup>33</sup> Further, the geometric distortion suffered by the resulting iminium ion in the case of the *syn*-enamines is found to be minimal when compared with an ideal planar geometry around the nitrogen atom, exhibiting closer resemblance with the product geometry. These factors would undoubtedly contribute toward improved stabilization for the *syn*-enamine TSs. The planarity of the putative iminium moiety for each TS is analyzed in detail using the  $C_{\text{ring}}-\text{N}-C-C_{\text{imminium}}$  dihedral angles, described as  $\theta_1-\theta_4$  (inset, Fig. 1).<sup>34</sup> Interesting correlations between the activation barriers and these dihedral angles emerge when different TSs are compared. Larger deviations from planarity are generally found for additions involving higher activation barriers. For instance, the  $\theta_1$  and  $\theta_3$  values in the lower-barrier *s-re* and *s-si* TSs for

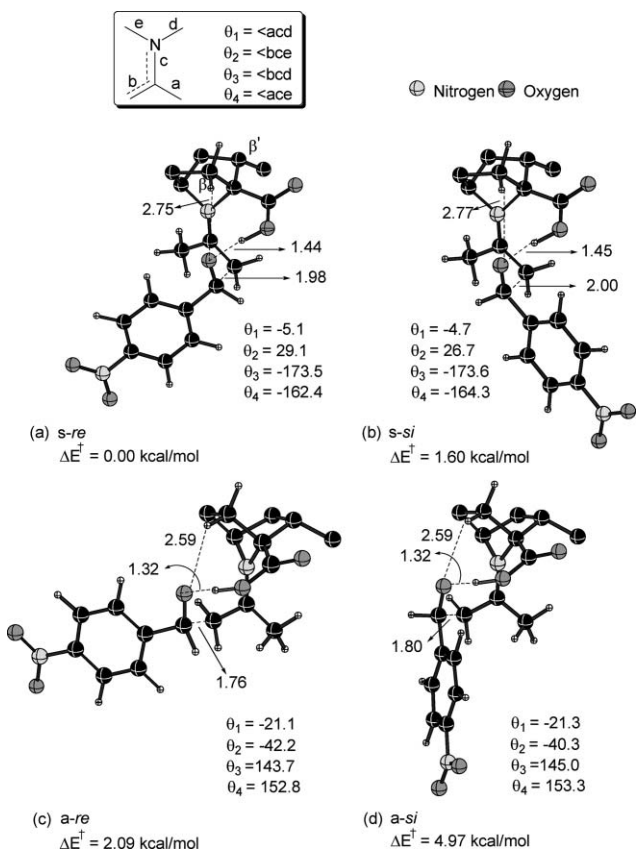


**Fig. 1** The B3LYP/6-31G\*-optimized transition state geometries for four unique stereochemical modes of addition for enamines derived from catalyst **1** to *p*-nitrobenzaldehyde. Only selected hydrogens on the catalyst are shown for clarity. Activation barriers  $\Delta E^\ddagger$  were obtained at the CPCM/B3LYP/6-311+G\*\*//B3LYP/6-31G\* level using DMSO as the solvent. Angles are given in degrees and distances in Å.

catalyst **1** imply a nearly planar geometry around the iminium nitrogen. The deviation for the *syn*-enamine additions are found to be only about  $\pm 5^\circ$ , whereas the corresponding values for the *a-re* and *a-si* TSs are of the order of  $\pm 35^\circ$ , indicating a larger geometric distortion for the developing iminium ion. Such deviations lead to reduced electrostatic stabilization in the TSs and perhaps result in higher activation barriers for *anti*-enamine additions than for *syn*-enamines. Interestingly, the differences in activation barriers between the *syn*- and *anti*-enamine additions are much more pronounced in [2.1.1] bicyclic catalysts (**3**, **5** and **7**) than in [2.2.1] bicyclic systems. It may be noticed that the rigidity of the [2.1.1] bicyclic framework leads to a less favourable proton transfer from the carboxylic acid group to the developing alkoxide in the *anti*-enamine TSs. Such a proton transfer is facilitated at the expense of greater geometric distortion around the developing iminium nitrogen.<sup>35</sup> Another contributing factor helping to achieve additional stabilization for the *s-re* TSs presumably originates from the C–H $\cdots$ π stabilizing interaction between the CH<sub>3</sub>-hydrogens of the enamine/iminium with the aryl group of the aldehyde (Fig. 1a).<sup>36</sup> Other stereoisomeric TSs involved in this example (*i.e.*, *s-si* as well as *a-re/a-si* TSs) lack such interactions. The relative activation barriers would eventually depend on the presence or absence of all these stabilizing interactions. The relative activation enthalpies calculated based on

**Table 1** Computed activation barriers ( $\Delta E^\ddagger$ ) obtained at the CPCM<sub>(DMSO)</sub>/B3LYP/6-311+G\*\*//B3LYP/6-31G\* level for the addition of enamines to *p*-nitrobenzaldehyde, and the corresponding enantiomeric excess for catalysts **1** to **7**<sup>a</sup>

Catalyst	Mode of approach	$\Delta E^\ddagger / \text{kcal mol}^{-1}$ <sup>b</sup>		
		Absolute	Relative	ee (%)
<b>1</b>	<i>a-re</i>	4.52 (6.77)	2.09 (2.20)	87 (87)
	<i>a-si</i>	7.40 (9.59)	4.97 (5.02)	
	<i>s-re</i>	4.13 (6.16)	0.00 (0.00)	
	<i>s-si</i>	5.73 (7.75)	1.60 (1.58)	
<b>2</b>	<i>a-re</i>	0.59 (3.95)	2.38 (2.84)	85 (85)
	<i>a-si</i>	3.56 (6.79)	5.35 (5.69)	
	<i>s-re</i>	4.93 (6.69)	0.00 (0.00)	
	<i>s-si</i>	6.43 (8.21)	1.50 (1.52)	
<b>3</b>	<i>a-re</i>	12.22 (15.35)	13.04 (14.57)	82 (87)
	<i>a-si</i>	15.28 (18.25)	16.11 (15.86)	
	<i>s-re</i>	0.59 (6.29)	0.00 (0.00)	
	<i>s-si</i>	1.96 (7.89)	1.37 (1.60)	
<b>4</b>	<i>a-re</i>	8.26 (10.47)	3.75 (4.02)	91 (92)
	<i>a-si</i>	11.22 (17.24)	6.72 (10.79)	
	<i>s-re</i>	7.16 (8.94)	0.00 (0.00)	
	<i>s-si</i>	8.99 (10.87)	1.82 (1.93)	
<b>5</b>	<i>a-re</i>	12.15 (15.69)	13.31 (14.28)	92 (89)
	<i>a-si</i>	31.32 (2.21)	32.48 (2.91)	
	<i>s-re</i>	3.25 (6.71)	0.00 (0.00)	
	<i>s-si</i>	5.18 (8.43)	1.93 (1.72)	
<b>6</b>	<i>a-re</i>	22.91 (25.75)	20.59 (20.52)	90 (91)
	<i>a-si</i>	10.17 (13.30)	7.85 (8.08)	
	<i>s-re</i>	11.02 (8.06)	0.00 (0.00)	
	<i>s-si</i>	12.81 (9.88)	1.79 (1.81)	
<b>7</b>	<i>a-re</i>	21.66 (22.33)	16.10 (16.24)	84 (85)
	<i>a-si</i>	24.87 (25.43)	19.31 (19.34)	
	<i>s-re</i>	-0.97 (1.16)	0.00 (0.00)	
	<i>s-si</i>	0.49 (2.67)	1.47 (1.50)	

<sup>a</sup> The graphic shows a schematic representation of the TSs corresponding to the attack of the *anti/syn*-enamine on the *re/si* face of the aldehyde (for catalyst **3**). <sup>b</sup> Gas-phase activation barriers  $\Delta H^\ddagger_{298\text{K}}$  including scaled zero-point energies obtained at the B3LYP/6-311+G\*\*//B3LYP/6-31G\* level are given in parentheses.

the lowest-energy TSs and the corresponding enantiomeric excess for all the proposed catalysts in this series are summarized in Table 1.

On the basis of the calculated absolute and relative activation barriers, it is noticed that the *syn*-enamines (*s-re*) derived from catalysts **1**–**7** tend to exhibit a general preference for *re*-face attack on the aldehyde. The TSs belonging to this series enjoy an additional C(β)H $\cdots$ O hydrogen bonding stabilization between the developing alkoxide and a suitably aligned C(β) hydrogen, as depicted in Fig. 1. The conformation of pyrrolidine in the bicyclic systems aids the formation of these favourable weak interactions, which could influence the relative stabilization of the diastereomeric TSs. As a rational design strategy, we envisaged that fine-tuning the acidity of C(β)H might have a direct bearing on the relative energies of the TSs. Thus, replacement of adjacent C(γ) methylene group of the azabicyclic system by more electronegative heteroatoms was considered. The presence of an α-heteroatom will impart enhanced acidity to the C(β) hydrogen and thus will

improve its ability towards stabilizing the developing alkoxide in the TS.<sup>37</sup> We have studied a series of  $\alpha$ -heteroatom-substituted azabicyclic catalysts (**4** to **7**). Computed enantiomeric excesses with these catalysts are indeed found to be encouraging (Table 1). The enantiomeric excess is consistently higher than the corresponding unmodified bicyclic catalysts as well as the parent proline. For example, the predicted enantiomeric excess for catalyst **3** is 82%, while that for **5** is as high as 92%. These values are noticeably higher than the experimental values (as well as the DFT-predicted values) for the proline-catalyzed direct aldol reaction.<sup>38</sup>

The nature and position of the substituents on the catalyst could be employed as an effective method in fine-tuning the stereoselectivity. This is evident from the modest improvement in the enantiomeric excess noticed for catalyst **1** when compared to **2**. When the methyl substituent is placed closer to the enamine, as in **1**, the stereoselectivity is found to be better. Further elaborations using larger substituents could be valuable for improving the overall selectivity, even for sterically unbiased substrates. Examination of the optimized TS geometries provided in Fig. 1 clearly shows that the C( $\beta$ ) substituent can directly influence the orientation of the carboxylic acid group, which in turn can affect the crucial proton transfer process. To confirm the existence of any such effects, the C( $\beta$ )H in a representative case (catalyst **4**) is substituted by a chlorine atom. As in the previously described approach, all four TSs for this modified catalyst are identified.

Geometric comparison between these catalysts can be performed with the help of the optimized geometries provided in Fig. 2. The orientation of the carboxylic acid group in the TSs when C( $\beta$ )-H is substituted with chlorine, labeled as **4**, is found to be different from that in catalyst **4** ((a) and (b) in Fig. 2).<sup>39</sup> The computed enantiomeric excess for **4** is found to be quite similar to that for the corresponding unsubstituted system (**4**). Another critical position on the catalyst framework is the C( $\beta$ ) position. In the lowest energy addition TSs for the [2.1.1] and [2.2.1] catalysts,

the C( $\beta$ )H  $\cdots$  O <sup>$\delta$ -</sup> interaction is found to be stronger in the [2.1.1] catalyst, according to the optimized distances (Fig. 2a,c).<sup>40</sup> The effect of the C( $\beta$ )H  $\cdots$  O=C-O interaction in influencing the carboxylic acid group orientation is found to be nearly nonexistent with the [2.1.1] system (a distance as large as 3.3 Å is noticed in the case of catalyst **5**). Interestingly, both these catalysts (**4** and **5**) are predicted to give nearly the same enantiomeric excess (Table 1). Therefore, the orientation of the carboxylic acid group does not seem to directly relate to the stereoselectivity, while the activation barriers are found to be different in catalysts **4** and **5**.

Computed activation barriers of the C-C bond formation step with the *syn*-enamine derived from [2.1.1] catalysts are found to be much lower than that with the [2.2.1] catalysts. Further, the energy differences between the TSs for *syn*- and *anti*-enamine additions to the electrophile are more pronounced in the [2.1.1] system. Inspection of the imaginary frequencies pertaining to the desired reaction coordinate convey interesting facts. While the imaginary frequency in the case of *anti*-enamines corresponds to the concomitant C-C bond formation and the proton transfer, it is dominated by the C-C bond formation in the case of the *syn*-enamines. On the basis of the C-C bond distances (in the range 1.95–2.10 Å with *syn*-enamines and 1.75–1.85 Å with *anti*-enamines)<sup>41</sup> and the proton transfer distances in the TSs, it is evident that the *syn*-enamines proceed through a relatively early transition state, whereas late transition states are noticed for the *anti*-enamines.

Another structurally different type of catalyst considered in this study has the C- $\beta$ (C-7) of the pyrrolidine ring at the apical position in the [2.2.1] bicyclic system (**8**). The *syn*-enamine generated from catalyst **8** is found to be marginally more stable than the corresponding *anti*-enamine. Among the four stereochemical modes of addition of enamine to the electrophile, the *a-re* TS is the lowest energy TS leading to C-C bond formation (Fig. 3). Geometrical features provided additional insights on the factors contributing to the energy differences between these TSs.

A network of stabilizing weak interactions is found to be relatively in favour of the *anti*-enamine TSs. These include (i) a hydrogen bonding interaction between the developing alkoxide and the partially positive hydrogen of carbon adjacent to nitrogen (Fig. 3,  $^{\delta+}$ NC( $\alpha$ )H  $\cdots$  O <sup>$\delta$ -</sup> = 2.62 Å in *a-re/a-si*), (ii) intramolecular hydrogen bonding between C( $\beta$ )H and the developing alkoxide (2.76 Å in *a-re* and 2.81 Å in *a-si*), and (iii) a Coulombic interaction between the incipient iminium nitrogen (N <sup>$\delta+$</sup> ) and the alkoxide (2.67 Å in *a-re* and 2.68 Å in *a-si*). In an effort to achieve optimal proton transfer distance between the carboxylic acid group and the developing alkoxide in *syn*-enamine TSs, change in orientation of the substituents around the incipient C-C bond takes place and results in lowering of intramolecular stabilizing interactions. The orientation of substituents around the forming C-C bond is more eclipsed in the *syn*-enamine TSs. The highest-eclipsing interactions are found with the *s-si* TS. (Fig. 3,  $\omega = -118^\circ$  in *s-si*) In all the TSs (derived both from *syn*-enamines and *anti*-enamines), the orientation of the carboxylic acid group is found to be assisted by an additional interaction between the -COOH group and C( $\beta$ )H (Fig. 3).

The computed activation barriers for the addition of *syn*-enamines derived from catalysts **8** are much higher than that for the corresponding *anti*-enamines. Now, among the two lower energy diastereomeric TSs from *anti*-enamines, the *a-re* TS is found to

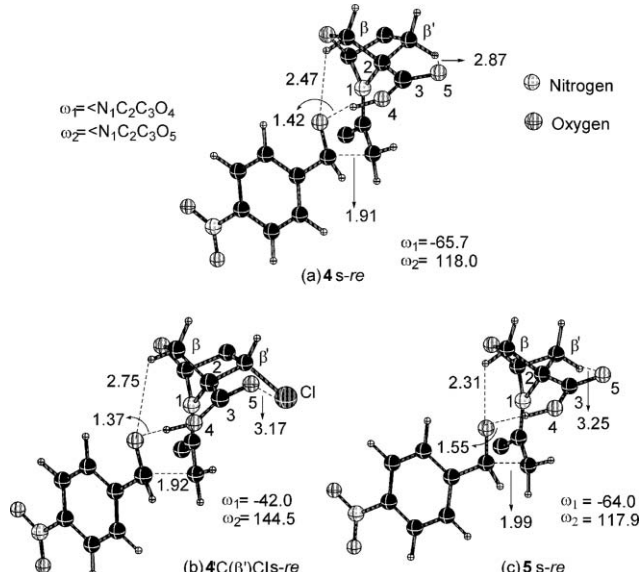
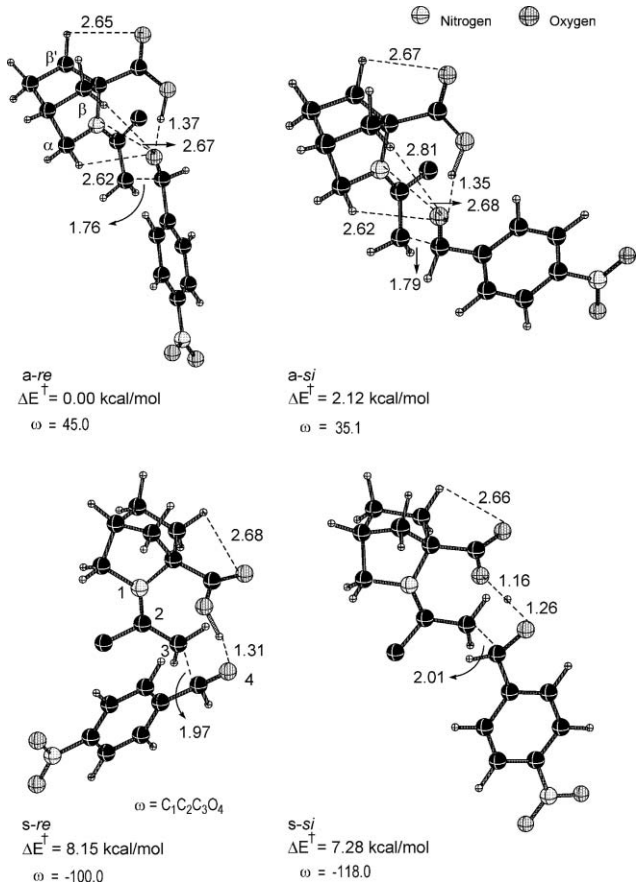


Fig. 2 The B3LYP/6-31G\*-optimized lowest-energy TSs of catalysts **4** and **5** (with Cl at the C( $\beta$ ) position) and **5**. Only selected hydrogens on the catalyst are shown for clarity. Angles are given in degrees and distances in Å.



**Fig. 3** The B3LYP/6-31G\*-optimized transition state geometries for four unique stereochemical modes of addition for enamines derived from catalyst **8** to *p*-nitrobenzaldehyde. The key weak interactions contributing to the transition state stabilization are shown. Only selected hydrogens on the catalyst are shown for clarity. Activation barriers,  $\Delta E^\ddagger$ , are obtained at the CPCM/B3LYP/6-311+G\*\*//B3LYP/6-31G\* level using DMSO as the solvent. Angles are given in degrees and distances in Å.

be the lowest energy TS, where the phenyl substituent is in the least-hindered position (Fig. 3). The energy difference between the two lower energy TSs (*a-re* and *a-si*) leading to diastereomeric products is found to be 2.12 kcal mol<sup>-1</sup>, corresponding to an enantiomeric excess of 95%. Comparison of activation barriers and enantiomeric excesses for this series of catalysts (**8**, **9** and **10**) are grouped together in Table 2.

In another group of catalysts considered in the present study, the envelope conformer of the parent proline is maintained, as part of a bicyclic system, as in **9** and **10**. These catalysts also exhibited a preference towards *anti*-enamine addition involving the *a-re* TS as the lowest energy pathway. A more staggered arrangement of substituents around the new C–C bond is noticed with the *anti*-enamine TSs, while it is more eclipsed with the *syn*-enamine TSs.<sup>35</sup> Such geometric features evidently lead to a higher-energy TSs for the *syn*-enamine addition pathway. Between the *anti*-enamine TSs, the *re*-facial attack on the aldehyde is favoured over the corresponding *si*-facial approach, since the aryl substituent on the aldehyde in the former is found to be sterically better positioned.<sup>42</sup>

Perhaps the most striking feature emerging from the present investigation relates to the correlation between the catalyst struc-

**Table 2** Computed activation barriers  $\Delta E^\ddagger$  obtained at the CPCM<sub>(DMSO)</sub>/B3LYP/6-311+G\*\*//B3LYP/6-31G\* level for the addition of enamines to *p*-nitrobenzaldehyde, and the corresponding enantiomeric excess for **8** to **11**

Catalysts	Mode of approach	$\Delta E^\ddagger/\text{kcal mol}^{-1}$ <sup>a</sup>		
		Absolute	Relative	ee (%)
<b>8</b>	<i>a-re</i>	6.55 (4.56)	0.00 (0.00)	95 (95)
	<i>a-si</i>	8.68 (6.76)	2.12 (2.20)	
	<i>s-re</i>	15.34 (13.94)	8.15 (8.61)	
	<i>s-si</i>	14.47 (12.23)	7.28 (6.90)	
<b>9</b>	<i>a-re</i>	3.56 (5.95)	0.00 (0.00)	75 (88)
	<i>a-si</i>	4.69 (7.62)	1.12 (1.66)	
	<i>s-re</i>	15.55 (13.03)	10.48 (2.77)	
	<i>s-si</i>	7.92 (13.91)	2.86 (3.64)	
<b>10</b>	<i>a-re</i>	7.90 (6.74)	0.00 (0.00)	80 (91)
	<i>a-si</i>	9.21 (8.62)	1.31 (1.87)	
	<i>s-re</i>	5.67 (9.23)	1.19 (2.02)	
	<i>s-si</i>	6.54 (10.06)	2.06 (2.84)	
<b>11</b>	<i>a-re</i>	7.87 (13.30)	3.62 (7.57)	5 (65.2)
	<i>a-si</i>	8.57 (12.88)	4.32 (7.16)	
	<i>s-re</i>	4.72 (5.95)	0.06 (0.00)	
	<i>s-si</i>	4.66 (6.88)	0.00 (0.92)	

<sup>a</sup> Gas-phase activation barriers  $\Delta H^\ddagger_{298\text{K}}$  including scaled zero-point energies computed at the B3LYP/6-311+G\*\*//B3LYP/6-31G\* level are given in parentheses.

ture and stereoselectivity. The agreement between the computed enantiomeric excess with that obtained experimentally for proline-catalyzed aldol reaction is found to be excellent. The ee predicted by DFT and the experimental value are 75% and 76% respectively.<sup>3a,38</sup> It is worthwhile to compare the enantiomeric excess calculated for catalysts **9** and **10** with that of proline, from a structure-selectivity point of view. The predicted ee for catalyst **9** is conspicuously quite close (74%) to the parent proline. In compounds **9** and **10**, even though the same proline conformation can be thought of as being constrained in a bicyclic framework, the increased rigidity of the [2.1.1] system is found to be good in improving the enantiomeric excess in **10** (Table 2).<sup>43</sup>

The position, orientation and acidity of the carboxylic acid group are known to be important in contributing to the catalytic ability of proline and its derivatives in promoting aldol reactions. For instance, proline and pyrrolidine-3-carboxylic acid have been reported to yield products of opposite stereochemistry in the Mannich reaction between 3-pentanone and *N*-PMP-protected  $\alpha$ -iminoester.<sup>44</sup> To verify how a bifunctional variant of proline (with a 1,3 relationship between the amino group and the carboxylic acid) performs compared to other bicyclic catalysts, we considered a [2.1.1] bicyclic system (Scheme 4, catalyst **11**). The computed activation barriers and the enantiomeric excess are given in Table 2. Though the carboxylic acid group is not adjacent to the enamine nitrogen, the distance is found to be close enough to facilitate the crucial proton transfer to the developing alkoxide.<sup>45</sup> In the case of catalyst **11**, the *syn*-enamine is found to be more stable than the *anti*-enamine. Further, the TSs resulting from the *syn*-enamines are much stable than those formed from the *anti*-enamines, but the energy difference between the *syn*-enamine TSs is very low. Hence the overall enantioselectivity of this catalyst is found to be the lowest among the present series of catalysts investigated. Based on the computed enantiomeric excess, it seems evident that the 1,2-relationship between the secondary amino group and the

carboxylic acid group is a highly desirable feature for amino acids to act as potential asymmetric catalysts for aldol reactions.

Encouraged by the enhanced stereoselectivity predicted for the bicyclic variants of proline, we have decided to examine how substrate-level changes (electrophilic aldehyde) will respond to these catalysts. Different substitutions on the aromatic aldehyde are therefore studied for their reaction with the enamine derived from a representative catalyst (**2**). Methyl substitution at the 2,6-positions of the aromatic aldehyde are found to be quite effective, increasing the enantiomeric excess up to 99%. Furthermore, the role of electronically active substituents (at the *para*-position) on the energetics of addition has also been investigated. The calculated activation barrier, as well as the enantiomeric excess, showed little variation compared to the original *p*-nitrobenzaldehyde.<sup>46</sup>

## Conclusions

The possible role of azabicyclic compounds (**1–10**) as potential organocatalysts in asymmetric aldol reaction between acetone and *p*-nitrobenzaldehyde are investigated. The stereoselectivity-determining step, similar to that of the established proline-catalyzed aldol reactions, are carefully examined by locating all stereochemically pertinent transition states using DFT methods. The calculations showed that these catalysts could be highly effective for aldol reactions, compared to popular organocatalysts such as proline. The simplest bicyclic analogues of proline are predicted to give better enantiomeric excesses. Suitable substitutions on these bicyclic frameworks are found to be a superior protocol in modulating the stereoselectivity of bifunctional secondary amino acids. Catalysts **1–8**, which are predicted to give enantiomeric excess from 82 to 95%, are expected to be superior over proline, for which the calculated enantiomeric excess is only 75%. The reaction is expected to proceed with greater ease, as the predicted activation energies are lower. Analysis of various intramolecular interactions, such as Coulombic and hydrogen bonding interactions, operating in the diastereomeric transition states, are found to be helpful in rationalizing the predicted stereoselectivity induced by these catalysts.

## Computational methods

Geometry optimization of reactants, intermediates, and transition states were carried out at the B3LYP/6-31G\* level of theory<sup>13,47</sup> using the Gaussian 98 and Gaussian 03 suites of quantum chemical programs.<sup>48</sup> All the stationary points on the respective potential energy surfaces were characterized at the same level of theory by evaluating corresponding Hessian indices. Enthalpies were obtained by adding scaled zero-point vibrational energy corrections (ZPVE)<sup>49</sup> and thermal contributions to the gas-phase energies using standard statistical mechanics procedures as implemented in the Gaussian suite. Careful verification of the unique imaginary frequencies for the transition states has been carried out to check whether the frequency indeed pertains to the desired reaction coordinate. Further, intrinsic reaction coordinate (IRC) calculations were carried out to authenticate the transition states.<sup>50,51</sup> Activation barriers refer to the enthalpy of activation, obtained as the energy difference between isolated reactants and the corresponding transition state structures. Enthalpies are calculated by adding scaled ZPVE (0.9806)<sup>49</sup> and

thermal contributions to the bottom-of-the-well energy values. Single-point energies were then calculated using a more flexible triple zeta quality basis set, namely the 6-311+G\*\* (with 6d-functions) with the continuum solvation model, using the SCRF-CPCM method,<sup>52</sup> with the united-atom Kohn–Sham (UAKS) radii. DMSO was used as the continuum solvent dielectric ( $\epsilon = 46.7$ ). All the SCRF calculations were performed with the default options implemented in Gaussian 03. These energy values include the solvent polarity effects, in the form of electrostatic terms, on the gas-phase-computed energies. Earlier reports have suggested that the electrostatic contributions are more important than the non-electrostatic terms in the continuum models.<sup>53</sup> The estimates based on these values are also found to be in very good agreement with the experimentally available selectivity known for proline.<sup>38</sup> Unless otherwise specified, the values reported within the SCRF-CPCM framework pertains to the free energy of solvation  $G_{\text{sol}}^{\text{el}}$  with all the electrostatic terms (denoted as  $E$  in the text). Full geometry optimizations with the continuum solvation model might lead to changes in geometries and energetics. Unfortunately, such calculations are prohibitively expensive on larger molecules (with regard to the level of theory) reported here. Further, the focus is on the relative energies of diastereomeric transition states than on the absolute activation parameters. One can therefore expect that the computed values should be sufficiently reliable to be able to draw meaningful conclusions.

## Acknowledgements

We are grateful to the Department of Science and Technology, New Delhi, for financial support (through SR/S1/OC-50/2003), and the IITB computer center for computing facilities. SCB acknowledges CSIR New Delhi for a Junior Research Fellowship.

## References and notes

- (a) G. Zhong, T. Hoffmann, R. A. Lerner, S. Danishefsky and C. F. Barbas, III, *J. Am. Chem. Soc.*, 1997, **119**, 8131; (b) G. Zhong, R. A. Lerner and C. F. Barbas, III, *Angew. Chem., Int. Ed.*, 1999, **38**, 3738; (c) P. I. Dalko and L. Moisan, *Angew. Chem., Int. Ed.*, 2001, **40**, 3726; (d) P. R. Schreiner, *Chem. Soc. Rev.*, 2003, **32**, 289; (e) P. I. Dalko and L. Moisan, *Angew. Chem., Int. Ed.*, 2004, **43**, 5138; (f) J. Seayad and B. List, *Org. Biomol. Chem.*, 2005, **3**, 719; (g) B. List and J. W. Yang, *Science*, 2006, **313**, 1584; (h) B. List, *Acc. Chem. Res.*, 2004, **37**, 548; (i) F. Cozzi, *Adv. Synth. Catal.*, 2006, **348**, 1367.
- (a) B. List, *Tetrahedron*, 2002, **58**, 5573; (b) M. Movassaghi and E. N. Jacobsen, *Science*, 2002, **298**, 1904; (c) A. B. Northrup and D. W. C. MacMillan, *J. Am. Chem. Soc.*, 2002, **124**, 6798; (d) A. B. Northrup, I. K. Mangion, F. Hettche and D. W. C. MacMillan, *Angew. Chem., Int. Ed.*, 2004, **43**, 2152; (e) M. Marigo, S. Bachmann, N. Halland, A. Braunto and K. A. Jorgenson, *Angew. Chem., Int. Ed.*, 2004, **43**, 5507.
- (a) K. Saktivel, W. Notz, T. Bui and C. F. Barbas, III, *J. Am. Chem. Soc.*, 2001, **123**, 5260; (b) E. R. Jarvo and S. J. Miller, *Tetrahedron*, 2002, **58**, 2481; (c) W. Notz, F. Tanaka and C. F. Barbas, III, *Acc. Chem. Res.*, 2004, **37**, 580; (d) E. Bellis and G. Kokotos, *Tetrahedron*, 2005, **61**, 8669; (e) Z. Tang, Z.-H. Yang, X.-H. Chen, L.-F. Cun, A.-Q. Mi, Y.-Z. Jiang and L.-Z. Gong, *J. Am. Chem. Soc.*, 2005, **127**, 9285; (f) J.-R. Chen, H.-H. Lu, X.-Y. Li, L. Cheng, J. Wan and W.-J. Xiao, *Org. Lett.*, 2005, **7**, 4543; (g) N. Halland, M. A. Lie, A. Kjærsgaard, M. Marigo, B. Schiott and K. A. Jorgenson, *Chem. Eur. J.*, 2005, **11**, 7083; (h) C. Cheng, C. Sun, C. Wang, Y. Zhang, S. Wei, F. Jiang and Y. Wu, *Chem. Commun.*, 2006, 215; (i) L. Gu, M. Yu, X. Wu, Y. Zhang and G. Zhao, *Adv. Synth. Catal.*, 2006, **348**, 2223.
- (a) Z. Tang, F. Jiang, L. Yu, X. Cui, L. Gong, A. Mi, Y. Jiang and Y. Wu, *J. Am. Chem. Soc.*, 2003, **125**, 5262; (b) K. N. Houk and P. H.-Y. Cheong, *Synthesis*, 2005, **9**, 1533.

- 5 (a) B. List, P. Pojarliev, W. T. Biller and J. M. Martin, *J. Am. Chem. Soc.*, 2002, **124**, 827; (b) S. Bahmanyar and K. N. Houk, *Org. Lett.*, 2003, **5**, 1249; (c) S. P. Brown, M. P. Brochu, C. J. Sinz and D. W. C. MacMillan, *J. Am. Chem. Soc.*, 2003, **125**, 10808; (d) N. Vignola and B. List, *J. Am. Chem. Soc.*, 2004, **126**, 450; (e) A. Fu, B. List and W. Thiel, *J. Org. Chem.*, 2006, **71**, 320.
- 6 Z. G. Hajos and D. R. Parrish, *J. Org. Chem.*, 1974, **39**, 1615.
- 7 (a) C. Agami, C. Puchot and J. Levisalles, *J. Chem. Soc., Chem. Commun.*, 1985, **441**; (b) C. Puchot, O. Samuel, E. Dunach, S. Zhao, C. Agami and H. B. Kagan, *J. Am. Chem. Soc.*, 1986, **108**, 2353.
- 8 S. Bahmanyar and K. N. Houk, *J. Am. Chem. Soc.*, 2001, **123**, 12911.
- 9 F. R. Clemente and K. N. Houk, *J. Am. Chem. Soc.*, 2005, **127**, 11294.
- 10 M. E. Jung, *Tetrahedron*, 1976, **32**, 3.
- 11 L. Hoang, S. Bahmanyar, K. N. Houk and B. List, *J. Am. Chem. Soc.*, 2003, **125**, 16.
- 12 (a) P. H.-Y. Cheong and K. N. Houk, *J. Am. Chem. Soc.*, 2004, **126**, 13912; (b) P. H.-Y. Cheong, H. Zhang, R. Thayumanavan, F. Tanaka, K. N. Houk and C. F. Barbas, III, *Org. Lett.*, 2006, **8**, 811.
- 13 (a) A. D. Becke, *J. Chem. Phys.*, 1993, **98**, 5648; (b) A. D. Becke, *Phys. Rev. A*, 1998, **38**, 3098; (c) C. Lee, W. Yang and R. G. Parr, *Phys. Rev. B*, 1998, **37**, 785.
- 14 (a) A. Córdova, *Angew. Chem., Int. Ed.*, 2005, **44**, 7028; (b) J. Joseph, D. B. Ramachary and E. D. Jemmis, *Org. Biomol. Chem.*, 2006, **4**, 2685.
- 15 (a) L. Hoang, S. Bahmanyar, K. N. Houk, H. J. Martin and B. List, *J. Am. Chem. Soc.*, 2003, **125**, 2475; (b) C. Allemand, R. Gordillo, F. R. Clemente, K. N. Houk and P. H.-Y. Cheong, *Acc. Chem. Res.*, 2004, **37**, 558.
- 16 M. S. Taylor and E. N. Jacobsen, *Angew. Chem., Int. Ed.*, 2006, **45**, 1520.
- 17 (a) K. N. Rankin, J. W. Gauld and R. J. Boyd, *J. Phys. Chem. A*, 2002, **106**, 5155; (b) L. R. Domingo and M. Arnó, *Theor. Chem. Acc.*, 2002, **108**, 232.
- 18 F. R. Clemente and K. N. Houk, *Angew. Chem., Int. Ed.*, 2004, **43**, 5766.
- 19 Gas phase activation enthalpies ( $\Delta H_{298K}$ ) have earlier been established to have smallest errors (when compared with experimentally determined activation parameters as well as enantioselectivities) for the proline-catalyzed asymmetric intermolecular aldol reaction between acetone or cyclohexanone with a number of electrophiles such as benzaldehyde, isobutyraldehyde and so on. See ref. 15a.
- 20 (a) G. Ujaque, F. Maseras and A. Lledós, *J. Am. Chem. Soc.*, 1999, **121**, 1317; (b) J. Vázquez, M. A. Pericas, F. Maseras and A. Lledós, *J. Org. Chem.*, 2000, **65**, 7303; (c) D. Balcells, F. Maseras and G. Ujaque, *J. Am. Chem. Soc.*, 2005, **127**, 3624.
- 21 (a) B. A. Grzybowski, A. V. Ishchenko, J. Shimada and E. I. Shakhnovich, *Acc. Chem. Res.*, 2002, **35**, 261; (b) H. M. Howard, T. Cenizal, S. Gutteridge, W. S. Hanna, Y. Tao, M. Totrov, V. A. Wittenbach and Y.-J. Zheng, *J. Med. Chem.*, 2004, **47**, 6669; (c) M. C. Kozlowski, S. P. Waters, J. W. Skudlarek and C. A. Evans, *Org. Lett.*, 2002, **4**, 4391; (d) M. Panda, M. C. Kozlowski and P.-W. Phuan, *J. Org. Chem.*, 2003, **68**, 564.
- 22 (a) J. A. Cobb, D. M. Shaw, D. A. Longbottom, J. B. Gold and S. V. Ley, *Org. Biomol. Chem.*, 2005, **3**, 84; (b) Y. Hayashi, T. Sumiya, J. Takahashi, H. Gotoh, T. Urushima and M. Shoji, *Angew. Chem., Int. Ed.*, 2006, **45**, 958; (c) L. Zu, J. Wang, H. Li and W. Wang, *Org. Lett.*, 2006, **8**, 3077; (d) S. Luo, X. Mi, L. Zhang, S. Liu, H. Xu and J.-P. Cheng, *Angew. Chem., Int. Ed.*, 2006, **45**, 3093.
- 23 For a report on 4,5-methanoprolines, see: K. N. Houk, J. S. Warrier, S. Hanessian and P. H.-Y. Cheong, *Adv. Synth. Catal.*, 2004, **346**, 1111.
- 24 (a) A. Córdova, W. Zou, I. Ibrahim, E. Reyes, M. Engqvist and W. Liao, *Chem. Commun.*, 2005, 3586; (b) A. Córdova, W. Zou, P. Dziedzic, I. Ibrahim, E. Reyes and Y. Xu, *Chem. Eur. J.*, 2006, **12**, 5383.
- 25 E. Czink and A. G. Császár, *Chem. Eur. J.*, 2003, **9**, 1008.
- 26 (a) J. K. M. Sanders, *Chem. Eur. J.*, 1998, **4**, 1378; (b) A. Wittkopp and P. R. Schreiner, *Chem. Eur. J.*, 2003, **9**, 407.
- 27 See Table S4† on the synthetic availability or other applications of some of these proposed molecules.
- 28 J. Gante, *Angew. Chem., Int. Ed. Engl.*, 1994, **33**, 1699.
- 29 S. F. Nelson, J. T. Ippoliti, T. B. Frigo and P. A. Petillo, *J. Am. Chem. Soc.*, 1989, **111**, 1776.
- 30 C. Aleman, A. I. Jimenez, C. Cativiela, J. J. Perez and J. Casanovas, *J. Phys. Chem. B*, 2005, **109**, 11836.
- 31 Interestingly, such a restricted pyrrolidine conformation has been found as part of the natural product epibatidine. See: T. F. Spande, H. M. Garraffo, M. W. Edwards, L. Panel and J. W. Daly, *J. Am. Chem. Soc.*, 1992, **114**, 3475.
- 32 See Table S5† for the relative energies of the *syn*- and *anti*-enamines formed between acetone and catalysts **1–11**.
- 33 Similar geometric features for TSs in proline-catalyzed aldol reactions have been noticed previously. See ref. 8,15a.
- 34 The planarity of enamines have been studied in detail using X-ray crystallographic techniques; see: K. L. Brown, L. Damm, J. D. Dunitz, A. Eschenmoser, R. Hobi and C. Kratky, *Helv. Chim. Acta*, 1978, **61**, 3108.
- 35 A full list of  $C_{\text{ring}}-\text{N}-\text{C}-\text{Cl}_{\text{minut}}$  dihedral angles (given in Fig. 1 as  $\theta_1-\theta_4$ ) are provided in Table S3†.
- 36 Hybrid Hartree–Fock DFT methods such as B3LYP can lead to systematic errors in estimating C–H $\cdots$  $\pi$  interactions. We have therefore carried out additional single-point energy calculations using the *ab initio* MP2 method. Interestingly, the enantiomeric excess calculated based on the energies obtained at the MP2/6-311G\*\*//B3LYP/6-31G\* level for a representative catalyst **1** (85%) is found to be in good agreement with the ee calculated at the CPCM<sub>(DMSO)</sub>/B3LYP/6-311G\*\*//B3LYP/6-31G\* level (87%). While inclusion of higher-order electron correlation might result in changes in the predicted enantiomeric excess, the trends are likely to remain the same across the range of catalysts proposed here. Considering the size of the catalyst–substrate complex, these calculations would be prohibitively expensive.
- 37 This is reminiscent of the  $\alpha$ -effect proposed in Diels–Alder reactions catalyzed by iminium ions; see: N. C. O. Tomkinson, J. L. Cavill and J. Peters, *Chem. Commun.*, 2003, 728.
- 38 The enantiomeric excess calculated based on the energies obtained at the CPCM<sub>(DMSO)</sub>/B3LYP/6-311G\*\*//B3LYP/6-31G\* level for the proline-catalyzed aldol reaction between acetone and *p*-nitrobenzaldehyde is given in Table S8†.
- 39 (a) A difference in dihedral angle value of 25° for the carboxylic acid orientation ( $\omega_2$ ) is noticed between unsubstituted and substituted cases; (b) the ee calculated for the **4** C(β)Cl-catalyzed aldol reaction is 90%.
- 40 The C(β)H $\cdots$ O $^{\delta-}$ alkoxide distance in the *s-re* TS geometry for catalyst **5** (Fig. 2c) is 2.31 Å, whereas the corresponding distance in catalyst **4** is 2.47 Å (Fig. 2a).
- 41 For a complete description of transition state structural parameters for all the catalysts, see Table S1 and S2†.
- 42 See Fig. S3†.
- 43 See Fig. S4† for optimized geometries of the lowest energy TSs for catalyst **10**.
- 44 (a) H. Zhang, M. Mifsud, F. Tanaka and C. F. Barbas, III, *J. Am. Chem. Soc.*, 2006, **128**, 9630; (b) S. Mitsumori, H. Zhang, P. H.-Y. Cheong, K. N. Houk, F. Tanaka and C. F. Barbas, III, *J. Am. Chem. Soc.*, 2006, **128**, 1040.
- 45 Depending on how the enamine double bond is positioned with respect to the carboxylic acid group (nearer or farther away), it is termed as a *syn*-enamine and *anti*-enamine, respectively. See Fig. S5†.
- 46 (a) Calculated activation barriers and enantiomeric excesses are summarized in Table S6 and S7†; (b) Please see Fig. S2† for the optimized geometries of the lowest energy TSs for the aldol reaction between acetone and 2,6-dimethyl-4-nitrobenzaldehyde catalyzed by **2**.
- 47 (a) R. Ditchfield, W. J. Hehre and J. A. Pople, *J. Chem. Phys.*, 1971, **54**, 724; (b) W. J. Hehre, R. Ditchfield and J. A. Pople, *J. Chem. Phys.*, 1972, **56**, 2257; (c) P. C. Hariharan and J. A. Pople, *Theor. Chim. Acta*, 1973, **28**, 213.
- 48 (a) M. J. Frisch, *Gaussian 98 (Revision A.11.4)*, Gaussian, Inc., Pittsburgh, PA, 2002; (b) M. J. Frisch, *Gaussian 03 (Revision C.02)*, Gaussian, Inc., Wallingford, CT, 2004. See the ESI† for the full citation.
- 49 A. P. Scott and L. Radom, *J. Phys. Chem.*, 1996, **100**, 16502.
- 50 (a) C. Gonzalez and H. B. Schlegel, *J. Chem. Phys.*, 1989, **90**, 2154; (b) C. Gonzalez and H. B. Schlegel, *J. Phys. Chem.*, 1990, **94**, 5523.
- 51 See Table S9† for the IRC profiles for the lowest energy transition states of catalysts **1–11**.
- 52 (a) M. Cossi, V. Barone, R. Cammi and J. Tomasi, *J. Chem. Phys. Lett.*, 1996, **255**, 327; (b) E. Cancès, B. Mennucci and J. Tomasi, *J. Chem. Phys.*, 1997, **107**, 3032.
- 53 (a) D. W. Tondo and J. R. Pliego, Jr., *J. Phys. Chem. A*, 2005, **109**, 507; (b) G. Alagona, C. Ghio and S. Monti, *Phys. Chem. Chem. Phys.*, 2002, **2**, 4884.

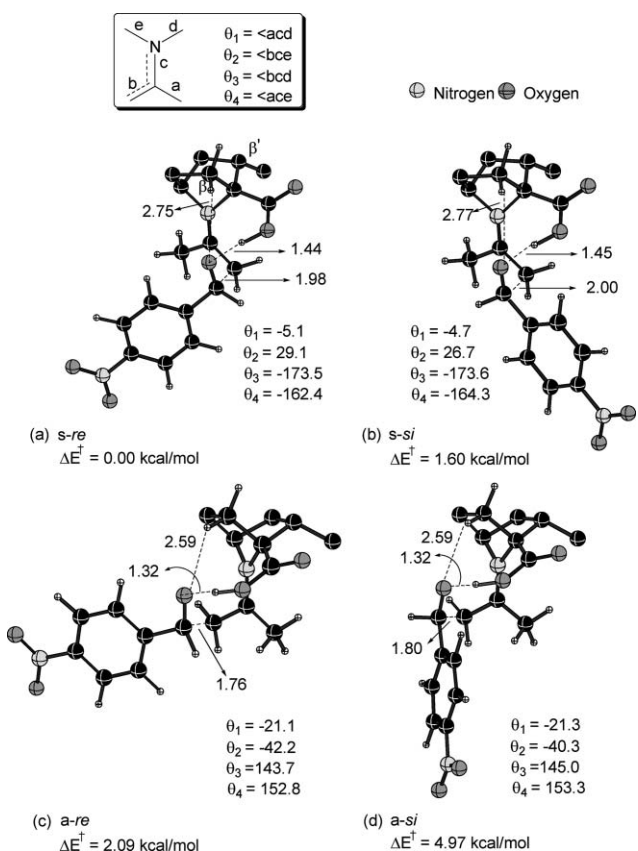


**Fig. 1** The B3LYP/6-31G\*-optimized transition state geometries for four unique stereochemical modes of addition for enamines derived from catalyst **1** to *p*-nitrobenzaldehyde. Only selected hydrogens on the catalyst are shown for clarity. Activation barriers  $\Delta E^\ddagger$  were obtained at the CPCM/B3LYP/6-311+G\*\*//B3LYP/6-31G\* level using DMSO as the solvent. Angles are given in degrees and distances in Å.

catalyst **1** imply a nearly planar geometry around the iminium nitrogen. The deviation for the *syn*-enamine additions are found to be only about  $\pm 5^\circ$ , whereas the corresponding values for the a-*re* and a-*si* TSs are of the order of  $\pm 35^\circ$ , indicating a larger geometric distortion for the developing iminium ion. Such deviations lead to reduced electrostatic stabilization in the TSs and perhaps result in higher activation barriers for *anti*-enamine additions than for *syn*-enamines. Interestingly, the differences in activation barriers between the *syn*- and *anti*-enamine additions are much more pronounced in [2.1.1] bicyclic catalysts (**3**, **5** and **7**) than in [2.2.1] bicyclic systems. It may be noticed that the rigidity of the [2.1.1] bicyclic framework leads to a less favourable proton transfer from the carboxylic acid group to the developing alkoxide in the *anti*-enamine TSs. Such a proton transfer is facilitated at the expense of greater geometric distortion around the developing iminium nitrogen.<sup>35</sup> Another contributing factor helping to achieve additional stabilization for the s-*re* TSs presumably originates from the C–H $\cdots$ π stabilizing interaction between the CH<sub>3</sub>-hydrogens of the enamine/iminium with the aryl group of the aldehyde (Fig. 1a).<sup>36</sup> Other stereoisomeric TSs involved in this example (*i.e.*, s-*si* as well as a-*re*/a-*si* TSs) lack such interactions. The relative activation barriers would eventually depend on the presence or absence of all these stabilizing interactions. The relative activation enthalpies calculated based on

**Table 1** Computed activation barriers ( $\Delta E^\ddagger$ ) obtained at the CPCM<sub>(DMSO)</sub>/B3LYP/6-311+G\*\*//B3LYP/6-31G\* level for the addition of enamines to *p*-nitrobenzaldehyde, and the corresponding enantiomeric excess for catalysts **1** to **7**<sup>a</sup>

Catalyst	Mode of approach	$\Delta E^\ddagger$ / kcal mol <sup>-1</sup> <sup>b</sup>		
		Absolute	Relative	ee (%)
<b>1</b>	a- <i>re</i>	4.52 (6.77)	2.09 (2.20)	87 (87)
	a- <i>si</i>	7.40 (9.59)	4.97 (5.02)	
	s- <i>re</i>	4.13 (6.16)		
	s- <i>si</i>	5.73 (7.75)	1.60 (1.58)	
<b>2</b>	a- <i>re</i>	0.59 (3.95)	2.38 (2.84)	85 (85)
	a- <i>si</i>	3.56 (6.79)	5.35 (5.69)	
	s- <i>re</i>	4.93 (6.69)	0.00 (0.00)	
	s- <i>si</i>	6.43 (8.21)	1.50 (1.52)	
<b>3</b>	a- <i>re</i>	12.22 (15.35)	13.04 (14.57)	82 (87)
	a- <i>si</i>	15.28 (18.25)	16.11 (15.86)	
	s- <i>re</i>	0.59 (6.29)	0.00 (0.00)	
	s- <i>si</i>	1.96 (7.89)	1.37 (1.60)	
<b>4</b>	a- <i>re</i>	8.26 (10.47)	3.75 (4.02)	91 (92)
	a- <i>si</i>	11.22 (17.24)	6.72 (10.79)	
	s- <i>re</i>	7.16 (8.94)	0.00 (0.00)	
	s- <i>si</i>	8.99 (10.87)	1.82 (1.93)	
<b>5</b>	a- <i>re</i>	12.15 (15.69)	13.31 (14.28)	92 (89)
	a- <i>si</i>	31.32 (2.21)	32.48 (2.91)	
	s- <i>re</i>	3.25 (6.71)	0.00 (0.00)	
	s- <i>si</i>	5.18 (8.43)	1.93 (1.72)	
<b>6</b>	a- <i>re</i>	22.91 (25.75)	20.59 (20.52)	90 (91)
	a- <i>si</i>	10.17 (13.30)	7.85 (8.08)	
	s- <i>re</i>	11.02 (8.06)	0.00 (0.00)	
	s- <i>si</i>	12.81 (9.88)	1.79 (1.81)	
<b>7</b>	a- <i>re</i>	21.66 (22.33)	16.10 (16.24)	84 (85)
	a- <i>si</i>	24.87 (25.43)	19.31 (19.34)	
	s- <i>re</i>	-0.97 (1.16)	0.00 (0.00)	
	s- <i>si</i>	0.49 (2.67)	1.47 (1.50)	

<sup>a</sup> The graphic shows a schematic representation of the TSs corresponding to the attack of the *anti/syn*-enamine on the *re/si* face of the aldehyde (for catalyst **3**). <sup>b</sup> Gas-phase activation barriers  $\Delta H^\ddagger_{298\text{K}}$  including scaled zero-point energies obtained at the B3LYP/6-311+G\*\*//B3LYP/6-31G\* level are given in parentheses.

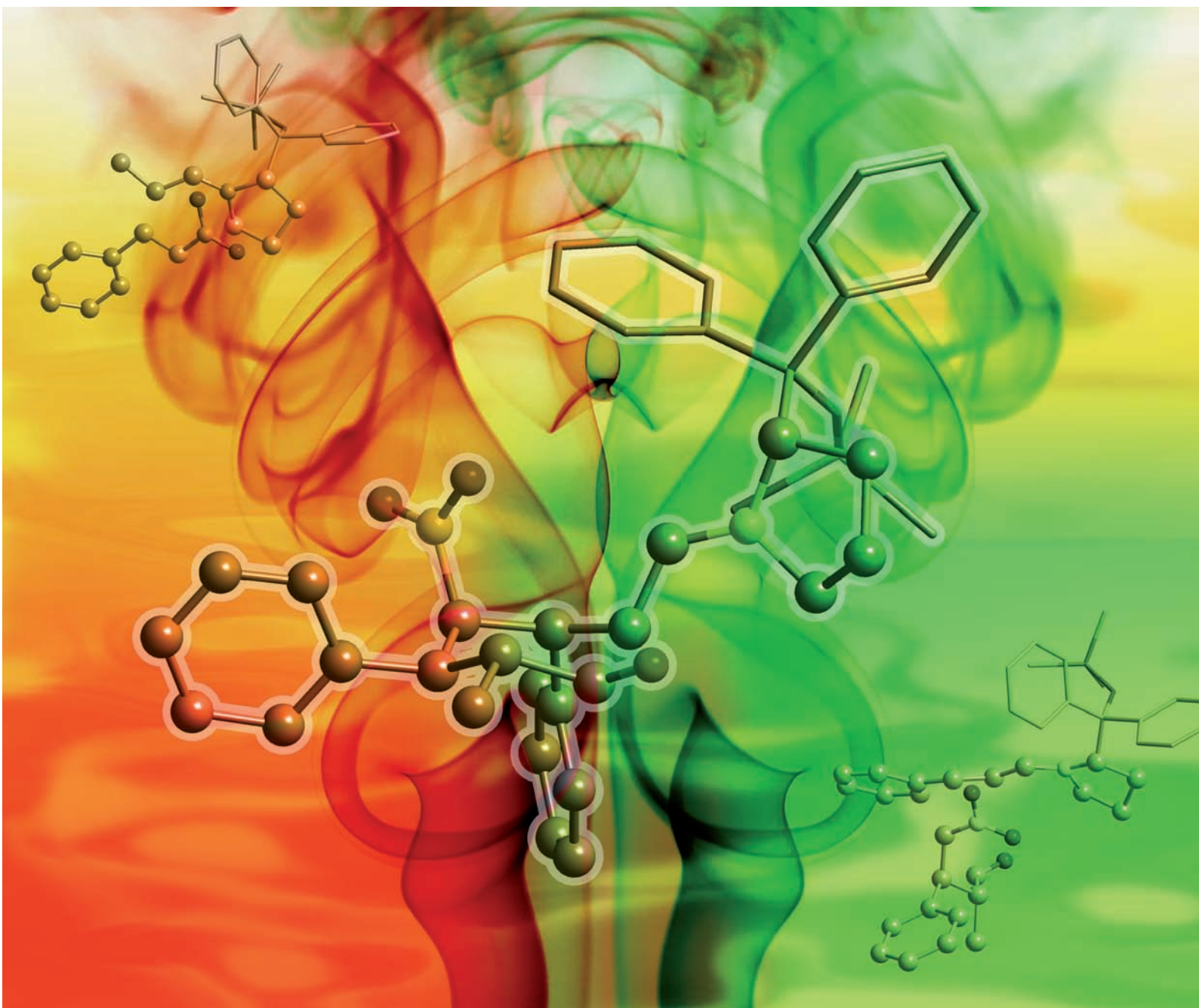
the lowest-energy TSs and the corresponding enantiomeric excess for all the proposed catalysts in this series are summarized in Table 1.

On the basis of the calculated absolute and relative activation barriers, it is noticed that the *syn*-enamines (s-*re*) derived from catalysts **1**–**7** tend to exhibit a general preference for *re*-face attack on the aldehyde. The TSs belonging to this series enjoy an additional C(β)H $\cdots$ O hydrogen bonding stabilization between the developing alkoxide and a suitably aligned C(β) hydrogen, as depicted in Fig. 1. The conformation of pyrrolidine in the bicyclic systems aids the formation of these favourable weak interactions, which could influence the relative stabilization of the diastereomeric TSs. As a rational design strategy, we envisaged that fine-tuning the acidity of C(β)H might have a direct bearing on the relative energies of the TSs. Thus, replacement of adjacent C(γ) methylene group of the azabicyclic system by more electronegative heteroatoms was considered. The presence of an α-heteroatom will impart enhanced acidity to the C(β) hydrogen and thus will

# Organic & Biomolecular Chemistry

www.rsc.org/obc

Volume 6 | Number 21 | 7 November 2008 | Pages 3865–4068



ISSN 1477-0520

RSC Publishing

**FULL PAPER**

C. B. Shinisha and Raghavan B. Sunoj  
Unraveling high precision  
stereocontrol in a triple cascade  
organocatalytic reaction

**Chemical Biology**

In this issue...



1477-0520(2008)6:21;1-J

# Unraveling high precision stereocontrol in a triple cascade organocatalytic reaction†

C. B. Shinisha and Raghavan B. Sunoj\*

Received 26th June 2008, Accepted 13th August 2008  
First published as an Advance Article on the web 12th September 2008  
DOI: 10.1039/b810901j

The mechanism and stereoselectivity in an organocatalyzed triple cascade reaction between an aldehyde, electron deficient olefin and an  $\alpha,\beta$ -unsaturated aldehyde are investigated for the first time using density functional theory. The factors responsible for high levels of observed stereoselectivity (Enders *et al.*, *Nature*, 2006, **441**, 861) towards the generation of cyclohexene carbaldehyde with four contiguous stereocentres are unravelled. The triple cascade reaction, comprising a Michael, Michael and aldol sequence as the key elementary reactions, is studied by identifying the corresponding transition states for the stereoselective C–C bond-formation. In the first Michael addition step between the enamine (derived from the chiral catalyst and propanal) and nitrostyrene, energetically the most preferred mode of addition is found to be between the *si*-face of (*E*)-*anti*-enamine on the *si*-face of nitrostyrene. The addition of the *si*-face of the nitroalkane anion on the *re*-face of the iminium ion (formed between the enal and the catalyst) is the lowest energy pathway for the second Michael addition step. The high level of asymmetric induction is rationalized with the help of relative activation barriers associated with the competitive diastereomeric pathways. Interesting weak interactions, along with the steric effects offered by the bulky  $\alpha$ -substituent on the pyrrolidine ring, are identified as critical to the stereoselectivity in this triple cascade reaction. The predicted stereoselectivities using computed energetics are found to be in perfect harmony with the experimental stereoselectivities.

## Introduction

Asymmetric multicomponent domino reactions have emerged as a powerful strategy for the synthesis of complex molecules with multiple stereocentres. The synthetic potential of domino reactions has been utilized in efficient and stereoselective construction of several targets, starting from relatively simple precursors.<sup>1</sup> Most significantly, the creation of many stereocentres is possible by using a single catalyst in *one pot*, without the isolation of intermediates or changing the reaction conditions. These domino reactions are reminiscent of biomimetic pathways, as they resemble the biosynthesis of complex natural products from simple precursors as building blocks.<sup>2</sup>

The recent overwhelming activities in organocatalysis<sup>3</sup> have set the stage for a number of interesting organocatalytic cascade reactions towards the construction of complex molecular structures.<sup>4</sup> The organocatalytic cascade reactions are often accompanied by high levels of stereocontrol achieved through chiral organocatalysts. The successful implementation of organocatalysts in cascade reactions can generate functionalized polycyclic bioactive molecules.<sup>5</sup> Among current organocatalysts, chiral secondary amines are more frequently employed to activate substrate(s) as enamine/iminium species, which in turn can participate in a range of reactions with a multitude of electrophiles.<sup>6</sup> The

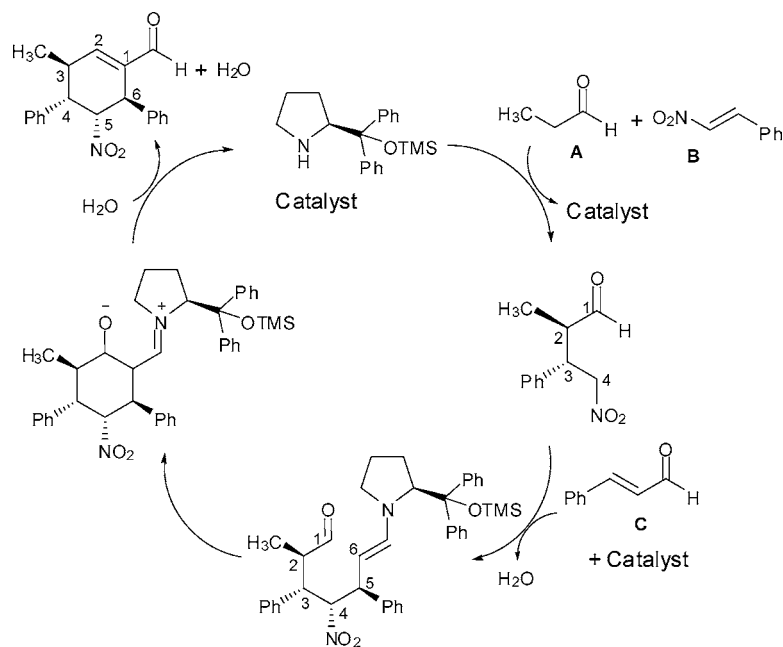
intermediates thus generated may not be stable enough and amenable for isolation, but permit quick transformation into more stable products through a subsequent reaction sequence. The stereoselectivity of these reactions is controlled in the bond formation step, either through hydrogen bond directed Brønsted acid catalysis as in proline<sup>7</sup> or a steric control approach as in diphenyl prolinol ethers.<sup>8</sup> The combination of different activation modes allows the design of innovative domino sequences to tackle high level stereochemical complexity of desired targets. Therefore, the organocatalytic reactions can ideally be exploited in designing tandem processes.

In a very recent study, Enders and co-workers have demonstrated an elegant asymmetric organocatalytic triple cascade reaction involving a linear aldehyde (**A**), a nitroalkene (**B**) and an  $\alpha,\beta$ -unsaturated aldehyde (**C**) towards constructing a tetrasubstituted cyclohexene carbaldehyde with a high degree of diastereoselectivity and complete enantiocontrol.<sup>9</sup> The reaction, as shown in Scheme 1, employed diphenylprolinol trimethylsilyl ether as the catalyst. It is also of interest to note that recently, diphenyl siloxy proline ethers have successfully been used as catalysts in a variety of reactions,<sup>10</sup> including cascade reactions.<sup>11</sup> Enders's triple cascade reaction is an exquisite example that includes the advantages of domino reactions as well as asymmetric organocatalysis. It should be noted that a suitably designed cascade reaction of this kind could open up convenient inroads into several polyfunctional cyclohexene building blocks with high levels of stereocontrol.

The present cascade reaction involves two conjugate additions followed by an intramolecular aldol cyclization. The first step is a Michael addition between propanal and nitrostyrene. The catalyst forms a chiral enamine with the aldehyde (**A**), which subsequently

Department of Chemistry, Indian Institute of Technology Bombay, Powai, Mumbai, 400076, India. E-mail: sunoj@chem.iitb.ac.in; Fax: 91-22-2572-3480 or 91-22-2576-7152

† Electronic supplementary information (ESI) available: The optimized geometries of all the transition states in the form of Cartesian coordinates, Figures S1–S4 and Tables S1–S10. See DOI: 10.1039/b810901j



**Scheme 1** Proposed catalytic cycle for the diphenylprolinol trimethylsilyl ether catalyzed triple cascade reaction for the generation of tetrasubstituted cyclohexene carbaldehydes.

adds to the nitroolefin.<sup>12</sup> A number of chiral pyrrolidines without a proton donating group have been remarkably successful in giving good yield and high enantioselectivity in such conjugate additions.<sup>13</sup> Here, the higher reactivity of the nitroolefin with the activated aldehyde can help supersede the possible iminium ion formation between the catalyst and the available  $\alpha,\beta$ -unsaturated aldehyde. After the first Michael addition, the catalyst liberated on hydrolysis can form an iminium ion<sup>14</sup> with the  $\alpha,\beta$ -unsaturated aldehyde (**C**) to accomplish the conjugate addition with the nitroalkane formed in the first step.<sup>15</sup> In the third step, the enamine intermediate formed from the second step undergoes cyclization through an intramolecular aldol reaction. The subsequent aldol cyclization and hydrolysis release the tetrasubstituted cyclohexene carbaldehyde. Enders *et al.* have further extended this domino reaction for the synthesis of poly substituted bicyclic and tricyclic carbon frameworks.<sup>16</sup>

Albeit qualitative proposals on the plausible mechanism of this organocatalytic cascade reaction are documented, clear insights into how such precise stereocontrol arises are evidently not reported. In this triple cascade reaction, four contiguous stereocentres are generated with such high precision that only two epimers are isolated out of 16 possible stereoisomers. Such remarkable stereocontrol prompted us to probe the origins of observed high stereoselectivity. As part of our ongoing efforts to understand stereoselectivities in organocatalytic reactions,<sup>17</sup> we have decided to investigate the energetics as well as the controlling factors contributing to stereoselectivity using computational methods. The present study offers the first comprehensive report on the stereoselectivity in organocatalytic cascade reactions. The insights obtained through modeling of experimentally known examples could later be utilized for rational design of new organocatalysts suitable for domino reactions. Also, the insights could help design cascade reactions towards specific target molecules with considerable structural and stereochemical complexity.

## Computational methods

A full DFT calculation on the present reaction, consisting of a fairly large number of atoms, will evidently be costly. On the other hand, semi-empirical approaches could be flawed by an imperfect description of the transition states leading to poorer energetic estimates. We have therefore used a combination of density functional theory (B3LYP/6-31G\*) and semi-empirical MO methods (AM1) with a hybrid ONIOM2 scheme denoted as ONIOM2(B3LYP/6-31G(d):AM1) using the Gaussian03 suite of quantum chemical programs.<sup>18,19</sup> In the ONIOM2(B3LYP/6-31G(d):AM1) approach, the energy of the *real* system at the *high* level can be estimated using an extrapolation scheme as,  $E(\text{ONIOM},\text{real}) = E(\text{high},\text{model}) + E(\text{low},\text{real}) - E(\text{low},\text{model})$ . This approach has been successful in explaining the mechanism as well as stereoselectivity of organic reactions.<sup>20</sup>

The geometry optimizations of reactants, intermediates, transition states and products were carried out using the ONIOM2 method described above. All of the transition states were characterized as first order saddle points and the imaginary frequencies were confirmed to represent the desired reaction coordinate. Additionally, we have carried out 10% displacement of the transition state geometry along the direction of the imaginary vibrational frequency and subsequently reoptimized the perturbed structure using the “calcfc” option available in the program. This was to ensure whether the transition state is genuine and connects reactants and product. The single-point energies were subsequently calculated at the B3LYP/6-31G\* level<sup>21,22</sup> using the ONIOM2 optimized geometries. The DFT single-point energies are used throughout the manuscript, unless otherwise specified.

According to the general recommendations given by Morokuma *et al.* for a multi-layer hybrid calculation, a substituent value test (*S*-value test) is performed. This is to examine how good the partition scheme and the corresponding model chemistries are for

the present system. The *S*-value is defined as  $S$  (level) =  $E$  (level, real) –  $E$  (level, model). The *S*-value is determined on the basis of the relative energies of **TS-1f** and **TS-1a** (*vide infra*). The  $\Delta S$  (high) and  $\Delta S$  (low) are respectively found to be only 0.07 and 1.04 kcal mol<sup>-1</sup>. The error associated with the ONIOM extrapolation is therefore ( $E_{(\text{ONIOM,real})} - E_{(\text{high, real})}$ ) estimated as 0.97 kcal mol<sup>-1</sup>, which is well within the recommended error tolerance limit of 2 kcal mol<sup>-1</sup>.<sup>18b</sup>

## Results and discussion

The stereoselectivity of the triple cascade reaction is studied by focusing on the critical C–C bond-formation steps. First, a fully optimized geometry of the catalyst obtained at the B3LYP/6-31G\* level is partitioned into two layers for subsequent optimization using the ONIOM2 method. The most crucial part of the reacting system (inner layer) is described using the density functional theory while the pyrrolidine  $\alpha$ -substituent (diphenyl(trimethyl)siloxymethyl group) is treated as the outer layer using the semi-empirical AM1 method.<sup>23</sup> The resulting dangling bond between the model system and the remainder of the molecule is saturated using a link atom. The geometric parameters of the catalyst optimized separately using the B3LYP/6-31G\* and ONIOM2 are found to be in good agreement with each other.<sup>24</sup> The lowest energy conformer of the catalyst with the same layering scheme is chosen for further calculations of the cascade reaction sequence using the ONIOM2 approach.<sup>25</sup>

For the Michael addition step between propanal-enamine and nitrostyrene,<sup>26</sup> multiple modes of approach are possible. We have considered additions involving the sterically unhindered face of the enamine intermediate on both the *re* and the *si* faces of (*E*)-nitrostyrene.<sup>27</sup> The enamine derived from propanal and the catalyst can have four key conformers arising from the *E/Z* configuration of the enamine double bond as well as the *syn/anti* orientations. The *syn* and *anti* descriptors denote the orientation of the enamine double bond with respect to the  $\alpha$ -substituent on

the pyrrolidine ring. These notations would be used hereafter to specify the enamine double bond orientations. In the addition step, the transition states are expected to maintain a staggered orientation of the substituents around the incipient C–C bond. The *re/si* face of (*E*)-nitrostyrene and enamine may adopt six staggered orientations around the developing C–C bond. Considering the four key conformers of enamine, the first step of the cascade cycle can have 24 transition states. The geometry optimization of various enamine configurations and conformers reveals that the *Z* isomer is in general higher in energy than the corresponding *E* isomer in both *syn* and *anti* enamines. In particular, the (*Z*)-*syn*-enamine is found to be 10.7 kcal mol<sup>-1</sup> higher in energy than the (*E*)-*anti*-enamine at the B3LYP/6-31G\* level of theory.<sup>28</sup> Further investigations therefore exclude (*Z*)-*syn*-enamine, leaving behind 18 key transition states leading to four possible diastereomeric products. A representative set of these transition state possibilities for the addition of (*E*)-*anti*-enamine to (*E*)-nitrostyrene (**1a–1f**) is provided in Fig. 1.

Among the various stereochemically relevant possibilities, the attack of the (*E*)-*anti*-enamine (using its *si*-face) on the *si*-face of nitrostyrene (**TS-1f**) is identified as energetically the most preferred transition state for the Michael addition. In fact, **TS-1f** is found to be relatively more stable by 5.0 kcal mol<sup>-1</sup> than the nearest lower energy transition state (**TS-1a**), which leads to the (*2R,3R*) diastereomer. It can be noticed from the computed activation barriers (Table 1) that the bulky substituent at the  $\alpha$ -position plays a steering role in promoting the Michael addition from the *anti*-enamine. The activation barriers associated with the *syn*-enamine additions are evidently higher than the corresponding *anti*-enamines. Further, the presence of a bulky  $\alpha$ -substituent effectively shields the *re*-face of the (*E*)-*anti*-enamine from Michael acceptors. The most interesting consequence of the above features offered by the catalyst and the accompanying energetics is high precision diastereoselectivity. The lowest energy transition state **TS-1f** leads to (*2R,3S*) nitroalkane, which is in perfect accordance with the experimental reports.<sup>30</sup> The predicted enantiomeric excess

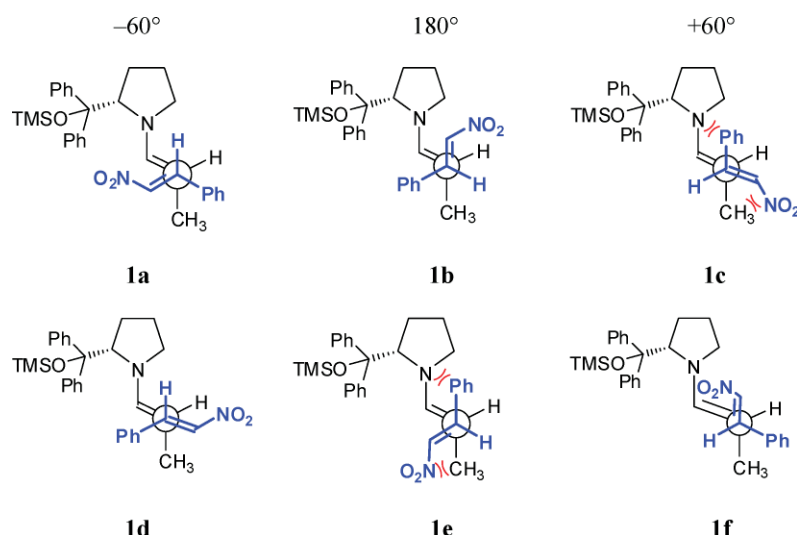


**Fig. 1** Key conformers of the transition states for the first Michael addition of (*E*)-*anti*-enamine to the *re/si* face of nitrostyrene. These conformers are grouped on the basis of the dihedral angle between the enamine double bond and the hydrogen of the nitrostyrene (as indicated) with dihedral angles of  $-60^\circ$ ,  $+180^\circ$  and  $+60^\circ$ .

**Table 1** The computed activation barriers ( $\Delta E^\ddagger$ ) at the B3LYP/6-31G\*//ONIOM2(B3LYP/6-31G\*:AM1) level for the addition of enamines to (*E*)-nitrostyrene

Enamine	Enamine-nitrostyrene prochiral faces	Product configuration	Transition state	$\Delta E^\ddagger$ in kcal mol <sup>-1</sup> <sup>a</sup>	
				Absolute	Relative
<i>(E)</i> -anti	<i>si</i> → <i>re</i>	( <i>R,R</i> )	<b>TS-1a</b>	28.4	5.0
	<i>si</i> → <i>re</i>	( <i>R,R</i> )	<b>TS-1b</b>	31.8	8.4
	<i>si</i> → <i>si</i>	( <i>R,S</i> )	<b>TS-1d</b>	31.7	8.3
	<i>si</i> → <i>si</i>	( <i>R,S</i> )	<b>TS-1f</b>	23.4	<b>0.0</b>
<i>(Z)</i> -anti	<i>re</i> → <i>re</i>	( <i>S,R</i> )	<b>TS-2a</b>	28.2	7.0
	<i>re</i> → <i>si</i>	( <i>S,S</i> )	<b>TS-2f</b>	29.1	7.9
<i>(E)</i> -syn	<i>re</i> → <i>re</i>	( <i>S,R</i> )	<b>TS-3a</b>	29.6	6.5
	<i>re</i> → <i>re</i>	( <i>S,R</i> )	<b>TS-3c</b>	33.3	10.2
	<i>re</i> → <i>si</i>	( <i>S,S</i> )	<b>TS-3e</b>	33.2	10.1
	<i>re</i> → <i>si</i>	( <i>S,S</i> )	<b>TS-3f</b>	33.6	10.5

<sup>a</sup> Absolute energy barriers are calculated with respect to the separated reactants and the relative energy barriers with respect to the energy of the lowest energy TS.

of >99% is found to be the same as the experimental reports by Hayashi *et al.* on the Michael addition between propanal enamine and nitrostyrene.<sup>30</sup>

While attempting to locate other transition state conformers for (*E*)-anti-enamine addition to the nitrostyrene, two important gauche interactions appeared quite prominent. These include the unfavorable interaction between (i) the phenyl ring on the

electrophile and the pyrrolidine ring, (ii) the nitro on the electrophile and the methyl of the enamine moiety. In general, it is noticed that such interactions tend to increase the energy of the addition transition states. Further, repeated attempts to identify **1c** and **1e** (Fig. 2) resulted in rotation around the incipient C–C bond during geometry optimization and it was found that they reverted to the nearest lower energy transition states such as **TS-1a**

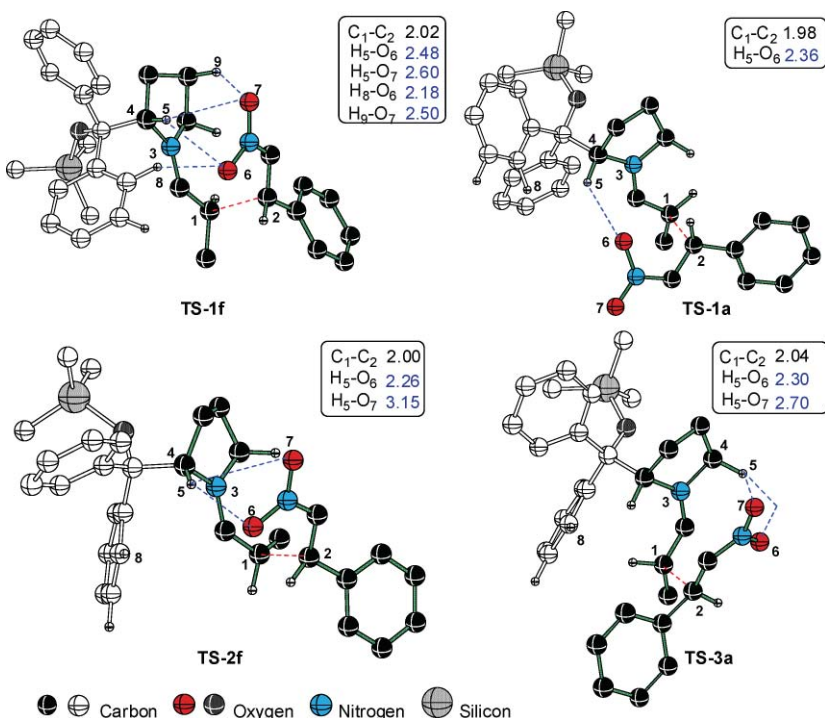


**Fig. 2** The ONIOM2(B3LYP/6-31G\*:AM1) optimized lower energy diastereomeric transition state geometries for the addition of enamine derived from the catalyst and propanal to (*E*)-nitrostyrene. Only selected hydrogens are shown for clarity. Distances are given in Å.

and **TS-1f**.<sup>31</sup> Interestingly, **TS-1a** and **TS-1f** are devoid of gauche interactions of the above kind. It is therefore evident that the substituents and geometries of the enamine and nitrostyrene exert a direct control on the stereochemical outcome of the reaction.

A number of stabilizing interactions are identified as responsible for the differential stabilization between the transition states. The developing nitroxide in **TS-1f** is found to be stabilized by a network of weak hydrogen bonding interactions as shown in Fig. 2. For instance, the distance between the methylene hydrogens of the pyrrolidine ring and the oxygens of the nitro group are between 2.5 and 2.6 Å. The optimized geometries of other diastereomeric transition states evidently reveal that the above-mentioned stabilizing interaction is not as effective as in **TS-1f**. Another noticeable stabilizing interaction in **TS-1f** is between the -NO<sub>2</sub> group and the aryl hydrogens of the α-substituent on the pyrrolidine ring. Such additional stabilizations in **TS-1f** are nearly absent in any other lower energy diastereomeric transition states. It is further noticed that the C-γ heads the envelope conformation of the pyrrolidine ring in **TS-1f**, whereas it is C-β in **TS-1a**. Hence in **TS-1f**, the C-γ hydrogen offers additional stabilization to the nitro group of the electrophile (as evident from the C-H···O distance of 2.5 Å). We have identified a bond path and the corresponding bond critical point (bcp) using the AIM theory for these interactions.<sup>32</sup> **TS-1a** on the other hand, lacks such additional weak interactions, except that due to the α-methylene of the pyrrolidine ring. Additionally, an electrostatic stabilization between the partially negative pyrrolidine nitrogen (developing iminium moiety in the TS) with the partially positive nitrogen of the electrophile is likely.<sup>33</sup> The N<sup>δ+</sup>···N<sup>δ-</sup> distance in **TS-1f** is found to be shorter (2.9 Å) than that in **TS-1a** (3.9 Å). In addition to the steric effects, hydrogen bonds, as described above, evidently contribute towards differentiating the diastereofacial approaches. All these factors contribute to the improved relative stabilization of **TS-1f**. On the basis of the analysis of intramolecular stabilizing interactions, as well as the computed activation barriers, it is now logical to state that the first step of this cascade reaction through **TS-1f** would lead to a high degree of stereocontrol.

More direct evidence in support of better kinetic preference of enamine towards nitrostyrene as opposed to enal (**C**) is gathered by separately evaluating the activation barriers for the addition. We have located transition states for the addition of enamine to α,β-unsaturated aldehyde. The calculated barriers are found to be higher by 7 kcal mol<sup>-1</sup> than the lowest energy TS for the addition of enamine to nitrostyrene.<sup>34</sup> If the first Michael addition occurs between enamine and enal, the products are going to be significantly different as compared to what has been reported experimentally.<sup>35</sup> It can also be noticed that the Michael adduct formed between nitrostyrene and enamine is detected experimentally.<sup>9,16b</sup> The computed activation barriers reveal that the lowest energy pathway should involve the addition of enamine to nitrostyrene as the first step. Although the reaction between enamine and enal cannot be completely ruled out, the experimental observation along with the computed data, clearly justify the reaction sequence as beginning with the addition of enamine to nitrostyrene in this triple cascade reaction.

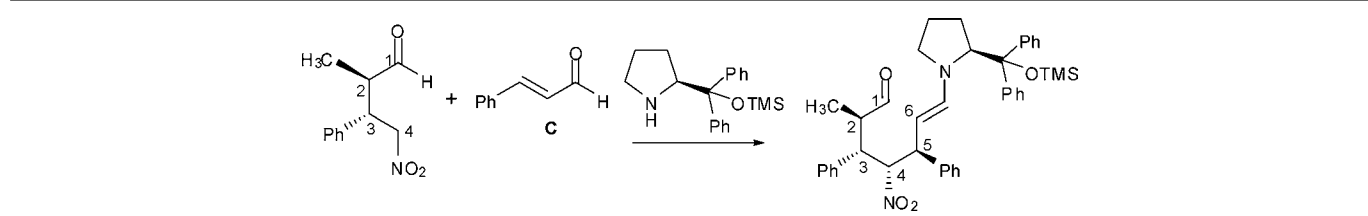
The generation of the third and fourth stereocentres takes place in the next step by the addition of the anion generated from the nitroalkane to the pre-activated enal (**C**).<sup>36</sup> The energetically more favored geometrical isomer of the iminium ion formed between enal

(**C**) and the catalyst is found to have *E,s-trans,E* stereochemistry.<sup>37</sup> This stereoisomer is chosen for further calculations. The formation of iminium ion renders more electrophilic character to the β-carbon of the α,β-unsaturated enal, thereby facilitating the second Michael addition with the nitroalkane anion generated in the preceding step.<sup>38</sup> The α-substituent on the pyrrolidine now comes into play in effectively differentiating the enantiotopic faces of the iminium ion to the approaching nucleophile. Since the *re* face is effectively shielded, the nucleophilic attack takes place on the *si* face of the iminium ion. The transition states for the Michael addition of nitroalkane anion to (*E,s-trans,E*)-iminium are identified wherein the configuration of nitroalkane is retained as (2*R*,3*S*), which is the major stereoisomer from the preceding step (Fig. 2). It is to be reckoned that the last step involves an intramolecular aldol cyclization (Scheme 1). The geometric requirement that the enamine and the electrophile (the CHO group) should be in reasonable proximity leads to only a limited number of conformers for the corresponding transition states. The nitroalkane anion can add to the Michael acceptor (iminium ion) using either the *re* face or *si* face as shown in Fig. 3. Hence the second Michael addition will result in the formation of products with an epimeric carbon.

The calculated absolute and relative activation barriers, respectively, with respect to the pre-reacting complex (between the reactants) and the lowest energy TS are tabulated in Table 2. Among the various possible modes of addition, the transition state **TS-4b** involving *si*-facial attack by the nitroalkane anion on the *re* face of the iminium is found to be the most favored mode. The optimized geometry conveys that the nitro and phenyl groups respectively on nucleophile and electrophile tend to remain antiperiplanar in the lower energy transition states. In other conformations, such as in **4a** and **4c**, the relative positions between the nitro and the phenyl groups are found to be gauche. These conformers are evidently higher in energy than **TS-4b**.<sup>39</sup> Three key transition states are considered for the addition of the *re*-face of the nitroalkane anion to the *re*-face of the iminium ion. The optimized geometry of **TS-4e** is found to prefer a conformation where the iminium double bond eclipses the -NO<sub>2</sub> group.<sup>40</sup> Only two unique transition states could be identified. Interestingly, during the course of transition state geometry optimization, the initial guess geometry of **TS-4f** converges to a structure identical to that of **TS-4d**.<sup>41</sup> The optimized structures of the lowest energy transition states leading to the formation of epimeric products are provided in Fig. 4.

Analysis of the geometries of lower energy transition states revealed several interesting facts. In both diastereomeric transition states (**TS-4b**, **TS-4d**), a preference for a staggered arrangement of the substituents around the incipient C-C bond is evident from the C<sub>10</sub>-C<sub>1</sub>-C<sub>2</sub>-H<sub>11</sub> dihedral angle. The hydrogen bonding between the α-hydrogens on the pyrrolidine ring (H<sub>s</sub>) and the -NO<sub>2</sub> group is found to be nearly the same in these transition states (Fig. 4). But a noticeable stabilizing interaction between the carbonyl oxygen and one of the methylene hydrogens of the pyrrolidine ring (O<sub>9</sub>-H<sub>s</sub>) is observed in **TS-4b**. The C=O···H distance is found to be 2.49 Å, implying a reasonably good hydrogen bonding stabilization. This interaction is totally absent in **TS-4d**, as the orientation of the carbonyl group is away from the pyrrolidine ring. Another interesting hydrogen bonding interaction is identified between the nitro group and the aryl

**Table 2** The computed activation barriers ( $\Delta E^\ddagger$ ) at the B3LYP/6-31G\*//ONIOM2(B3LYP/6-31G\*:AM1) level for the addition of a nitroalkane anion to the iminium derived from the enal (C)



Transition state	Prochiral face of nitroalkane anion	$\Delta E^\ddagger$ in kcal mol <sup>-1</sup>	
		Absolute <sup>a</sup>	Relative
<b>TS-4b</b>	<i>si</i>	5.4	0.0
<b>TS-4c</b>	<i>si</i>	7.8	4.2
<b>TS-4f <math>\rightarrow</math> TS-4d</b>	<i>re</i>	11.7	2.2
<b>TS-4e</b>	<i>re</i>	2.8	2.5

<sup>a</sup> Here the absolute barrier refers to the energy difference between the respective pre-reacting complexes and corresponding transition states.

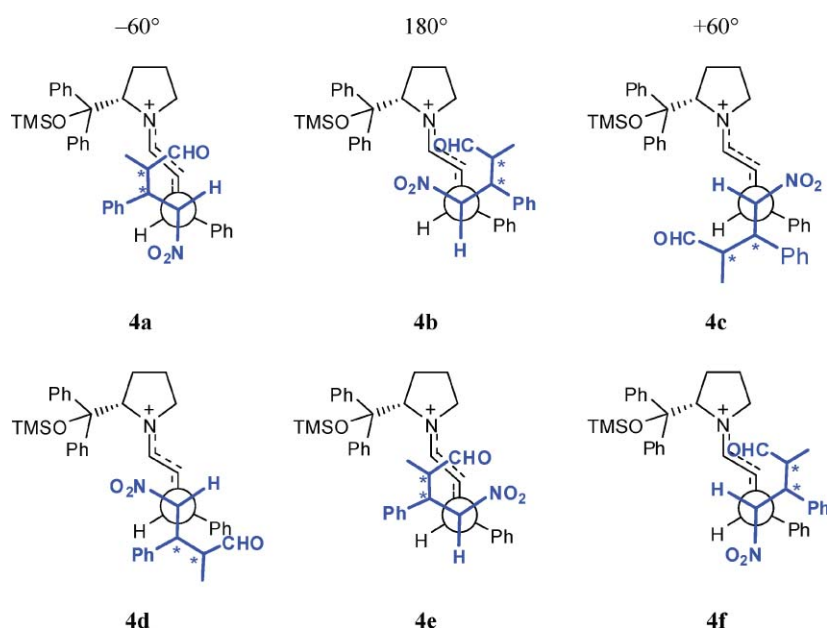


**Fig. 3** Key conformers of the transition states for the second Michael addition step. These conformers are grouped on the basis of the dihedral angle between the iminium double bond and the hydrogen of the nitroalkane (as indicated) with dihedral angles of  $-60^\circ$ ,  $+180^\circ$  and  $+60^\circ$ .

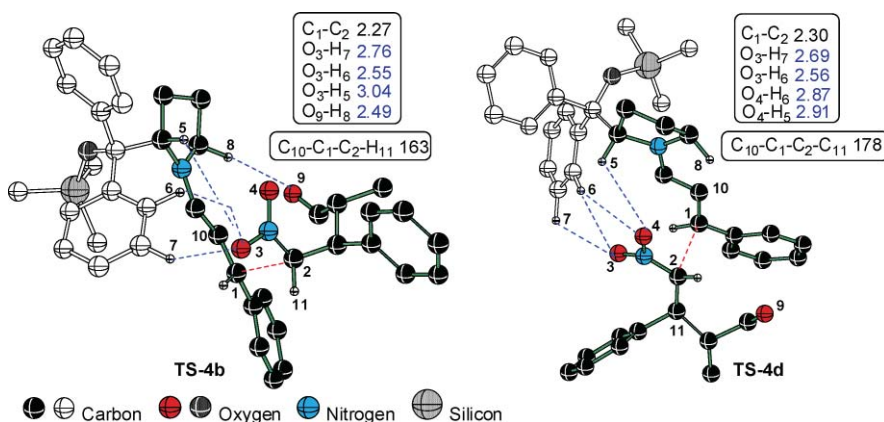


**Fig. 4** The ONIOM2(B3LYP/6-31G\*:AM1) optimized geometries of lower energy transition states for the second Michael addition step between the nitroalkane anion and the iminium ion (formed between pyrrolidine and  $\alpha,\beta$ -unsaturated aldehyde). Only selected hydrogens are shown for clarity. Angles are given in degrees and distances in Å.

hydrogens of the pyrrolidine  $\alpha$ -substituent as shown in Fig. 4.<sup>32</sup> This highlights the importance of weak stabilizing interactions offered by the  $\alpha$ -substituent in contributing toward the extra stabilization of **TS-4b** and **TS-4d**, a feature that is lacking in all other transition state possibilities (**TS-4c**, **TS-4e**). Interestingly, the lower energy transition states in both Michael addition steps (**TS-1f**, **1a** and **TS-4b**, **4d**) in this cascade reaction exhibited the above stabilizing interaction. The cumulative effect of such interactions results in an energy difference of 2.2 kcal mol<sup>-1</sup> between **TS-4b** and the diastereomeric **TS-4d**, which corresponds to a diastereomeric excess of 95% in favor of the (2*R*,3*S*,4*S*,5*S*)-2-methyl-4-nitro-3,5-diphenyl enamine intermediate. This prediction is in accordance with the experimental results obtained for diphenyl prolinol silyl ether catalyzed reactions between  $\alpha,\beta$ -unsaturated aldehyde and  $\gamma$ -nitroketone.<sup>15</sup> However, quantitative agreement with the experimental observation (diastereomeric excess) could vary depending on the choice of theory and basis sets.<sup>42</sup>

The enamine thus formed should participate in an intramolecular aldol cyclization. A schematic representation indicating the

key conformational possibilities is given in Fig. 5. The geometric requirement that the enamine and the electrophile stay in reasonable proximity for the aldol reaction to take place severely restricts the number of reactive conformers for the ensuing C–C bond-forming step. The enamine intermediate generated in the preceding Michael addition step through pathways **4a**, **4b**, and **4c** (Fig. 3) can in principle undergo ring closure either through **5a** or **5d**. Further, **5b** and **5c** correspond to possible transition states for the intramolecular aldol cyclization of the enamine precursors generated from **4d** and **4f**.

The optimized geometries of lower energy transition states for the intramolecular cyclization of the enamine intermediate are provided in Fig. 6. The lowest energy transition state (**TS-5a**)<sup>43</sup> is found to be 9.1 kcal mol<sup>-1</sup> more stable than the other possibilities, such as **TS-5c**. Both these TSs are found to maintain a chair conformation where the nitro group and the phenyl ring occupy the axial positions. An additional methyl group at the axial position contributes to the higher energy of **TS-5c**.<sup>44</sup> Among the weak interactions stabilizing the developing alkoxide, the hydrogen

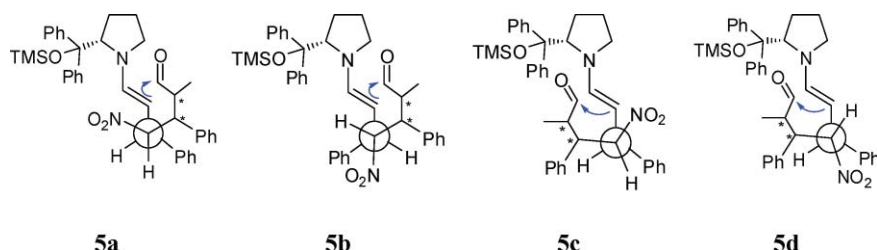


**Fig. 5** Key conformers of the transition states for the intramolecular cyclization of the enamine with favorable geometric disposition between the aldehyde and enamine.

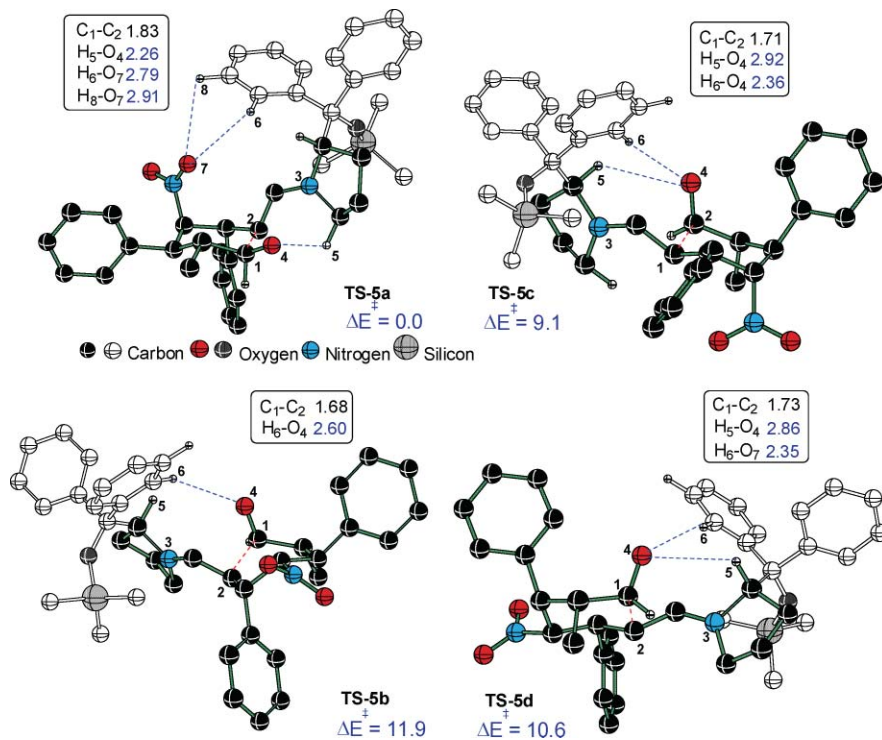


**Fig. 6** The ONIOM2(B3LYP/6-31G\*:AM1) optimized geometries for the lower energy transition states of intramolecular aldol cyclization. Only selected hydrogens are shown for clarity. Distances are given in Å. Relative energies ( $\Delta E^\ddagger$  in kcal) are obtained at the B3LYP/6-31G\*/ONIOM2(B3LYP/6-31G\*:AM1) level of theory.

bonding between the C $\alpha$  methylene hydrogen (adjacent to the pyrrolidine N) is more prominent in **TS-5a** with a distance of 2.26 Å than that in **TS-5c**, which has a distance of interaction of 2.92 Å.<sup>32</sup> An additional weak C–H(aryl)…O interaction in **TS-5a** arises due to the orientation of the nitro group towards the phenyl ring of the pyrrolidine substituent. On the basis of the computed energies, it is clear that the intramolecular aldol reaction through **TS-5a** would lead to ring closure. The cascade reaction eventually generates (3*S*,4*S*,5*R*,6*R*)-3-methyl-5-nitro-4,6-diphenyl cyclohex-1-ene carbaldehyde with four contiguous stereocentres with a high degree of stereoselectivity. This feature is evidently achieved by using a diphenyl prolinol silyl ether catalyst for promoting asymmetric Michael reactions in the cascade sequence.

## Conclusions

Mechanistic features of an interesting triple cascade Michael–Michael–Aldol reaction towards the generation of a cyclohexene carbaldehyde have been established using density functional theory calculations. We have been able to shed light on the controlling factors responsible for the high stereoselectivity observed experimentally. This has been achieved by precisely identifying all the stereochemically relevant transition states for three most important C–C bond-forming reactions in the cascade reaction sequence. The reaction pathways for the first two asymmetric Michael additions proceed through enamine as well as iminium activation modes, respectively, for aldehyde and  $\alpha,\beta$ -unsaturated enal. The examination of various stereochemically important modes of additions between enamine and nitrostyrene conveyed that the *si*-face of enamine (derived from the catalyst and propanal) adding to the *si*-face of nitrostyrene possesses the lowest activation energy. In the case of the second Michael addition step, the addition of the *si*-face of the nitroalkane anion to the *re*-face of the iminium ion (derived from enal and the catalyst) was found to be the lowest energy transition state. The predicted stereoselectivities are found to be in perfect concurrence with the experimental observation as reported by Enders and co-workers. The present results support the steric control approach, wherein efficient shielding of one face of the iminium/enamine intermediates is crucial to high levels of asymmetric induction. We anticipate that these insights into how stereoselectivity is achieved in a triple cascade reaction could be useful in designing novel one pot sequences towards highly complex target molecules.

## Acknowledgements

We thank the Department of Science and Technology (DST), New Delhi for financial support (through SR/S1/OC-50/2003) and the IITB computer centre for generous computing facilities. SCB acknowledges CSIR New Delhi for the senior research fellowship.

## References

- (a) D. J. Ramón and M. Yus, *Angew. Chem., Int. Ed.*, 2005, **44**, 1602; (b) H.-C. Guo and J.-A. Ma, *Angew. Chem., Int. Ed.*, 2006, **45**, 354.
- (a) P. J. Parson, C. S. Penkett and A. J. Shell, *Chem. Rev.*, 1996, **96**, 195; (b) L. F. Tietze, *Chem. Rev.*, 1996, **96**, 115; (c) K. C. Nicolaou, T. Montagnon and S. A. Snyder, *Chem. Commun.*, 2003, 551; (d) H. Pellisier, *Tetrahedron*, 2006, **62**, 2143; (e) D. Enders, C. Grondal and M. R. M. Hüttl, *Angew. Chem., Int. Ed.*, 2007, **46**, 1570.
- (a) P. I. Dalko and L. Moisan, *Angew. Chem., Int. Ed.*, 2001, **40**, 3726; (b) P. I. Dalko and L. Moisan, *Angew. Chem., Int. Ed.*, 2004, **43**, 5138; (c) D. B. Ramachary and C. F. Barbas III, *Chem.–Eur. J.*, 2004, **10**, 5323; (d) J. Seayad and B. List, *Org. Biomol. Chem.*, 2005, **3**, 719; (e) M. J. Gaunt, C. C. C. Johansson, A. McNally and N. T. Vo, *Drug Discovery Today*, 2007, **12**, 8.
- (a) Y. Huang, A. M. Walji, C. H. Larsen and D. W. C. MacMillan, *J. Am. Chem. Soc.*, 2005, **127**, 15051; (b) Y. Hayashi, T. Okano, S. Aratake and D. Hazelard, *Angew. Chem., Int. Ed.*, 2007, **46**, 4922; (c) L. Zu, H. Xie, J. Wang, W. Jiang, Y. Tang and W. Wang, *Angew. Chem., Int. Ed.*, 2007, **46**, 3732.
- (a) K. C. Nicolaou, D. J. Edmonds and P. G. Bulger, *Angew. Chem., Int. Ed.*, 2006, **45**, 7134; (b) S.-L. Cui, X.-F. Lin and Y.-C. Wang, *Eur. J. Org. Chem.*, 2006, 5174.
- (a) A. B. Northrup and D. W. C. MacMillan, *J. Am. Chem. Soc.*, 2002, **124**, 2458; (b) I. K. Mangion, A. B. Northrup and D. W. C. Macmillan, *Angew. Chem., Int. Ed.*, 2004, **43**, 6722; (c) B. List, *Acc. Chem. Res.*, 2004, **37**, 548; (d) B. List, *Chem. Commun.*, 2006, 819; (e) A. Erkkilä, I. Majander and P. M. Pihko, *Chem. Rev.*, 2007, **107**, 5416; (f) S. Mukherjee, J. W. Yang, S. Hoffmann and B. List, *Chem. Rev.*, 2007, **107**, 5471.
- (a) B. List, P. Poirier and H. J. Martin, *Org. Lett.*, 2001, **3**, 2423; (b) C. Allemann, R. Gordillo, F. R. Clemente, P. H.-Y. Cheong and K. N. Houk, *Acc. Chem. Res.*, 2004, **37**, 558.
- C. Palomo and A. Mielgo, *Angew. Chem., Int. Ed.*, 2006, **45**, 7876.
- D. Enders, M. R. M. Hüttl, C. Grondal and G. Raabe, *Nature*, 2006, **441**, 861.
- (a) M. Marigo, J. Franzén, T. B. Poulsen, W. Zhuang and K. A. Jørgensen, *J. Am. Chem. Soc.*, 2005, **127**, 6964; (b) J. Franzén, M. Marigo, D. Fielenbach, T. C. Wabnitz, A. Kjærsgaard and K. A. Jørgensen, *J. Am. Chem. Soc.*, 2005, **127**, 18296; (c) Y. Chi and S. H. Gellman, *Org. Lett.*, 2005, **7**, 4253; (d) G.-L. Zhao and A. Córdova, *Tetrahedron Lett.*, 2006, **47**, 7417; (e) A. Carbone, M. Marigo, C. North, A. Landa and K. A. Jørgensen, *Chem. Commun.*, 2006, 4928; (f) C. Palomo, S. Vera, I. Velilla, A. Mielgo and E. Gómez-Benagoa, *Angew. Chem., Int. Ed.*, 2007, **46**, 8054.
- (a) M. Marigo, T. Schulte, J. Franzén and K. A. Jørgensen, *J. Am. Chem. Soc.*, 2005, **127**, 15710; (b) M. Marigo, S. Bertelsen, A. Landa and K. A. Jørgensen, *J. Am. Chem. Soc.*, 2006, **128**, 5475; (c) W. Wang, H. Li, J. Wang and L. Zu, *J. Am. Chem. Soc.*, 2006, **128**, 10354; (d) S. Branda, E. Maerten and K. A. Jørgensen, *J. Am. Chem. Soc.*, 2006, **128**, 14986; (e) D. B. Ramachary and M. Kishor, *J. Org. Chem.*, 2007, **72**, 5056; (f) A. Carbone, S. Cabrera, M. Marigo and K. A. Jørgensen, *Angew. Chem., Int. Ed.*, 2007, **46**, 1101.
- (a) For such Michael additions, nitrostyrenes in general are found to be very effective: D. Enders and A. Seki, *Synlett*, 2002, 26; (b) O. M. Berner, L. Tedeschi and D. Enders, *Eur. J. Org. Chem.*, 2002, 1877; (c) R. Ballini, G. Bosica, D. Fiorini, A. Palmieri and M. Petrini, *Chem. Rev.*, 2005, **105**, 933; (d) D. Enders and S. Chow, *Eur. J. Org. Chem.*, 2006, 4578; (e) S. B. Tsogoeva, *Eur. J. Org. Chem.*, 2007, 1701; (f) K. Albertshofer, R. Thayumanavan, N. Utsumi, F. Tanaka and C. F. Barbas III, *Tetrahedron Lett.*, 2007, **48**, 693.
- (a) O. Andrey, A. Alexakis, A. Tomassini and G. Bernardinelli, *Adv. Synth. Catal.*, 2004, **346**, 1147; (b) T. Ishii, S. Fujioka, Y. Sekiguchi and H. Kotsuki, *J. Am. Chem. Soc.*, 2004, **126**, 9558; (c) W. Wang, J. Wang and H. Li, *Angew. Chem., Int. Ed.*, 2005, **44**, 1369.
- (a) Significant recent developments in organocatalytic Michael reactions involving enamine or iminium intermediates have been reported; (b) D. Almási, D. A. Alonso and C. Nájera, *Tetrahedron: Asymmetry*, 2007, **18**, 299; (c) J. L. Vicario, D. Badía and L. Carrillo, *Synthesis*, 2007, **14**, 2065; (d) S. Hanessian and V. Pham, *Org. Lett.*, 2000, **2**, 2975; (e) N. Halland, R. G. Hazell and K. A. Jørgensen, *J. Org. Chem.*, 2002, **67**, 8331; (f) N. Halland, P. S. Aburel and K. A. Jørgensen, *Angew. Chem., Int. Ed.*, 2003, **42**, 661; (g) A. Prieto, N. Halland and K. A. Jørgensen, *Org. Lett.*, 2005, **7**, 3897; (h) H. Gotoh, H. Ishikawa and Y. Hayashi, *Org. Lett.*, 2007, **9**, 5307.
- D. Enders, A. A. Narine, T. R. Benninghaus and G. Raabe, *Synlett*, 2007, **11**, 1667.
- (a) D. Enders, M. R. M. Hüttl, J. Runsink, G. Raabe and B. Wendt, *Angew. Chem., Int. Ed.*, 2007, **46**, 467; (b) D. Enders, M. R. M. Hüttl, G. Raabe and J. W. Bats, *Adv. Synth. Catal.*, 2008, **350**, 267.
- (a) D. Roy and R. B. Sunoj, *Org. Lett.*, 2007, **9**, 4873; (b) M. P. Patil and R. B. Sunoj, *J. Org. Chem.*, 2007, **72**, 8202; (c) D. Janardanan and R. B. Sunoj, *J. Org. Chem.*, 2007, **72**, 331; (d) D. Janardanan and R. B. Sunoj,

- Chem.–Eur. J.*, 2007, **13**, 4805; (e) C. B. Shinisha and R. B. Sunoj, *Org. Biomol. Chem.*, 2007, **5**, 1287.
- 18 (a) S. Dapprich, I. Komáromi, K. S. Byun, K. Morokuma and M. J. Frisch, *J. Mol. Struct. (THEOCHEM)*, 1999, **461–462**, 1; (b) T. Vreven and K. Morokuma, *J. Comput. Chem.*, 2000, **21**, 1419; (c) K. Morokuma, *Bull. Korean Chem. Soc.*, 2003, **24**, 797; (d) K. Morokuma, *Philos. Trans. R. Soc. London, Ser. A*, 2002, **360**, 1149; (e) T. Vreven, K. S. Byun, I. Komáromi, S. Dapprich, J. A. Montgomery, Jr., K. Morokuma and M. J. Frisch, *J. Chem. Theory Comput.*, 2006, **2**, 815.
- 19 M. J. Frisch, G. W. Trucks, H. B. Schlegel, G. E. Scuseria, M. A. Robb, J. R. Cheeseman, J. A. Montgomery, Jr., T. Vreven, K. N. Kudin, J. C. Burant, J. M. Millam, S. S. Iyengar, J. Tomasi, V. Barone, B. Mennucci, M. Cossi, G. Scalmani, N. Rega, G. A. Petersson, H. Nakatsuji, M. Hada, M. Ehara, K. Toyota, R. Fukuda, J. Hasegawa, M. Ishida, T. Nakajima, Y. Honda, O. Kitao, H. Nakai, M. Klene, X. Li, J. E. Knox, H. P. Hratchian, J. B. Cross, V. Bakken, C. Adamo, J. Jaramillo, R. Gomperts, R. E. Stratmann, O. Yazyev, A. J. Austin, R. Cammi, C. Pomelli, J. Ochterski, P. Y. Ayala, K. Morokuma, G. A. Voth, P. Salvador, J. J. Dannenberg, V. G. Zakrzewski, S. Dapprich, A. D. Daniels, M. C. Strain, O. Farkas, D. K. Malick, A. D. Rabuck, K. Raghavachari, J. B. Foresman, J. V. Ortiz, Q. Cui, A. G. Baboul, S. Clifford, J. Cioslowski, B. B. Stefanov, G. Liu, A. Liashenko, P. Piskorz, I. Komaromi, R. L. Martin, D. J. Fox, T. Keith, M. A. Al-Laham, C. Y. Peng, A. Nanayakkara, M. Challacombe, P. M. W. Gill, B. G. Johnson, W. Chen, M. W. Wong, C. Gonzalez and J. A. Pople, *GAUSSIAN 03 (Revision C.02)*, Gaussian, Inc., Wallingford, CT, 2004.
- 20 (a) T. Dudding and K. N. Houk, *Proc. Natl. Acad. Sci. U. S. A.*, 2004, **101**, 5770; (b) V. P. Ananikov, R. Szilagyi, K. Morokuma and D. G. Musaev, *Organometallics*, 2005, **24**, 1938; (c) D. Balcells, F. Maseras and G. Ujaque, *J. Am. Chem. Soc.*, 2005, **127**, 3624; (d) X. Zhang, H. Du, Z. Wang, Y.-D. Wu and K. Ding, *J. Org. Chem.*, 2006, **71**, 2862.
- 21 (a) A. D. Becke, *J. Chem. Phys.*, 1993, **98**, 5648; (b) A. D. Becke, *Phys. Rev. A*, 1998, **38**, 3098; (c) C. Lee, W. Yang and R. G. Parr, *Phys. Rev. B*, 1998, **37**, 785.
- 22 (a) R. Ditchfield, W. J. Hehre and J. A. Pople, *J. Chem. Phys.*, 1971, **54**, 724; (b) W. J. Hehre, R. Ditchfield and J. A. Pople, *J. Chem. Phys.*, 1972, **56**, 2257; (c) P. C. Hariharan and J. A. Pople, *Theor. Chim. Acta*, 1973, **28**, 213.
- 23 Two-layered ONIOM partition scheme for the catalyst is given in Fig. S1 (ESI†).
- 24 The geometric parameters are summarized in Table S1 in the ESI. The average correlation coefficient ( $R^2$ ) for the important structural parameters obtained through full B3LYP and ONIOM2(B3LYP:AM1) optimized geometries for the catalyst is found to be 0.9.
- 25 Different conformations arising due to the rotation of the  $\alpha$ -substituent around the pyrrolidine ring are considered. The most favored conformer is found to have a dihedral angle of +60° between the N–C(2) and C–O bond of the substituent. This geometry is found to be relatively more stable by 2.9 kcal mol<sup>-1</sup> than the next highest energy conformer. See Table S2 in the ESI for the relative energies of various conformers of the catalyst. The ring conformational features of the catalyst are not investigated in this study.
- 26 (a) The computed GRDs are found to be evidently in favor of nitrostyrene as the preferred electrophile to react with the enamine rather than enal. The computed electronegativity ( $\chi$ ), hardness ( $\eta$ ) and electrophilicity index ( $\omega$ ) are tabulated in Table S5 (ESI). R. G. Parr and R. G. Pearson, *J. Am. Chem. Soc.*, 1983, **105**, 7512; (b) W. Yang and W. J. Mortier, *J. Am. Chem. Soc.*, 1986, **108**, 5708; (c) R. G. Parr, L. v. Szentháry and S. Liu, *J. Am. Chem. Soc.*, 1999, **121**, 1922; (d) H. Chermette, *J. Comput. Chem.*, 1999, **20**, 129; (e) L. R. Domingo, P. Pérez and R. Contreras, *Tetrahedron*, 2004, **60**, 6585.
- 27 (a) The (*E*)-isomer of the electrophile is found to be energetically more stable. This orientation is maintained in the present study; (b) For experimental evidence see T. Ohwada, T. Ohta and K. Shudo, *J. Am. Chem. Soc.*, 1986, **108**, 3029.
- 28 See Table S3 for the relative energies of *E/Z* isomers of *syn/anti*-enamines formed between the catalyst and propanal.
- 29 Other possible conformers for the addition of (i) (*Z*)-*anti*-enamine to (*E*)-nitrostyrene (**2a–2f**) and (ii) (*E*)-*syn*-enamine to (*E*)-nitrostyrene (**3a–3f**) are given in Fig. S2 in the ESI.
- 30 Y. Hayashi, H. Gotoh, T. Hayashi and M. Shoji, *Angew. Chem., Int. Ed.*, 2005, **44**, 4212.
- 31 Some of the possible conformers for the addition transition states of (*Z*)-*anti*-enamine and (*E*)-nitrostyrene as well as (*E*)-*syn*-enamine and (*E*)-nitrostyrene (**2b–e** and **3b,d** as in Fig. S2 in the ESI) could not be located. For more details, see the ESI.
- 32 (a) The electron density at the *bcp* along the key stabilizing interactions is provided in Fig. S3 of the ESI; (b) R. F. W. Bader, *Atoms in Molecules: A Quantum Theory*, Clarendon Press, Oxford, 1990; (c) AIM2000, version 2.0; The Buro für Innovative Software, SBK-Software, Bielefeld, Germany.
- 33 Partial charges on nitrogens rendering electrostatic interaction are confirmed by examining the corresponding Mulliken as well as natural charges. Details of MCA and NPA analyses are provided in Table S4 (ESI†).
- 34 We located TSs for the addition of enamine to iminium formed by the  $\alpha,\beta$ -unsaturated aldehyde. Although the activation barrier is less compared to other pathways, the product formed is highly unstable. Hence this pathway involving such double activation is likely to be very reversible. Moreover, entropic disadvantages are going to be higher as well. See Table S6 (ESI) for the optimized geometries and energetics of lower energy TSs for the addition of enamine to enal.
- 35 Plausible pathways leading to such products are provided in the ESI (Fig. S4).
- 36 In this step of the cascade reaction sequence, the third reactant, namely  $\alpha,\beta$ -unsaturated aldehyde, first forms an iminium ion with the catalyst. This serves as the Michael acceptor for the C–C bond formation.
- 37 (a) Important geometrical isomers of the iminium ion are individually optimized. The (*E,s-trans,E*) isomer is found to be more stable than the (*Z,s-trans,E*) geometrical isomer by 1.5 kcal mol<sup>-1</sup>; (b) Relative energies of possible isomers of the iminium ion are given in Table S6 in the ESI.
- 38 (a) P. Melchiorre and K. A. Jørgensen, *J. Org. Chem.*, 2003, **68**, 4151; (b) S. Bertelsen, M. Marigo, S. Brandes, P. Dinér and K. A. Jørgensen, *J. Am. Chem. Soc.*, 2006, **128**, 12973.
- 39 Even after repeated attempts, we could not locate the TS corresponding to conformer **4a**. The destabilizing interaction between the phenyl group of the pyrrolidine  $\alpha$ -substituent and the substituents on nitroalkane is found to be prominent. It is therefore safe enough to assume that **4a** would be a higher energy conformer. All our initial guess geometries have developed oscillatory behavior, leading to lack of convergence or resulting in rotation around the incipient C–C bond towards **4c** during geometry optimization. This situation would not affect the conclusions drawn on the stereoselectivities.
- 40 In spite of repeated attempts, all initial guess transition state geometries with a staggered orientation of substituents around the incipient C–C bond (**4e** in Fig. 4) converge to an eclipsed conformation during geometry optimization.
- 41 Several attempts toward optimizing **TS-4f** have been carried out. These include constrained optimization of the key dihedral angles, a range of initial guess geometries with a number of local rotamers etc.. Invariably, all such efforts eventually cascaded down to **TS-4d**.
- 42 By using single-point energies at the B3LYP/6-31+G\*//ONIOM2-(B3LYP/6-31G\*:AM1) and B3LYP/6-31+G\*\*//ONIOM2(B3LYP/6-31G\*:AM1) levels, the computed relative energies of all the TSs for the first and second step of the reaction are found to show some variations with respect to the numbers obtained using the 6-31G\* basis set. For comparison between these results, see Table S9 and S10 of the ESI.
- 43 We could not locate **TS-5a** using the ONIOM2 method. Optimizations were therefore carried out at the HF/6-31G\* level. Relative energies and activation barriers were then computed by evaluating single-point energy at the B3LYP/6-31G\* level.
- 44 Absolute and relative activation barriers for the intramolecular aldol cyclization are tabulated in Table S8 (ESI†).

# On the Origins of Kinetic Resolution of Cyclohexane-1,2-diols Through Stereoselective Acylation by Chiral Tetrapeptides

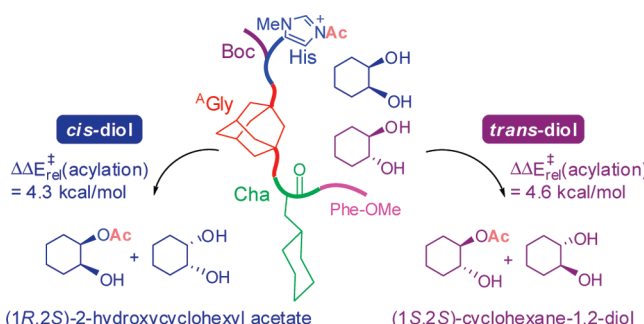
C. B. Shinisha and Raghavan B. Sunoj\*

Department of Chemistry, Indian Institute of Technology Bombay, Powai,  
Mumbai 400076, India

*sunoj@chem.iitb.ac.in*

Received May 27, 2009

## ABSTRACT



The relative energies of cyclohexane-1,2-diols and chiral tetrapeptide (2 (Boc) or 3 (Moc)) complexes calculated using DFT indicate a thermodynamic preference for chiral recognition toward  $(1R,2R)_{e,e-\alpha}$  isomer. The barrier for stereoselective acyl transfer is identified as lower for *trans*- $(1R,2R)$ -cyclohexane-1,2-diol, leading to the kinetic resolution (KR) of *trans*- $(1S,2S)$ -cyclohexane-1,2-diol. The prediction is in concert with the reported experiments for *trans*-diols, while that for hitherto unknown *cis*-diol demands experimental verification. It is proposed that desymmetrization would enable the resolution of *cis*- $(1R,2S)$ -2-hydroxycyclohexyl acetate.

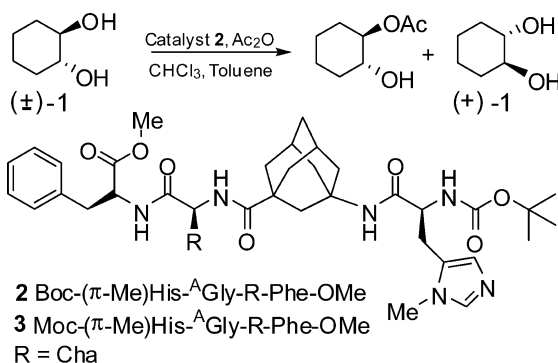
Kinetic resolutions (KRs) are recognized as an effective protocol toward the generation of enantiopure compounds.<sup>1</sup> Both enzymatic and nonenzymatic KRs have found useful applications with a spectrum of organic compounds.<sup>2</sup> Among the nonenzymatic approaches, KR of alcohols through asymmetric acylation has attracted considerable attention in recent years.<sup>3</sup> An interesting strategy popularized by Miller and co-workers employs small peptides functionalized with nucleophilic *N*-methylimidazole as catalysts for KR of

secondary alcohols.<sup>4</sup> Another impressive example on the use of small peptide catalysts due to Schreiner and co-workers demonstrated successful resolution of 1,2-*trans* cycloalkane diols (Scheme 1).<sup>5</sup> These approaches in general rely either on substrate specificity arising due to hydrogen bonding interactions or/and the propensity to exhibit improved order through secondary structures.<sup>6</sup> While the design of newer peptide catalysts for KR continues to grow, efforts toward

- (1) Vedejs, E.; Jure, M. *Angew. Chem., Int. Ed.* **2005**, *44*, 3974.
- (2) (a) Reetz, M. T. *Angew. Chem., Int. Ed.* **2001**, *40*, 284. (b) Keith, J. M.; Larwo, J. F.; Jacobsen, E. N. *Adv. Synth. Catal.* **2001**, *343*, 5. (c) Robinson, D. E. J. E.; Bull, S. D. *Tetrahedron: Asymmetry* **2003**, *14*, 1407.
- (3) (a) Copeland, G. T.; Miller, S. J. *J. Am. Chem. Soc.* **2001**, *123*, 6496. (b) Jarvo, E. R.; Evans, C. A.; Copeland, G. T.; Miller, S. J. *J. Org. Chem.* **2001**, *66*, 5522. (c) Ishihara, K.; Kosugi, Y.; Akakura, M. *J. Am. Chem. Soc.* **2004**, *126*, 12212.

(4) (a) Miller, S. J.; Copeland, G. T.; Papaioannou, N.; Horstmann, T. E.; Ruel, E. M. *J. Am. Chem. Soc.* **1998**, *120*, 1629. (b) Jarvo, E. R.; Copeland, G. T.; Papaioannou, N.; Bonitatebus, P. J., Jr.; Miller, S. J. *J. Am. Chem. Soc.* **1999**, *121*, 11638. (c) Vasbinder, M. M.; Jarvo, E. R.; Miller, S. J. *Angew. Chem., Int. Ed.* **2001**, *40*, 2824. (d) Miller, S. J. *Acc. Chem. Res.* **2004**, *37*, 601. (e) Davie, E. A. C.; Mennen, S. M.; Xu, Y.; Miller, S. J. *Chem. Rev.* **2007**, *107*, 5759.

(5) Müller, C. E.; Wanka, L.; Jewell, K.; Schreiner, P. R. *Angew. Chem., Int. Ed.* **2008**, *47*, 6180.

**Scheme 1.** Enantioselective Acylation Reaction Catalyzed by **2**<sup>5</sup>

unravelling the molecular origins of such catalysis are not widely reported.<sup>7</sup> Detailed insights on the mechanism as well as the crucial kinetic factors would indeed help improve the efficiency of such promising methods.

In this letter, we intend to shed light on the origins of KR of 1,2-diols achieved through a chiral tetrapeptide-catalyzed stereoselective acyl transfer reaction. The objectives here are 2-fold: (i) to provide a mechanistic framework toward rationalizing the KR of racemic *trans*-cyclohexane-1,2-diols and (ii) to apply the insights thus obtained toward predicting the likely outcome of, hitherto unknown, meso *cis*-cyclohexane-1,2-diols. Schreiner's tetrapeptide catalysts (**2**), derived from a rigid non-natural  $\gamma$ -amino acid, denoted as Boc-( $\pi$ -Me)His- $^A$ Gly-Cha-Phe-OMe and Moc-( $\pi$ -Me)His- $^A$ Gly-Cha-Phe-OMe, are chosen for the present investigation.<sup>8</sup>

A hybrid DFT (B3LYP/6-31G\*) and semiempirical MO (PM3) treatment using the ONIOM2 methodology is employed for geometry optimization. All the intermediates and transition states are, respectively, characterized as minima and first-order saddle points using frequency analysis. Additionally we have carried out 10% displacement of the transition geometry along the direction of the imaginary frequency and reoptimized the perturbed structure using the “calcfc” option available in the program. This was to ensure whether the transition state is genuine and connects the reactant and the product. Energies of such stationary points are subsequently refined using single-point energy calcula-

(6) (a) France, S.; Guerin, D. J.; Miller, S. J.; Lectka, T. *Chem. Rev.* **2003**, *103*, 2985. (b) Formaggio, F.; Barazzza, A.; Bertocco, A.; Toniolo, C.; Broberman, Q. B.; Kaptein, B.; Brasola, E.; Pengo, P.; Pasquato, L.; Scrimin, P. *J. Org. Chem.* **2004**, *69*, 3849. (c) Doyle, A. G.; Jacobsen, E. N. *Chem. Rev.* **2007**, *107*, 5713.

(7) Although KRs of diols with the help of peptides are largely unexplored, DFT studies on stereoselective acyl transfer in secondary alcohol as well as certain desymmetrization reactions are recently reported. See: (a) Xu, S.; Held, I.; Kempf, B.; Mayr, H.; Steglich, W.; Zipse, H. *Chem.—Eur. J.* **2005**, *11*, 4751. (b) Li, X.; Liu, P.; Houk, K. N.; Birman, V. B. *J. Am. Chem. Soc.* **2008**, *130*, 13836. (c) Oh, S. H.; Rho, H. S.; Lee, J. W.; Youk, S. H.; Chin, J.; Song, C. E. *Angew. Chem., Int. Ed.* **2008**, *47*, 7872.

(8) (a)  $^A$ Gly =  $\gamma$ -amino acid. (b) In the real system on which experiments were performed, only Boc protection is employed. See ref 5.

tions at the B3LYP/6-31G\* level of theory.<sup>9</sup> Such approaches have been successfully used in explaining the mechanism and stereoselectivity of organic reactions.<sup>10</sup> The most crucial part of the reacting system including the diol and ( $\pi$ -Me)His-acylum fragments is described using density functional theory (higher layer), while the peptide backbone is treated as a lower layer using the semiempirical PM3 method.

The KR is envisaged to proceed first through the formation of inclusion complexes facilitated by chiral recognition between the host peptide and diols, and then a stereoselective acyl transfer reaction takes place under the chiral environment. While the latter reaction holds the key to KR, the initial inclusion complexes can be equally critical. The problem is therefore approached in two important steps. The identification of important lower energy inclusion complexes between different stereoisomers of the diol and the host peptide is undertaken first. The stereoselective acyl transfer reactions are then studied by precisely identifying the corresponding transition states. The chiral recognition of diols offered by two tetrapeptides Moc-( $\pi$ -Me)His- $^A$ Gly-Cha-Phe-OMe (**3**) and Boc-( $\pi$ -Me)His- $^A$ Gly-Cha-Phe-OMe (**2**)<sup>11</sup> is examined by considering a series of likely inclusion complexes as shown in Figure 1. The stabilization of these complexes appears to depend on the relative stereochemical disposition between the diol hydroxyl groups and the extent of intermolecular interactions with the peptide residues. In the lowest-energy inclusion complex for the *trans*-diol, the configuration is identified as (1*R*,2*R*)<sub>e,e</sub>- $\alpha$ . It is identified that these complexes are primarily stabilized by an anchoring hydrogen bonding interaction between the C=O group of the amino acid backbone of the catalyst and the diol hydroxyl group. Interestingly, such an interaction is noticed in all of the lower-energy complexes. A representative geometry of an inclusion complex depicting this is provided in Figure 2a.

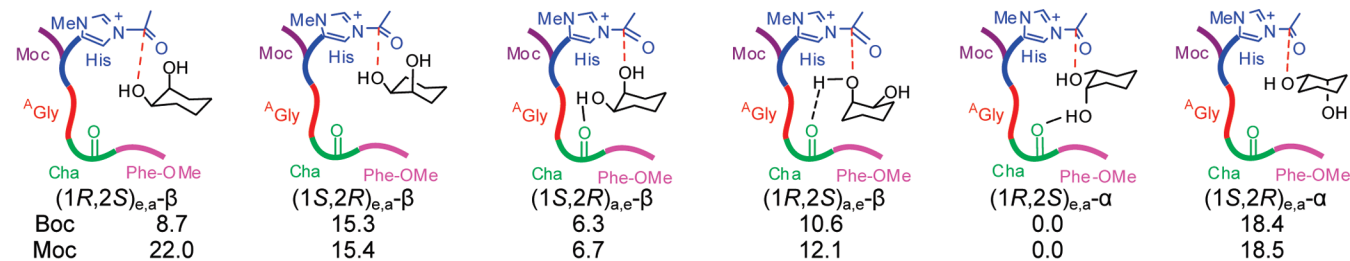
A comparison of the computed relative energies of *trans*- and *cis*-1,2-cyclohexanediol complexes is given in Figure 1. It is noticed that the *trans*-(1*R*,2*R*)-diol $\cdots$ acylum complex is more stable by 4.3 kcal/mol than the energetically nearest diastereomeric *trans*-(1*S*,2*S*)-diol $\cdots$ acylum complex. In the case of *cis*-diols, the *cis*-(1*R*,2*S*)-diol $\cdots$ acylum complex is found to be the most preferred complex. The relative energies of these complexes suggest a likely thermodynamic propensity toward selective chiral recognition by the host peptide. The differential binding of diastereomeric diols can be

(9) (a) From a computational standpoint, the present catalyst–substrate complexes are relatively large, in particular for transition state searches, for full DFT calculations. We have therefore resorted to hybrid ONIOM2 calculations where the higher and lower layers are, respectively, treated at the B3LYP/6-31G\* and PM3 methods. The approach is denoted as ONIOM2(B3LYP/6-31G\*:PM3). (b) All calculations have been performed using Gaussian03 suite: Frisch, M. J. *Gaussian 03*, Rev C.02; Gaussian Inc. (full citation is provided in Supporting Information). (c) Dapprich, S.; Komáromi, I.; Byun, K. S.; Morokuma, K.; Frisch, M. J. *J. Mol. Struct. (THEOCHEM)* **1999**, 461. (d) Vreven, T.; Morokuma, K. *J. Comput. Chem.* **2000**, *21*, 1419. (e) Morokuma, K. *Bull. Korean Chem. Soc.* **2003**, *24*, 797.

(10) (a) Dudding, T.; Houk, K. N. *Proc. Natl. Acad. Sci. U.S.A.* **2004**, *101*, 5770. (b) Zhang, X.; Du, H.; Wang, Z.; Wu, Y.-D.; Ding, K. *J. Org. Chem.* **2006**, *71*, 2862. (c) Shinisha, C. B.; Sunoj, R. B. *Org. Biomol. Chem.* **2008**, *6*, 3921.

(11) Wanka, L.; Cabrele, C.; Vanejews, M.; Schreiner, P. R. *Eur. J. Org. Chem.* **2007**, 1474.

### *cis*-Cyclohexane-1,2-diols



### *trans*-Cyclohexane-1,2-diols

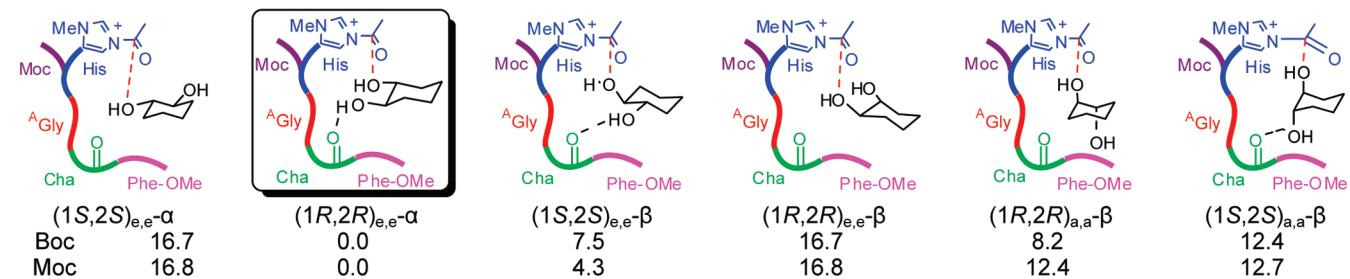


**Figure 1.** Computed relative energies ( $\Delta E$  in kcal/mol) at the B3LYP/6-31G\*//ONIOM2(B3LYP/6-31G\*:PM3) level of theory for catalyst-acylium $\cdots$ diol complexes. The relative energies for *trans*- and *cis*-diols are reported separately, on the basis of the lowest-energy inclusion complex in each case.

envisioned to offer a congenial template for the ensuing acylation reaction. It is logical to assume that the acyl transfer reaction is more likely to take place soon after the correct inclusion complexes are generated. Next, the TSs for acyl transfer to diols are located. The relative energies with respect to the lowest-energy TS for both *trans*- and *cis*-diols are provided in Table 1. The TS for the acyl transfer reaction,  $(1R,2R)_{e,e}\text{-}\alpha^\ddagger$ ,<sup>12</sup> leading to the formation of  $(1R,2R)$ -2-hydroxycyclohexyl acetate is found to be the lowest-energy TS. The enantiomeric excess calculated on the basis of relative activation energy of the next higher energy diastereomeric TS  $(1S,2S)_{e,e}\text{-}\beta^\ddagger$  giving rise to the corresponding

enantiomer is above 99%. The computed ee is larger than the experimentally reported value of 75%.<sup>5</sup> Though the calculated ee is quantitatively higher than the observed value, the predicted sense of stereoselectivity toward acylation is same as that observed experimentally. The protecting groups (Boc or Moc) do not seem to influence the stereochemical outcome, as those are farther from the reaction site.

The optimized geometries of the lower-energy TSs are provided in Figure 2. Comparison of the geometrical features of the TSs reveals that the hydrogen bonding between the diol hydroxyl groups and the C=O group of the amino acid backbone play a vital role toward stabilizing the TSs. For

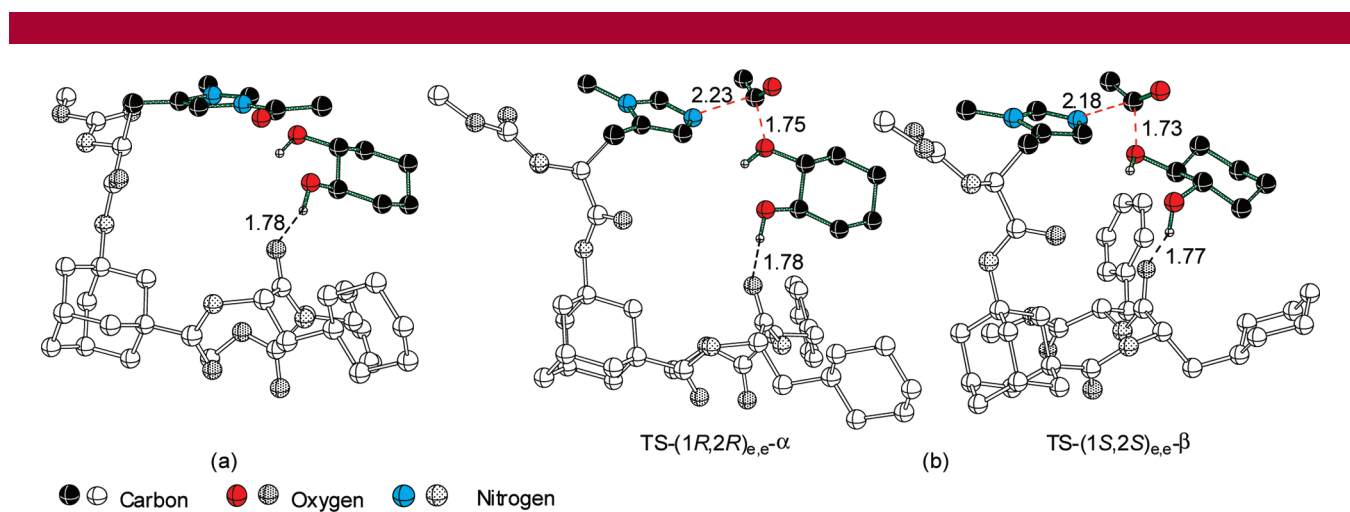


**Figure 2.** ONIOM2(B3LYP/6-31G\*:PM3) optimized geometry of (a)  $(1R,2R)_{e,e}$ -cyclohexane-1,2-diol $\cdots$ acylium complex, and (b) the lower-energy TSs for the acetyl transfer to *trans*-diol. Only selected hydrogens are shown for improved clarity. Lighter gray and darker colored shadings, respectively, represent the lower (PM3) and higher (B3LYP) layers in the ONIOM2 partitioning. Distances are given in Å.

**Table 1.** Computed Relative Energies of Transition States Obtained at the B3LYP/6-31G\*\*//ONIOM(B3LYP/6-31G\*:PM3) Level of Theory for the Acyl Transfer<sup>a</sup>

diol	transition states	relative $\Delta E^\ddagger$ (in kcal/mol)	
		Boc ( <b>2</b> )	Moc ( <b>3</b> )
trans-diol	(1S,2S) <sub>e,e</sub> - $\alpha^\ddagger$ <sup>b</sup>	13.5	13.4
	(1S,2S) <sub>e,e</sub> - $\beta^\ddagger$	4.6	4.5
	(1S,2S) <sub>a,a</sub> - $\beta^\ddagger$	7.6	7.7
	(1R,2R) <sub>e,e</sub> - $\alpha^\ddagger$	<b>0.0</b>	<b>0.0</b>
	(1R,2R) <sub>e,e</sub> - $\beta^\ddagger$	11.5	11.6
	(1R,2R) <sub>a,a</sub> - $\beta^\ddagger$	9.7	11.6
	(1R,2S) <sub>e,a</sub> - $\alpha^\ddagger$	<b>0.0</b>	<b>0.0</b>
	(1R,2S) <sub>e,a</sub> - $\beta^\ddagger$	16.1	16.3
	(1R,2S) <sub>a,e</sub> - $\beta^\ddagger$	12.5	12.6
	(1S,2R) <sub>e,a</sub> - $\alpha^\ddagger$	12.7	12.7
cis-diol	(1S,2R) <sub>e,a</sub> - $\beta^\ddagger$	14.9	15.0
	(1S,2R) <sub>a,e</sub> - $\beta^\ddagger$	4.3	4.4

<sup>a</sup> See Tables S1 and S2 in the Supporting Information, respectively, for values obtained using the 6-31G\*\* basis set as well as the activation barriers with respect to the prereacting complexes. <sup>b</sup> The notations  $\alpha$  and  $\beta$  refer to the orientations of  $-\text{OH}$  in the diol to which the acetyl is transferred.

instance, the hydrogen bonding distance in TS (1R,2R)<sub>e,e</sub>- $\alpha^\ddagger$  is found to be 1.78 Å. The separation between the cyclohexyl groups, respectively, of catalyst **2** and the diol is found to increase from the prereacting complex to the lowest-energy acyl transfer TS. The distances of the acyl group from histidine nitrogen and diol oxygen indicate a product-like TS for acyl transfer. The conformation of the peptide backbone in the higher-energy TSs is identified to exhibit larger deviations as compared to that with the lower-energy TS.<sup>13</sup> In particular, the orientation of the cyclohexyl group of the backbone is found to be progressively different for higher-energy TSs. In TS (1S,2S)<sub>e,e</sub>- $\beta$ , the incipient C–O bond develops 1,3-diaxial interaction with the C( $\beta$ )H, which is absent in the lowest-energy TS (1R,2R)<sub>e,e</sub>- $\alpha^\ddagger$ . A stabilizing hydrogen bonding interaction between the acyl oxygen and cyclohexane C( $\alpha$ )H of the diol offers additional stabilization for (1R,2R)<sub>e,e</sub>- $\alpha^\ddagger$ .<sup>14</sup> The cumulative effects of the stereoelectronic features as noted above will help achieve the vital

(12) In the nomenclature used for inclusion complexes and transition states, the subscripts a (axial) or e (equatorial) refer to the position of  $-\text{OAc}$  and  $-\text{OH}$  in the product and notations  $\alpha$  and  $\beta$  refer to the orientations of  $-\text{OH}$  in the diol to which the acetyl group is transferred.

(13) A comprehensive comparison of such deviations is given in Figure S3 in Supporting Information.

(14) Figure S4 showing these interactions is given in Supporting Information.

energy separation between the diastereomeric acyl transfer TSs. In other words, the *trans*-(1R,2R)<sub>e,e</sub> cyclohexane diol is predicted to undergo stereoselective acylation, leaving behind the (1S,2S)<sub>e,e</sub> stereoisomer amenable to KR.

After having established the molecular origins of stereoselective acylation of *trans*-diols, we became curious to learn how *cis*-diols would respond to acylation under the chiral template. Among the various acylation TSs considered for *cis*-diols, it is found that TS (1R,2S)<sub>e,a</sub>- $\alpha^\ddagger$  is the lowest-energy TS. A hydrogen bonding interaction between one of the carbonyl groups of the backbone and the diol hydroxyl is found to dominate in the lower-energy TSs. An additional TS, TS (1R,2S)<sub>e,a</sub>- $\alpha^\ddagger$ , wherein this hydrogen bonding interaction is weaker, is found to have higher energy.<sup>15</sup> The next higher-energy TS leading to the opposite enantiomer, i.e., TS (1S,2R)<sub>a,e</sub>- $\beta^\ddagger$ , is 4.3 kcal/mol higher than the lowest-energy (1R,2S)<sub>e,a</sub>- $\alpha^\ddagger$  in the case of Boc-protected peptide.<sup>16</sup> Such a larger difference in the activation barriers between the kinetically significant acylation step evidently suggest that the separation of *cis*-(1R,2S)-cyclohexane-1,2-diol through monoacylation using catalyst **2** appears to be a feasible option. The resulting product of desymmetrization is predicted as (1R,2S)-2-hydroxycyclohexyl acetate. We hope that the prediction would be subjected to experimental verification in the near future.

In summary, we have been able to explain the observed product stereochemistry in the kinetic resolution of *trans*-cyclohexane-1,2-diol. The predicted outcome is in concurrence with the available experimental results. The bifunctional nature of the catalyst is illustrated where one end offers nucleophilic catalysis while the backbone helps to achieve chiral recognition.

**Acknowledgment.** Generous computing facilities from IITB computer centre and a senior research fellowship from CSIR New Delhi (SCB) are gratefully acknowledged.

**Supporting Information Available:** Details on computational methods, full citation of ref 9b, optimized geometries of lower-energy transition states, and optimized coordinates of various transition states and their energies are given. This material is available free of charge via the Internet at <http://pubs.acs.org>.

OL9011822

(15) A comparison of these transition state features is given in Figure S2 of Supporting Information.

(16) The optimized geometries of lower-energy transition states for the acylation reaction of *cis*-cyclohexane-1,2-diol are given in Figure S1 of Supporting Information.

# Synthesis of Azoaromatic Dyes via Redox Driven C—N Bond Fusion

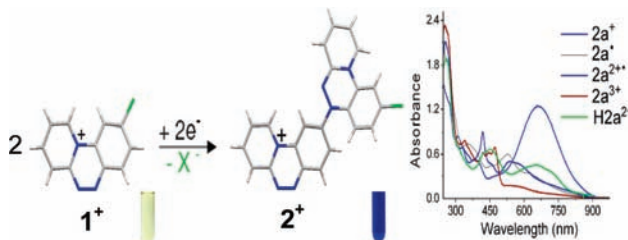
Mominul Sinan,<sup>†</sup> Manashi Panda,<sup>†</sup> Priyabrata Banerjee,<sup>†</sup> C. B. Shinisha,<sup>‡</sup>  
Raghavan B. Sunoj,<sup>\*,‡</sup> and Sreebrata Goswami<sup>\*,†</sup>

Department of Inorganic Chemistry, Indian Association for the Cultivation of Science,  
Kolkata 700 032, India, and Department of Chemistry, Indian Institute Technology  
Bombay, India

*icsg@iacs.res.in; sunoj@chem.iitb.ac.in*

Received May 21, 2009

## ABSTRACT



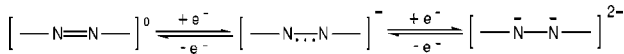
Two novel organic azo-dyes ( $2^+$ ) that feature an intense intramolecular charge transfer transition with end absorption reaching into the NIR region are introduced. Syntheses of these compounds were achieved by an unusual redox-driven C—N bond fusion of the tricyclo azoaromatic compounds ( $1^+$ ). The compounds show reversible electro- as well as proton chromism. The results have generated further scope of research in the area of designed syntheses of functional azoaromatics.

Azo-aromatic compounds have been studied extensively over the years owing to their versatile optical and redox properties. Low-lying vacant azo-centered  $\pi^*$  molecular orbitals in azoaromatic compounds are responsible for their long wavelength transitions<sup>1</sup> and nonlinear optical properties.<sup>2</sup> The  $\pi^*$  MO of these may also be directly populated<sup>3</sup> by one or two electrons, chemically or electrochemically. The resulting two-step redox system (Scheme 1) contains a radical anion<sup>4</sup> as

that contain azo functions in variable oxidation states may be anticipated to constitute charge transfer molecules with absorption in the red wavelength region. Redox-active compounds that absorb intensely in the long wavelength region attract considerable attention as functional materials.

In this communication we introduce two novel examples of donor–acceptor molecules containing azo functions in two different oxidation states. The compounds are bright blue ( $\lambda_{\text{max}}$  near 640 nm) with large molar extinction coefficients ( $>18,000 \text{ M}^{-1} \text{ cm}^{-1}$ ) and undergo multiple electron transfer

**Scheme 1.** Successive Azo Reduction



an intermediate and a 1,2-disubstituted hydrazido(2-) species<sup>5</sup> as a fully reduced form. Thus di- and polymeric compounds

(1) (a) *Industrial Dyes: Chemistry, Properties, Applications*; Hunger, K., Ed.; Wiley-VCH: Weinheim, Germany, 2003. (b) Kim, J. J.; Funabiki, K.; Muramatsu, H.; Shibata, K.; Kim, S. H.; Shiozaki, H.; Hortmann, H.; Matsui, M. *Chem. Commun.* **2000**, 753.

(2) (a) Ishow, E.; Bellaïche, C.; Bouteiller, L.; Nakatani, K.; Delaire, J. A. *J. Am. Chem. Soc.* **2003**, 125, 15744. (b) Luo, J.; Qin, J.; Kang, H.; Ye, C. *Chem. Mater.* **2001**, 13, 927. (c) Qiu, F.; Cao, Y.; Xu, H.; Jiang, Y.; Zhou, Y.; Liu, J. *Dyes Pigments*. **2007**, 75, 454.

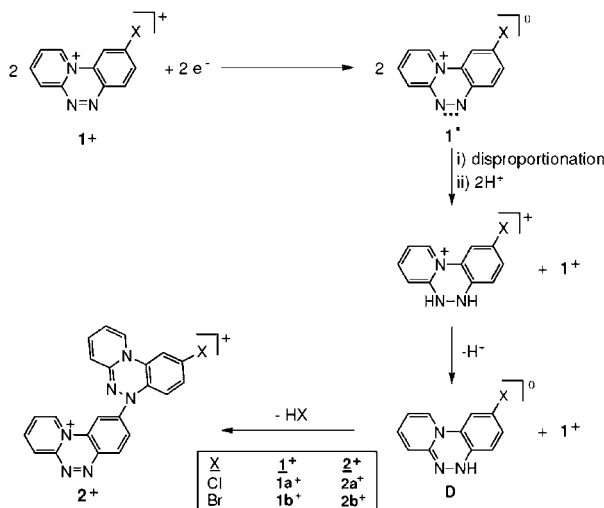
(3) (a) Sadler, J. L.; Bard, A. J. *J. Am. Chem. Soc.* **1968**, 90, 1979. (b) Goswami, S.; Mukherjee, R.; Chakravorty, A. *Inorg. Chem.* **1983**, 22, 2825.

(4) (a) Samanta, S.; Singh, P.; Fiedler, J.; Záliš, S.; Kaim, W.; Goswami, S. *Inorg. Chem.* **2008**, 47, 1625. (b) Pramanik, K.; Shivakumar, M.; Ghosh, P.; Chakravorty, A. *Inorg. Chem.* **2000**, 39, 195, and references therein.

(5) Drug, E.; Gozin, M. *J. Am. Chem. Soc.* **2007**, 129, 13784.

reversibly at low potentials. These are obtained as stable crystalline materials from a novel one-pot redox-driven C–N bond fusion<sup>6</sup> reaction (Scheme 2) of heterocyclic azoaromatics (**1**<sup>+</sup>) that was recently reported<sup>7</sup> by us. The level of oxidation states of the donor and acceptor units in these compounds differ by two units. As far as we are aware, examples of such azo-organic dyes are not available in the literature. The most closely related dimers are the aryl/saturated hydrocarbon bridged bis-hydrazines<sup>8</sup> and their corresponding radical cations reported by Nelsen et al.

Scheme 2. Synthetic Reaction



The 6-Cl(Br)-substituted yellow compounds **1a**<sup>+</sup> and **1b**<sup>+</sup> upon electrochemical one electron reduction in water produced the intense blue monocations **2a**<sup>+</sup> and **2b**<sup>+</sup>, respectively. Notably this transformation does not occur in dry acetonitrile. The neutral radical compound **1a**<sup>•</sup> is stable in dry solvent and showed characteristic single line EPR. It may thus be concluded that a proton source is essential for the reference transformation. Subsequently, we found that chemical reduction of an aqueous solution of **1**<sup>+</sup> by the use of aqueous sodium dithionite also produced **2**<sup>+</sup> in high yields (ca. 80%). These were isolated as their perchlorate or chloride salts. The mechanism of the reaction remains unresolved as yet. However, one of the most plausible mechanisms is depicted in Scheme 2. The reaction is initiated by one electron reduction of the triazinium cation. The triazene radical, thus produced, undergoes rapid disproportionation in aqueous medium to produce a tricyclo nuleophilic

intermediate **[D]**, which on subsequent reaction with **1**<sup>+</sup> produces the cationic dimer **2**<sup>+</sup> with the elimination of HX. Further propagation of the fusion reaction via X substitution in **2**<sup>+</sup> was not possible due to nonlability of X bonded to the reduced tricyclo moiety in **2**<sup>+</sup>. Thus reduction of the azo chromophore is the primary prerequisite for the above dimerization reaction. Interestingly, catalytic hydrogenation of **1a**<sup>+</sup> in methanol on 10% Pd/C also produced **2a**<sup>+</sup>, confirming our above proposition further. The intermediate **[D]** appears to be highly reactive and combines instantaneously (see below) with the unreacted **1a**<sup>+</sup> to form **2a**<sup>+</sup>. Thermodynamic feasibility for the formation of **2a**<sup>+</sup> is assessed on the basis of the calculated enthalpy for each step. The overall reaction is found to be highly exothermic, which includes one electron reduction of **1a**<sup>+</sup> as well as disproportionation<sup>9</sup> of the ensuing triazene radical. In the last step, formation of the cationic dimer **2a**<sup>+</sup> is also found to be favored with a heat of formation of -24.7 kcal/mol.

Micro analytical, positive-ion ESI-mass spectra, together with NMR spectral data (Figures S1–S3, Supporting Information) of the compounds, [2]A (A = ClO<sub>4</sub>, Cl) convincingly support their formulations. X-ray structure determination of a representative compound, [2a]ClO<sub>4</sub> confirms its formation. A molecular view of the cationic compound is shown in Figure 1 (for its ORTEP see Figure S4, Supporting Information).

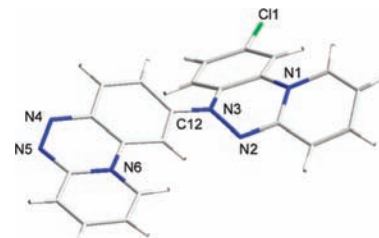


Figure 1. Molecular view of **2a**<sup>+</sup>.

The most significant observation in this structure is that an essentially planar triazinium unit (acceptor) is bonded to a boat-shaped two electron reduced unit (donor) through a newly formed C(12)–N(3) bond. The N–N length in the acceptor unit indicates a double<sup>10</sup> bond (N(4)–N(5), 1.311(3) Å), whereas that in the reduced unit is a single<sup>11</sup> bond (N(2)–N(3), 1.411(3) Å). The connecting C(12)–N(3) bond is shorter than a single bond, indicating electron delocalization between the two rings.

Cyclic voltammetry (CV) studies (Figure 2) of **2**<sup>+</sup> revealed two one electron oxidative waves associated with the formation of the dication radical **2**<sup>2+</sup> and the trication, **2**<sup>3+</sup>, respectively. In addition to the above anodic responses, a

(6) (a) Samanta, S.; Goswami, S. *J. Am. Chem. Soc.* **2009**, *131*, 924, and references therein. (b) Barder, T. E.; Buchwald, S. L. *J. Am. Chem. Soc.* **2007**, *129*, 12003. (c) Hartwig, J. F. *Acc. Chem. Res.* **2008**, *41*, 1534.

(7) Sinan, M.; Panda, M.; Ghosh, A.; Dhara, K.; Fanwick, P. E.; Chattopadhyay, D. J.; Goswami, S. *J. Am. Chem. Soc.* **2008**, *130*, 5185.

(8) (a) Nelsen, S. F.; Konradsson, A. E.; Clennan, E. L.; Singleton, J. *Org. Lett.* **2004**, *6*, 285. (b) Lockard, J. V.; Zink, J. I.; Konradsson, A. E.; Weaver, M. N.; Nelsen, S. F. *J. Am. Chem. Soc.* **2003**, *125*, 13471. (c) Nelsen, S. F.; Ismagilov, R. F.; Gentile, K. E.; Powell, D. R. *J. Am. Chem. Soc.* **1999**, *121*, 7108. (d) Nelsen, S. F.; Chang, H.; Wolff, J. J.; Adamus, J. *J. Am. Chem. Soc.* **1993**, *115*, 12276.

(9) Electron affinity of **1a**<sup>+</sup> is -131.5 kcal/mol, and calculated heat of reaction for disproportionation followed by protonation is -245.6 kcal/mol (B3LYP/6-31G\*).

(10) Mostad, A.; Rømning, C. *Acta Chim. Scand.* **1971**, *25*, 3361.

(11) Morino, Y.; Iijima, T.; Mutara, Y. *Bull. Chem. Soc. Jpn.* **1960**, *33*, 46.

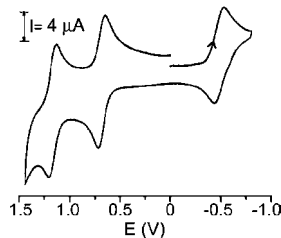


**Figure 2.** Cyclic voltammogram of  $\mathbf{2a}^+$ .

reductive response at  $-0.49$  V signifies the formation of a neutral radical,  $\mathbf{2}^\bullet$ . For comparison, the parent triazinium salt [ $\mathbf{1a}$ ]ClO<sub>4</sub> displayed<sup>7</sup> a reductive one electron wave at  $-0.17$  V forming a neutral triazene radical,  $\mathbf{1a}^\bullet$ .

The electrolytically generated compounds,  $\mathbf{2a}^{2+*}$  and  $\mathbf{2a}^\bullet$ , each showed a single line sharp EPR spectrum at  $g = 2.004$  and  $2.006$ , respectively, characterizing the formation of the free radicals. The trication,  $\mathbf{2a}^{3+}$  is, however, EPR silent as expected (Figures S5–S8, Supporting Information).

To gather further insights into the molecular origin of these redox reactions, we have analyzed the B3LYP/6-31G\* optimized geometries of these species.<sup>12</sup> The agreement between the experimental structural parameters and that obtained through DFT calculations for  $\mathbf{2a}^+$  are found to be excellent (Table 1). The geometric comparison between  $\mathbf{2a}^+$  and the corresponding one electron reduced species,  $\mathbf{2a}^\bullet$ , reveals an elongation of N(4)–N(5) bond. Further, the spin orbital contours of  $\mathbf{2a}^\bullet$  (Figure 3) indicate a relatively larger localization of spin density on N(4). It is therefore concluded that the reduction of  $\mathbf{2a}^+$  is predominantly centered at the acceptor part. The oxidation of  $\mathbf{2a}^+$ , on the other hand, is identified to impart double bond character to the N(3)–N(2) bond.

**Table 1.** Essential Structural Parameters of Compounds from DFT Calculations<sup>a</sup>

	bond lengths			torsional angle
	N(5)–N(4)	N(3)–N(2)	N(3)–C(12)	N(2)–N(3)–C(12)–C(22)
$\mathbf{2a}^\bullet$	1.343	1.414	1.409	-18
$\mathbf{2a}^+$	1.307 (1.311)	1.406 (1.411)	1.364 (1.372)	-9 (-4)
$\mathbf{2a}^{2+*}$	1.277	1.349	1.425	-37
$\mathbf{2a}^{3+}$	1.269	1.297	1.466	-55

<sup>a</sup> Experimental data available for  $\mathbf{2a}^+$  is given in parentheses

Spin density of the first oxidized product  $\mathbf{2a}^{2+*}$  is primarily at the N(3)–N(2) bond of the donor unit. The LUMO of the subsequent oxidized species  $\mathbf{2a}^{3+}$  is also found to be localized on the N(3)–N(2) bond (Figure S9, Supporting Information). Moreover, both oxidation and reduction of  $\mathbf{2a}^+$  result in out-of-plane geometric disposition of the two rings.

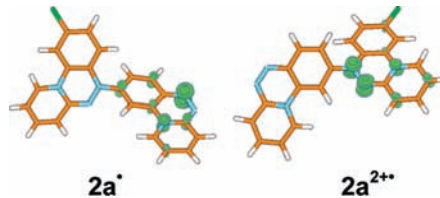


**Figure 3.** DFT calculated spin orbitals of the compounds  $\mathbf{2a}^\bullet$  and  $\mathbf{2a}^{2+*}$ .

The intense blue color of the parent compound,  $\mathbf{2a}^+$ , upon electrolyses faded considerably along with blue shift (electrochromic effect) of the transition bands (Figure 4). The analyses of frontier MOs of  $\mathbf{2a}^+$  indicate that the HOMO and HOMO–1 are localized on the donor triazinium, while the unoccupied orbitals such as LUMO and LUMO+1 are localized primarily on the acceptor unit. On the basis of values of the oscillator strength predicted using TD-DFT, the most intense transition at 634 nm for the compound  $\mathbf{2a}^+$  is ascribed to the excitation from HOMO to LUMO.<sup>13</sup>

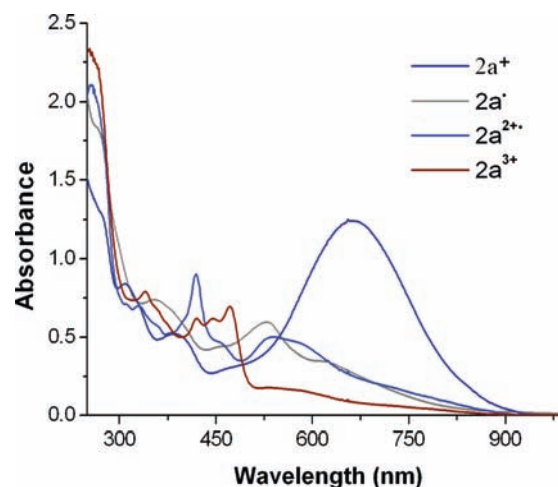


**Figure 4.** UV–vis spectra of  $\mathbf{2}^\bullet$ ,  $\mathbf{2}^+$ ,  $\mathbf{2}^{2+*}$ , and  $\mathbf{2}^{3+}$ .

Moreover, upon addition of H<sup>+</sup> to a solution of the compound  $[\mathbf{2a}]^+$  in MeOH–H<sub>2</sub>O (1:1 v/v), the intense blue color became light yellowish green, which is attributed to protonation of N2 resulting in loss of conjugation with the C5 atom.<sup>14</sup> The effect of H<sup>+</sup> in the above spectral change is reversible with a sharp isosbestic point at 510 nm (Figure 5).

(12) All electronic structure calculations were performed using Gaussian 03: Frisch, M. J. et al., *Gaussian 03*; Gaussian, Inc.: Wallingford, CT, 2004 (see Supporting Information for full citation). All stationary points are characterized by frequency calculations on the optimized geometries.

(13) Frontier molecular orbitals of  $\mathbf{2a}^+$  as well as list of computed vertical excitations of  $\mathbf{2a}^\bullet$ ,  $\mathbf{2a}^+$ ,  $\mathbf{2a}^{2+*}$ ,  $\mathbf{2a}^{3+}$ , and  $\mathbf{1a}^+$  are given in Supporting Information.

(14) An increase in N(2)–C(5) distance from 1.309 to 1.409 Å is noticed upon protonation of  $\mathbf{2a}^+$  (see Supporting Information).

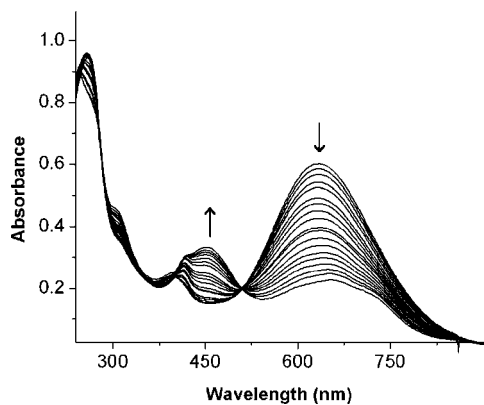


**Figure 5.** UV-vis spectral change of  $\mathbf{2a}^+$  as a function of  $[\text{H}^+]$ .

In summary, we have introduced a redox-driven one-pot synthesis of two novel azoaromatic dyes that feature intense intramolecular charge transfer bands with end absorption reaching into the NIR region. These compounds show appealing optoelectronic and redox properties. The applications of these azo dyes as functional materials<sup>15</sup> are under scrutiny.

**Acknowledgment.** The research was supported by the DST, India funded project SR/S1/IC-24/2006. Crystallography was performed at the DST-funded National Single Crystal Diffractometer Facility at the Department of Inorganic Chemistry, IACS. M.S. and C.B.S. are thankful to the CSIR for Fellowship support. Thanks are due to Dr. K. Ghosh of Kalyani University, India for useful discussion. IIT Bombay Computer Center is acknowledged for generous CPU time.

**Supporting Information Available:** X-ray crystallographic table of  $[\mathbf{2a}]\text{ClO}_4$ , TD-DFT calculations results, relevant figures as noted in the text, and experimental and computational details. This material is available free of charge via the Internet at <http://pubs.acs.org>.

OL9011184

(15) (a) Kim, S.-H.; Matsumoto, S. *Dyes Pigments*. **2007**, *72*, 406. (b) Li, G.; Zhou, Y.-F.; Cao, X.-B.; Bao, P.; Jiang, K.-J.; Lin, Y.; Yang, L.-M. *Chem. Commun.* **2009**, 2201, and references therein. (c) Steckler, T. T.; Zhang, X.; Hwang, J.; Honeyager, R.; Ohira, S.; Zhang, X.-H.; Grant, A.; Ellinger, S.; Odom, S. A.; Sweat, D.; Tanner, D. B.; Rinzler, A. G.; Barlow, S.; Brédas, J.-L.; Kippelen, B.; Marder, S. R.; Reynolds, J. R. *J. Am. Chem. Soc.* **2009**, *131*, 2824.

# The Pivotal Role of Chelation as a Stereochemical Control Element in Non-Evans *Anti* Aldol Product Formation

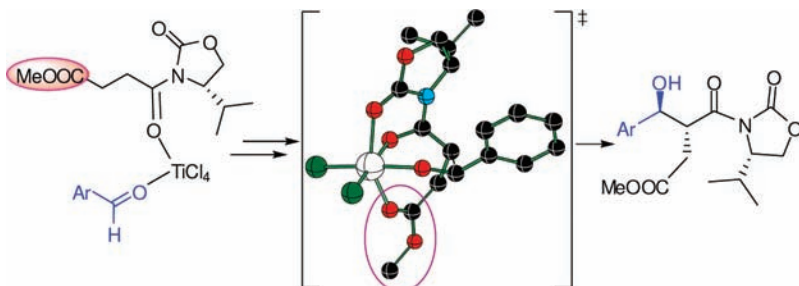
C. B. Shinisha and Raghavan B. Sunoj\*

Department of Chemistry, Indian Institute of Technology Bombay, Powai,  
Mumbai 400076, India

[sunoj@chem.iitb.ac.in](mailto:sunoj@chem.iitb.ac.in)

Received April 28, 2010

## ABSTRACT



The origin of stereoselective formation of Evans *syn* and non-Evans *anti* aldol products in the reaction between titanium enolate derived from *N*-succinyl oxazolidinone and benzaldehyde is established by using transition-state modeling. The chelated transition-state model is found to hold the key to otherwise less likely non-Evans *anti* aldol product, whereas the nonchelated model offers a convincing rationalization toward Evans *syn* aldol product. The computed results are in agreement with the reported experimental observations.

Asymmetric aldol reactions employing oxazolidinones as chiral auxiliaries have been a domain of considerable activity in organic chemistry for nearly three decades.<sup>1</sup> The use of oxazolidinones and its variants has found an increasingly large number of applications in total synthesis of natural products and compounds of pharmaceutical significance.<sup>2</sup> The precedence in oxazolidinone-mediated aldol reactions encompasses the synthesis of both *syn* and *anti* aldol products.<sup>3,4</sup> While most of the early efforts provided access to *syn* aldol products, the synthesis of *anti* aldol received

great attention in more recent times. The approach toward the latter generally relies on stoichiometric control, changes in the nature of reagents, and the chiral auxiliaries.<sup>5</sup> For example, *anti*-selective aldol reactions were achieved by (a) varying the nature of Lewis acids in boron enolate mediated reactions,<sup>5c</sup> (b) introducing magnesium halide as catalyst,<sup>5d</sup> and (c) using thiazolidinethione as the chiral auxiliary.<sup>5e</sup> It

(1) (a) Evans, D. A.; Bartroli, J.; Shih, T. L. *J. Am. Chem. Soc.* **1981**, *103*, 2127. (b) Evans, D. A.; Ennis, M. D.; Mathre, D. J. *J. Am. Chem. Soc.* **1982**, *104*, 1737. (c) Evans, D. A.; Urpi, F.; Somers, T. D.; Clark, J. S.; Bilodeau, M. T. *J. Am. Chem. Soc.* **1990**, *112*, 8215. (d) Evans, D. A.; Starr, J. T. *Angew. Chem., Int. Ed.* **2002**, *41*, 1787.

(2) (a) Crimmins, M. T.; King, B. W. *J. Am. Chem. Soc.* **1998**, *120*, 9084. (b) Hawkins, J. M.; Watson, T. J. N. *Angew. Chem., Int. Ed.* **2004**, *43*, 3224. (c) Crimmins, M. T.; Christie, H. S.; Chaudhary, K.; Long, A. *J. Am. Chem. Soc.* **2005**, *127*, 13810. (e) Patel, J.; Clavé, G.; Renard, P.-Y.; Franck, X. *Angew. Chem., Int. Ed.* **2008**, *47*, 4224. (f) Tessier, A.; Lahmar, N.; Pytkowicz, J.; Briguad, T. *J. Org. Chem.* **2008**, *73*, 2621.

(3) (a) Evans, D. A. *Aldrichim. Acta* **1982**, *15*, 23. (b) Evans, D. A.; Rieger, D. L.; Bilodeau, M. T.; Urpi, F. *J. Am. Chem. Soc.* **1991**, *113*, 1047. (c) Crimmins, M. T.; King, B. W.; Tabet, E. A.; Chaudhary, K. *J. Org. Chem.* **2001**, *66*, 894.

(4) Details of the stereochemical descriptions and product nomenclature are provided in the Supporting Information.

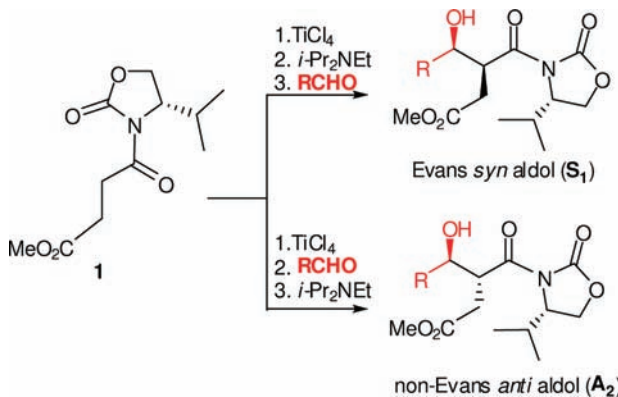
(5) (a) Danda, H.; Hansen, M. M.; Heathcock, C. H. *J. Org. Chem.* **1990**, *55*, 173. (b) Bonner, M. P.; Thornton, E. R. *J. Am. Chem. Soc.* **1991**, *113*, 1299. (c) Walker, M. A.; Heathcock, C. H. *J. Org. Chem.* **1991**, *56*, 5747. (d) Evans, D. A.; Tedrow, J. S.; Shaw, J. T.; Downey, C. W. *J. Am. Chem. Soc.* **2002**, *124*, 392. (e) Evans, D. A.; Downey, C. W.; Shaw, J. T.; Tedrow, J. S. *Org. Lett.* **2002**, *4*, 1127. (f) Crimmins, M. T.; McDougall, P. J. *Org. Lett.* **2003**, *5*, 591. (g) Itoh, Y.; Yamanaka, M.; Mikami, K. *J. Am. Chem. Soc.* **2004**, *126*, 13174.

is noteworthy that large majority of oxazolidinone mediated aldol reactions offer access to *syn*-diastereoselectivity.

In a very recent study, Hajra et al. reported the synthesis of both *syn* and *anti* aldol products, beginning from the same substrates, just by altering the sequence of generation of the enolate.<sup>6</sup> The reaction was performed by using *N*-acyloxazolidinones bearing a  $\gamma/\delta$ -chelating functional group, as shown in Scheme 1. What is interesting here is that when the normal sequence of addition of reagents was followed, Evans *syn* aldol (**S<sub>1</sub>**) was formed. More intriguing, however, was the formation of non-Evans *anti* aldol (**A<sub>2</sub>**), when the electrophile was introduced prior to the addition of base (inverse sequence of addition). Further, with unfunctionalized substrates Evans *syn* aldol only was isolated, irrespective of whether a normal or an inverse sequence of additions of reagents were followed. This observation evidently alludes to the potential role of the pendent functional group in steering the stereochemical course of the reaction.

It is surprising to note that the very premise on which the stereochemical outcome of oxazolidinone based asymmetric induction have been thus far rationalized relies on qualitative transition state (TS) models.<sup>5b</sup> The insights on the electronic structure of such crucial TSs are seldom found in literature.<sup>7</sup> We have recently examined the nature of stereocontrolling TSs in the reaction of titanium enolates, derived from Evans as well as Crimmins chiral auxiliaries, with benzaldehyde.<sup>8</sup> In this paper, we intend to shed light on the molecular origin of stereoselectivity-controlling chelation in *N*-acyloxazolidinones bearing a pendent functional group.

**Scheme 1.** Oxazolidinone-Mediated Aldol Reaction Yielding *Syn* and *Anti* Aldol Products (See Ref 6)



The key intermediates and TSs associated with the reaction of titanium enolate derived from *N*-succinyl-2-oxazolidinone

(6) Hajra, S.; Giri, A. K.; Karmakar, A.; Khatua, S. *Chem. Commun.* **2007**, 2408.

(7) Except for a rare account on oxazolidinone based stereoinduction by using boron enolates, see: Goodman, J. M.; Paton, R. S. *Chem. Commun.* **2007**, 2124.

(8) Our efforts toward rationalizing the formation of Evans and non-Evans *syn* aldol products through chelated and nonchelated transition-state models to date is the only computational study on oxazolidinone mediated asymmetric aldol reaction between Ti-enolate and aldehydes. Shinisha, C. B.; Sunoj, R. B. Manuscript in preparation.

(**1** in Scheme 1) and benzaldehyde is identified by using the density functional theory calculations. Computations are performed at the B3LYP/6-311+G\*\*//B3LYP/6-31G\* level of theory.<sup>9,10</sup> All calculations were carried out by using Gaussian03 suite of quantum chemical programs.<sup>11</sup> To establish the influence of different coordination patterns around the oxophilic titanium, several likely possibilities are analyzed and their effect on the stereochemical course of the reaction is delineated herein.

One of the most important roles of the titanium center is to anchor together the reactants viz., **1** and benzaldehyde, through coordination. The coordinations that can most readily occur is between titanium and the carbonyl oxygens of the (i) *N*-acyl group and (ii) benzaldehyde. Additional coordination possibilities as well are likely with the carbonyl of the oxazolidinone ring or/and the pendent ester group.<sup>12</sup> The terminologies “chelated” and “nonchelated”, respectively, refer to the presence or absence of coordination between the ring carbonyl of oxazolidinone and titanium.<sup>13</sup> The effect of such preorganization is expected to be critical in the stereocontrolling C–C bond formation step. The TSs for the addition of *si/re* face of chiral titanium enolate on the *si/re* face of benzaldehyde are identified.<sup>14</sup> To distinguish different TSs arising as a result of differing chelation modes, following scheme is adopted in the TS notations. The representations are as follows: **2**, nonchelation, **3**, chelation with the ring carbonyl of the oxazolidinone, **3'**, chelation with the pendent group, and **4**, chelation with both ring carbonyl and the pendent groups.

Under the conditions of normal sequence of addition of reagents, it is logical to assume that the titanium enolate will be generated from a precoordinated  $\text{TiCl}_4$  substrate complex.<sup>15</sup> It is identified that when a nonchelated TS model is employed for the stereoselective C–C bond formation, the computed relative energies of the TSs indicate the formation of Evans *syn* aldol product as most likely.<sup>16</sup> The addition by the less hindered *re* face of the enolate on the *si* face of benzaldehyde is found to be the most favored mode. The lowest energy TS **TS-S<sub>1</sub>-2** leads to the formation of Evans *syn* aldol (**S<sub>1</sub>**) (Table 1, entry 1).<sup>8</sup>

(9) All the intermediates and TSs were respectively characterized as minima and first-order saddle points by using frequency calculations. Further, intrinsic reaction coordinate (IRC) calculations were performed to authenticate the TSs. Calculations on the critical TSs were further repeated at the mPW1K level of theory. See the Supporting Information for further details.

(10) The solvent effects were incorporated with the continuum solvation model by using the SCRF-PCM framework. Dichloromethane was taken as the continuum solvent dielectric ( $\epsilon = 8.93$ ). The results are tabulated in Tables S1 and S2 in the Supporting Information.

(11) Frisch, M. J. *Gaussian 03*, Revision C.02; Gaussian, Inc.: Wallingford, CT, 2004. See the full citation in the Supporting Information.

(12) The TSs **S<sub>1</sub>**, **S<sub>2</sub>**, **A<sub>1</sub>**, and **A<sub>2</sub>** correspond to Evans *syn*, non-Evans *syn*, Evans *anti*, and non-Evans *anti* products.

(13) Qualitative models that are generally employed in rationalizing the stereoselectivity in oxazolidinone mediated aldol reaction are summarized in Scheme S1 in the Supporting Information.

(14) A schematic representation of all these modes of addition are given in Scheme S2 in the Supporting Information.

(15) Marrone, A.; Renzetti, A.; De Maria, P.; Gérard, S.; Sapi, J.; Fontana, A.; Re, N. *Chem.–Eur. J.* **2009**, *15*, 11537.

(16) Such a nonchelated working model has been documented: (a) Nerz-Stormes, M.; Thornton, E. R. *J. Org. Chem.* **1991**, *56*, 2489. (b) Siegel, C.; Thornton, E. R. *J. Am. Chem. Soc.* **1989**, *111*, 5722. (c) Crimmins, M. T.; Shamszad, M. *Org. Lett.* **2007**, *9*, 149. (d) See Scheme S1 in the Supporting Information.

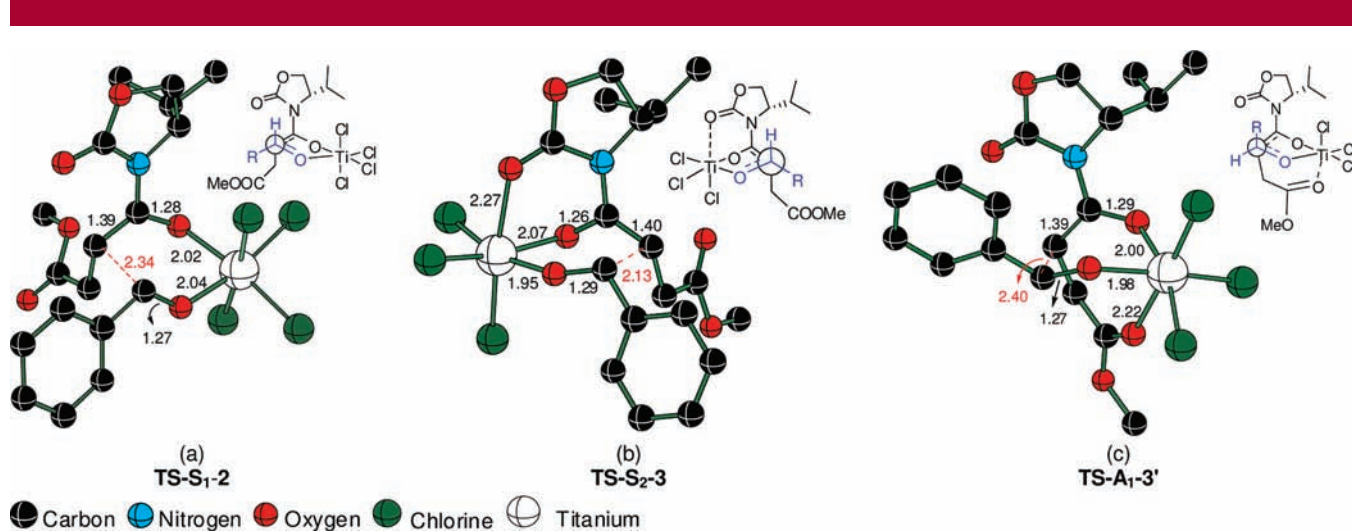


**Figure 1.** B3LYP/6-31G\*-optimized geometries of lower energy diastereomeric transition states for the addition of titanium enolate (derived from *N*-succinyl-2-oxazolidinone) to benzaldehyde. Different coordination modes are depicted by using the lowest energy transition state in each case.

The optimized geometry of the lowest energy **TS-S<sub>1</sub>-2**, as given in Figure 1a, reveals a chairlike structure, wherein the phenyl group occupies a pseudoequatorial position. It can further be noticed that the pendent group in this nonchelated model is oriented away from the aryl group as well as from the coordination sphere of titanium. This implies that under the conditions of normal sequence of addition of reagents, a nonchelated pathway guiding toward Evans *syn* aldol product is quite likely to operate. Further, the presence of potential chelating group in the pendent arm might not directly influence the stereoselectivity in this TS model.

Next, the chelated TSs wherein the ring carbonyl is coordinated to titanium are identified, and the associated energetics are summarized in Table 1. The addition by nonhindered *si* face of the enolate on the *re* face of benzaldehyde is identified as the most favored mode. The optimized geometry of the lowest energy **TS-S<sub>2</sub>-3** is provided in Figure 1b. The lowest energy TS exhibits a chairlike geometry with the phenyl group on benzaldehyde positioned farther from the chiral auxiliary. The preferred diastereofacial approach through **TS-S<sub>2</sub>-3** would lead to non-Evans *syn* aldol product. From these results it is evident that the presence of the pendent group is perhaps not influencing in the stereo-differentiation, so long as a conventional chelated and nonchelated TS model is invoked. In fact, our prediction concurs with the literature precedence, where the chelated TS model is proposed to be responsible for the formation of non-Evans *syn* aldol (**S<sub>2</sub>**), under suitable reaction conditions.<sup>3c,5b</sup>

With the chelated TS model suggesting the formation of non-Evans *syn* aldol, we turned our attention to another model as follows. As mentioned earlier, a non-Evans *anti* aldol (**A<sub>2</sub>**) product is produced, upon following an inverse sequence of addition of reagents. Besides the aforementioned

**Table 1.** Relative Energies (in kcal/mol) of Important Transition States Obtained at the B3LYP/6-311+G\*\*//B3LYP/6-31G\* Level of Theory for the C–C Bond Formation between Titanium Enolate and Benzaldehyde

transition states	$\Delta E^\ddagger$	$\Delta H^\ddagger$	$\Delta G^\ddagger$
	(a)		
<b>TS-S<sub>1</sub>-2</b>	<b>0.0</b>	<b>0.0</b>	<b>0.0</b>
<b>TS-S<sub>2</sub>-2</b>	4.8	4.8	5.0
<b>TS-A<sub>1</sub>-2</b>	<sup>a</sup>	<sup>a</sup>	<sup>a</sup>
<b>TS-A<sub>2</sub>-2</b>	8.7	8.5	8.8
	(b)		
<b>TS-S<sub>1</sub>-3</b>	4.8	4.7	5.4
<b>TS-S<sub>2</sub>-3</b>	<b>0.0</b>	<b>0.0</b>	<b>0.0</b>
<b>TS-A<sub>1</sub>-3</b>	2.8	2.7	3.3
<b>TS-A<sub>2</sub>-3</b>	0.2	0.2	0.3
	(c)		
<b>TS-S<sub>1</sub>-3'</b>	1.1	1.4	1.5
<b>TS-S<sub>2</sub>-3'</b>	3.5	3.4	3.3
<b>TS-A<sub>1</sub>-3'</b>	<b>0.0</b>	<b>0.0</b>	<b>0.0</b>
<b>TS-A<sub>2</sub>-3'</b>	2.7	2.7	3.1

<sup>a</sup> The transition state could not be located after repeated attempts.

chelations, a new TS model where the additional functionality from the pendent group coordinates to titanium is studied.<sup>17</sup>

The stereochemical course could be quite different when the second scenario, as described in Scheme 1, is operating. When benzaldehyde is introduced prior to the generation of titanium enolate, different coordination possibilities can arise. The TSs exhibiting coordination of the pendent carbonyl group are located and the relative energies are provided in Table 1. In this model, the addition of the *re* face of the enolate on the *re* face of benzaldehyde through a boat-like

(17) Several key possibilities belonging to this category are presented in Scheme S2 of the Supporting Information.

TS (TS-A<sub>1</sub>-3' in Figure 1c) is identified as the most preferred mode. The TS-A<sub>1</sub>-3' can lead to Evans *anti* aldol (A<sub>1</sub>) product. In the next higher energy TS, namely TS-S<sub>1</sub>-3', the aryl group occupies a pseudoequatorial position in a chairlike conformation and is oriented toward the pendent coordination.<sup>18</sup> It is of significance, at this juncture, to reckon that the predicted stereochemical outcome is at variance with the reported experimental results (Scheme 1). Refinements to TS models hitherto considered are therefore evidently in order.

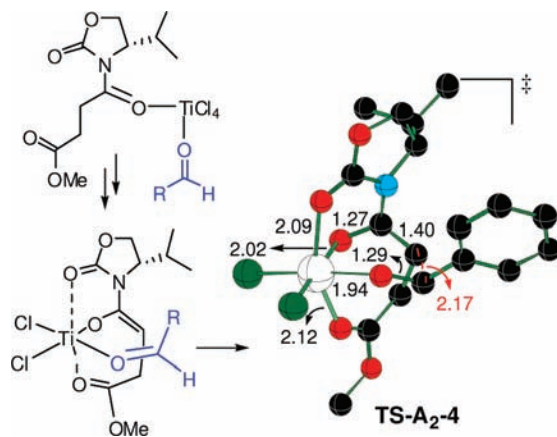


**Figure 2.** B3LYP/6-31G\*-optimized geometry of the TS for the C–C bond formation wherein the pendent group is coordinated. Distances are given in angstroms.

Further refinements have been done in which the coordination of both carbonyl groups of oxazolidinone ring and the pendent group with titanium is included. The optimized TS geometry, as given in Figure 2, reveals a six-membered boatlike arrangement. The carbonyl groups of oxazolidinone, enolate, pendent ester group, and benzaldehyde together constitute a distorted octahedral topology around the titanium center.<sup>19</sup> The relative energies of the key TSs with respect to the lowest energy TS are summarized in Table 2.<sup>20</sup> The lowest energy **TS-A<sub>2</sub>-4** is found to involve the addition of *si* face of enolate on the *si* face of benzaldehyde. The next

(18) Optimized TS geometries are given in Figure S1 in the Supporting Information.

(19) (a) The axial ligands are found to be tilted toward the substrate. (b) Similar topologies around titanium have earlier been noticed for TiCl<sub>4</sub>-promoted C–C bond formation reactions. See: Patel, C.; Sunoj, R. B. *J. Org. Chem.* **2010**, *75*, 359.

(20) The relative energies obtained from single-point calculations by using the PCM model at various levels of theory are provided in Table S2 of the Supporting Information.

(21) See Figure S2 in the Supporting Information.

(22) **TS-S<sub>2</sub>-4** appears to be more constrained (Figure S2, Supporting Information), leading to a higher degree of destabilization between the ester and the phenyl groups. It is to be noted that the computational methodology employed here, although adequate for the assessment of relative energies, may not provide an accurate description of van der Waals repulsions.

higher energy TS (**TS-S<sub>2</sub>-4**) presents a chairlike conformation with the phenyl group occupying a pseudoequatorial position.<sup>21</sup> The higher energy of this TS perhaps is due to the destabilizing interaction with the pendent carboxylic group coordinated to titanium.<sup>22</sup> The resulting product from **TS-S<sub>1</sub>-4** would be Evans *syn* aldol and involves the attack by the hindered face of enolate on the electrophile. Hence, when both the ring carbonyl and pendent carbonyl groups are in coordination with titanium, the stereoselective C–C bond formation would lead to non-Evans *anti* aldol (**A<sub>2</sub>**) as the most favored product.

Since TSs in this model is most vital to the conclusions, we have examined how the predicted trends hold across different levels of theory and basis set combinations. The results provided in Table 2 readily suggest a close mutual agreement between the computed values.

**Table 2.** Computed Relative Energies (in kcal/mol) of Important Transition States with Pendent Group Coordination<sup>a</sup> for the C–C Bond Formation between Titanium Enolate and Benzaldehyde

transition states	relative energy (in kcal/mol)					
	L1	L2	L3	L1	L2	L3
ΔH <sup>‡</sup>	ΔG <sup>‡</sup>	ΔH <sup>‡</sup>	ΔG <sup>‡</sup>	ΔH <sup>‡</sup>	ΔG <sup>‡</sup>	ΔG <sup>‡</sup>
<b>TS-A<sub>2</sub>-4</b>	<b>0.0</b>	<b>0.0</b>	<b>0.0</b>	<b>0.0</b>	<b>0.0</b>	<b>0.0</b>
<b>TS-S<sub>2</sub>-4</b>	1.1	1.0	1.6	1.1	1.3	1.2
<b>TS-S<sub>1</sub>-4</b>	2.6	3.2	<sup>b</sup>	<sup>b</sup>	2.8	3.2

<sup>a</sup> L1 = B3LYP/6-311+G\*\*//B3LYP/6-31G\*; L2 = mPW1K/6-311+G\*\*//mPW1K/6-31G\*; L3 = B3LYP/LANL2DZ(Ti), 6-31+G\*\*. <sup>b</sup> Transition state could not be located after repeated attempts.

In summary, we could rationalize the formation of non-Evans *anti* aldol (**A<sub>2</sub>**) product by invoking a chelated TS model in which the metal is coordinated with ring carbonyl and the  $\gamma$ -functionality. The formation of Evans *syn* aldol, on the other hand, is explained through nonchelated transition states. Our results are in accordance with the known experimental results.

**Acknowledgment.** Computing resources from the IITB computer center, Center for Modeling Simulation and Design Hyderabad, and a fellowship from CSIR New Delhi (S.C.B) are acknowledged. We are thankful to Prof. S. Hajra (IIT Kharagpur) for bringing our attention to the reagent sequence-dependent product variations.

**Supporting Information Available:** Details on computational methods, full citation of ref 11, and optimized coordinates of various transition states and their energies. This material is available free of charge via the Internet at <http://pubs.acs.org>.

OL100969F